

**Design, Deployment, Performance and Baseline Data Assessment
of Surface Tiltmeter Array Technology in Aquistore Geologic CO₂
Storage Project**

by

Yazhao Wang

A thesis submitted in partial fulfillment of the requirements for the degree of

Master of Science
in
GeoEnvironmental Engineering

Department of Civil and Environmental Engineering
University of Alberta

© Yazhao Wang, 2015

Abstract

Tiltmeters have been widely applied in the engineering field for precise angle measurement. The recent adoption of surface tiltmeter array in monitoring geologic CO₂ storage has further expanded the reach of this technology. During reservoir surveillance, tiltmeter array detects sub-millimeter level surface movement, delivers valuable input for reservoir management, and provides safety assurance to the general public. While achieving the high sensitivity, tiltmeter array also bears negative effect from the amplified environmental and cultural noise. The control and quantification of noise signals become more important in reservoir surveillance as noise signals approach injection signals in both temporal scale and amplitude. A surface array consisting of 15 tiltmeters is deployed in the Aquistore geologic CO₂ storage site southwest of Estevan, Saskatchewan, Canada. The design and deployment of tiltmeter array successfully delivers satisfactory reservoir coverage and sustains an insulated operational environment. In the baseline phase two years of tilt data are collected and analyzed for the composition of noise signals. Earth tides, surface meteorological conditions and seismic activities all contribute to the observed baseline tilt pattern. In order to remove the impact of noise signals, three general methods are proposed based on the revealed signal characteristics. A statistical regression method is used to quantify linearly-provoked tilt signal such as that from solid earth tide. For complex processes such as the impact of surface precipitation, a numerical modelling approach is adopted to estimate the scale of induced tilt signal. As tiltmeter sensors exhibit temperature dependent behavior, a

calibration method is proposed. With the removal of noise signals from tilt measurement, the tiltmeter array technology is improved with more accurate and unbiased surveillance output monitoring CO₂ injection and storage.

Acknowledgement

This thesis becomes a reality with the kind support of many individuals. I would like to extend my sincere thanks to all of them.

Foremost, I would like to express my truthful gratitude to my supervisor, Dr. Richard Chalaturnyk, for his continuous support during my master's study. His motivation, enthusiasm and immense knowledge added considerably to my graduate experience.

I am also grateful for my co-supervisor, Dr. Gonzalo Zambrano, for his invaluable guidance during my research. I appreciate his insightful suggestions, inspiring comments and encouragement that helped me making solid progress.

I would like to thank all friends and colleagues at the Reservoir Geomechanics Research Group. In particular, I thank Hrishikesh Adhikari, Jakob Brandl, Sander Osinga and Kais Ben Abdallah for their help and companionship in those many field trips to Estevan. Our time together in that edge of the world were not only fruitful, but also filled with laughter and joy. I thank Steve Gamble and Gilbert Wong for their professional assistance in the lab. And I appreciate Hope Walls for her administrative support.

My deepest gratitude goes to my family for their unflagging love and support. This dissertation is simply impossible without them.

Table of Contents

CHAPTER 1 Introduction	1
1.1 Statement of problem	1
1.2 Research objective.....	1
1.3 Scope and methodology	2
1.4 Organization of thesis.....	2
CHAPTER 2 Overview of Monitoring Geologic CO ₂ Storage	3
2.1 Carbon capture and storage	3
2.2 Measuring, monitoring and verification	4
2.3 Surface deformation monitoring.....	5
2.4 Tiltmeter and tiltmeter array.....	6
CHAPTER 3 Project Descriptions	9
3.1 Aquistore project	9
3.2 Tiltmeter array reservoir surveillance study	12
3.2.1 Design phase.....	12
3.2.2 Installation phase	12
3.2.3 Baseline phase	12
3.2.4 Monitoring phase.....	12
CHAPTER 4 Tiltmeter Array Design, Deployment and Operation	14
4.1 Tiltmeter array design.....	14
4.1.1 Array aerial distribution.....	14
4.1.2 Burial depth	16
4.2 Field instrumentation.....	17
4.2.1 Tiltmeter	17
4.2.2 Data acquisition system.....	19
4.2.3 Weather station.....	21
4.3 Installation procedures.....	21

4.4 Data collection and system performance	22
4.4.1 Data management	22
4.4.2 Baseline performance	23
CHAPTER 5 Baseline Tilt Pattern Characterization and Modelling.....	27
5.1 Overview	27
5.2 Earth tide signal.....	30
5.2.1 Introduction	30
5.2.2 Literature review	31
5.2.3 Statistical analysis	31
5.2.4 Modelling	32
5.2.5 Discussion	35
5.3 Barometric signal	36
5.3.1 Introduction	36
5.3.2 Statistical analysis	37
5.3.3 Modelling	37
5.3.4 Discussion	38
5.4 Rainfall signal.....	39
5.4.1 Introduction	39
5.4.2 Literature review	39
5.4.3 Statistical analysis	42
5.4.4 Discussion	44
5.5 Thermal signal.....	45
5.5.1 Introduction	45
5.5.2 Temperature dependent behavior of sensor.....	45
5.5.3 Thermoelastic tilt.....	49
5.5.4 Discussion	54
5.6 Seismic signal.....	54
5.6.1 Introduction	54

5.6.2 Observed seismic signals.....	54
5.6.3 Discussion	55
CHAPTER 6 Numerical Modelling of Episodic Rainfall Tilt Pattern.....	57
6.1 Framework of modelling.....	57
6.1.1 Infiltration modelling.....	58
6.1.2 Seepage modelling.....	60
6.1.3 Deformation modelling.....	63
6.2 Modelling description.....	65
6.2.1 Dimension and geometry.....	66
6.2.2 Infiltration modelling.....	68
6.2.3 Seepage modelling.....	71
6.2.4 Deformation modelling.....	75
6.3 Results	77
6.3.1 2D model	77
6.3.2 3D model	84
6.4 Discussion	91
CHAPTER 7 Conclusion and Recommendation.....	93
References	96
Appendix A Standard Working Procedure for Tiltmeter Station Installation.....	101
Appendix B Field Installation Logs.....	106
Appendix C Tiltmeter Temperature Compensation Test.....	108

List of Tables

Table 2-1: A summary of common technologies utilized in MMV (After Plasynski et. al [8]).....	4
Table 2-2: A comparison of three surface deformation monitoring technologies	5
Table 3-1: Distribution of surface deformation monitoring instruments in Aquistore	10
Table 4-1: Tech Specs for Pinnacle Series 5000 Tiltmeters.....	18
Table 5-1: Major sources of baseline ground motion.....	27
Table 5-2: Characteristics of captured noise signals in Aquistore.....	29
Table 5-3: Summary of tiltmeter response to earth tide compared to modelled results.....	35
Table 5-4: Tilting angle and regression coefficient determined for barometric pressure signal.....	38
Table 5-5: Back calculated Thermoelasticity parameters for site NW02	54
Table 5-6: Calculated seismic wave speed compared to theoretical seismic wave speed	56
Table 6-1: Soil VWC and SWCC used in seepage analysis	71
Table 6-2: Soil unsaturated permeability used in deformation analysis	72
Table 6-3: Soil properties adopted in deformation modelling	76
Table 7-1: Characterized noise signals in Aquistore	93
Table C-1: Data obtained from temperature compensation test	110
Table C-2: A sample calculation for temperature dependency coefficient.....	110

List of Figures

Figure 2-1: Schematic diagram of an electrolytic level sensor.....	6
Figure 2-2: Interpreting horizontal surface deformation from surface tiltmeter array.....	7
Figure 2-3: Interpreting vertical deformation from downhole tiltmeter array	7
Figure 3-1: Location Map showing the Williston Basin and the enlarged area with the CO ₂ source and Aquistore’s injection and observation wells (After Worth et. al [16]).....	9
Figure 3-2: Baseline vertical ground displacement obtained from InSAR data in Aquistore (after Francisco et. al [18]).....	11
Figure 3-3: An Aquistore ground station showing surface instruments from different surveillance systems	11
Figure 4-1: Preliminary simulation results of CO ₂ footprint after injection (Whittaker and Worth, [19]).....	15
Figure 4-2: Tiltmeter array distribution map	15
Figure 4-3: Coverage of tiltmeter array in Aquistore	16
Figure 4-4: Tiltmeter borehole design in Aquistore	17
Figure 4-5: Pinnacle series 5000 tiltmeter utilized in Aquistore	18
Figure 4-6: Tiltmeter station surface enclosure	19
Figure 4-7: an individual radio unit contained within a completed tiltmeter station.....	19
Figure 4-8: Master radio unit and antennas	20
Figure 4-9: Tiltmeter data transmission map.....	20
Figure 4-10: Dedicated weather station for surface tiltmeter array	21
Figure 4-11: Photo of a completed tiltmeter station alongside the central communication station and the dedicated weather station.....	22
Figure 4-12: TiltTalk interface used to manage tiltmeter array.....	23
Figure 4-13: Baseline tiltmeter data from site TL06 between November 2012 and November 2013	23
Figure 4-14: Baseline tiltmeter data from site NW01 between November 2012 and November 2013	24
Figure 4-15: Two level sensors and a re-leveling motor contained inside a tiltmeter housing.....	24

Figure 4-16: Tiltmeter temperature sensor reading in the first six months.....	25
Figure 4-17: Initial compass reading from two tiltmeters	26
Figure 4-18: Combined vector map with existing tiltmeters in Aquistore in 2015	26
Figure 5-1: Baseline Tiltmeter reading showing short, intermediate and long term fluctuations...	28
Figure 5-2: General mechanism of noise signals and methodology in removing their effects	29
Figure 5-3: Earth heave and depression under solid earth tide	30
Figure 5-4: Tilt time series from tiltmeter station TL06 during 2013	32
Figure 5-5: Power spectrum of N-S tilt reading from tiltmeter station TL06.....	32
Figure 5-6: Power spectrum of E-W tilt reading from tiltmeter station TL06.....	32
Figure 5-7: Tidal amplitude calculated for Aquistore using program SOLID.....	33
Figure 5-8: Calculated East-West tidal tilt in Aquistore.....	33
Figure 5-9: Calculated East-West tidal tilt in Aquistore.....	33
Figure 5-10: Observed tilt signal from TL06 station and theoretical earth tide tilt	34
Figure 5-11: Cross-correlation plot for both directions of tiltmeter data.....	34
Figure 5-12: Tiltmeter data before (Red) and after (Blue) removing earth tide signals	36
Figure 5-13: Cross-correlation analysis between tilt and barometric pressure	37
Figure 5-14: Subtracting barometric signals from baseline tiltmeter data.....	38
Figure 5-15: Baseline tilt pattern during a period of heavy rainfalls.....	42
Figure 5-16: Daily variation tilt data from two tiltmeter in Aquistore and daily precipitation data	43
Figure 5-17: Cross-correlation function between daily tilt data and daily precipitation	44
Figure 5-18: Tilt readings from laboratory zero-vibration temperature test.....	46
Figure 5-19: Shift in scale factor after a shift in environmental temperature.....	47
Figure 5-20: Thermal compensation test setup.....	47
Figure 5-21: Tiltmeter 6536 showing a linear dependency between scale factor and temperature	48
Figure 5-22: Tiltmeter 6490 showing a non-linear dependency between scale factor and temperature.....	48
Figure 5-23: Tiltmeter 6751 showing a negative correlation between calibration factor and temperature.....	48

Figure 5-24: Downhole temperature record in 2013	51
Figure 5-25: Downhole temperature and tilt reading after installation from TL06	53
Figure 5-26: Downhole temperature and tilt reading after installation from NW01	53
Figure 5-27: Tiltmeter data showing the impact from repositioning of the tool.....	53
Figure 5-28: Tilt signals reflecting by seismic activities.....	55
Figure 5-29: Illustrative figures showing magnitude distance of earthquake, and corresponding movement of tiltmeter TL06	55
Figure 6-1: Framework of rainfall-tilt model	57
Figure 6-2: Flowchart of simulation components in the rainfall-tilt model.....	58
Figure 6-3: 2D model geometry	66
Figure 6-4: Planar view of modelling areas of 3D model.....	67
Figure 6-5: 2D surface geometry of Model A	67
Figure 6-6: 2D surface geometry of Model B	68
Figure 6-7: Daily and cumulative precipitation data used for modelling	69
Figure 6-8: Daily air temperature data used for modelling.....	70
Figure 6-9: Daily wind speed data used for modelling.....	70
Figure 6-10: Daily relative humidity data used for modelling	70
Figure 6-11: Saturated permeability 0.89 m/day (Left) and 0.089 m/day (Right).....	72
Figure 6-12: Surface boundaries with differential horizontal infiltration applied in 2D simulation	74
Figure 6-13: Schematic graph showing 3D spatial variation in induced groundwater table change after rainfallOutput.....	74
Figure 6-14: Grid distribution in 2D model.....	74
Figure 6-15: Grid distribution in 3D model.....	75
Figure 6-16: General boundary conditions adopted in deformation modelling.....	76
Figure 6-17: Full net boundary flux obtained from infiltration modelling in 2D setup.....	78
Figure 6-18: Head profile at the end of 2D seepage simulation	78
Figure 6-19: Horizontal head profile at -30m at the end of 2D seepage simulation.....	79
Figure 6-20: Displacement profile at the end of deformation analysis.....	79

Figure 6-21: A zoomed view showing displacement vectors at the center of the model.....	80
Figure 6-22: Tilt pattern from five locations from the 2D model.....	81
Figure 6-23: Modelled and observed tilt pattern for SW-NE sensor, NW01.....	81
Figure 6-24: Modelled and observed tilt pattern for NW-SE sensor, NW01.....	82
Figure 6-25: Modelled and observed tilt pattern for E-W sensor, TL06	82
Figure 6-26: Modelled and observed tilt pattern for N-S sensor, TL06	82
Figure 6-27: Scatterplot between porewater gradient and horizontal displacement.....	83
Figure 6-28: Tilt and displacement at (100m, -30m).....	84
Figure 6-29: Boundary flux over time for both models.....	85
Figure 6-30: End of simulation porewater head contour at -30m depth for Model A	85
Figure 6-31: End of simulation porewater head profile for model A	86
Figure 6-32: End of simulation porewater head contour at -30m depth for Model B.....	86
Figure 6-33: End of simulation porewater head profile for model B.....	87
Figure 6-34: Porewater pressure head at SW-NE direction.....	87
Figure 6-35: Porewater pressure head at NW-SE direction.....	87
Figure 6-36: Porewater pressure head at W-E direction.....	88
Figure 6-37: Porewater pressure head at N-S direction.....	88
Figure 6-38: Porewater pressure gradient.....	88
Figure 6-39: End of simulation displacement (-30m) vector map from Model A	89
Figure 6-40: End of simulation displacement (-30m) profile from Model A	89
Figure 6-41: Modelled tilt pattern compared with filtered original data	90
Figure 7-1: Systematic approach in reducing tiltmeter noise signals	95
Figure A-1: Solar panel and radio box setup on steel pole.....	102
Figure A-2: setup inside radio box	103
Figure A-3: Cable wiring and connection	103
Figure A-4: Setup tab of TiltTalk shows all tiltmeters information	104
Figure A-5: “Expand” tool array table shows all active tiltmeter information, “Refresh All” to detect new tiltmeters.....	104

Figure A-6: Control tab of TiltTalk shows command window for each tiltmeter, including acquire status, changing settings and download data	104
Figure A-7: Finished tiltmeter station	105
Figure C-1: Rotation arm and testing frame	108
Figure C-2: Temperature control device and environmental chamber	109
Figure C-3: Measuring gauges and LVDT	109
Figure C-4: Temperature dependency coefficient at -1°C	111
Figure C-5: Calibration factor with temperature	111

CHAPTER 1 Introduction

1.1 Statement of problem

The Aquistore project broke ground in southeast Saskatchewan, Canada in 2012. As Canada's first deep saline formation carbon dioxide (CO₂) storage project, it intends to demonstrate that storing liquid CO₂ underground is a safe, workable solution to reduce greenhouse gas emission to the atmosphere. Aquistore project has a comprehensive measuring, monitoring and verification (MMV) program that provides critical information to ensure the safe, effective and environmentally acceptable implementation of CO₂ storage. Surface tiltmeter array is a monitoring component applied within the MMV program that assesses near surface displacements during the injection of CO₂. The adoption of tiltmeter array in Aquistore aims at capturing sufficient surveillance information to evaluate the feasibility of long-term utilization of this technology.

A tiltmeter is a very sensitive instrument that can resolve tilt as little as one billionth of a radian. Tiltmeter array is ideal for monitoring the expected millimeter-scale surface deformation in Aquistore. However, one disadvantage of tiltmeter also amplifies in this application, the high noise-signal ratio. The surface of the earth naturally moves miniscule amounts every day due to environmental disturbance, human activities, etc. Tiltmeters will pick up noise signals from these environmental and cultural effects and deliver the composite pattern as surveillance results. Noise signals may obscure or even alter the signals from injection and therefore reduce the accuracy and reliability of the monitoring outcome. Noise signals can be managed and quantified. The scale of noise signal can be reduced through adequate design and installation precautions, as well as post-deployment data analysis and processing. In the design and installation phase, a sufficiently distributed and tight-insulated tiltmeter array can greatly increase effectiveness. During monitoring phase, characterization and quantification of noise signals can reduce the uncertainty.

1.2 Research objective

The utilization of tiltmeter array in monitoring geologic CO₂ storage is still a fresh practice for this technology. The performance of tiltmeter array is highly associated to the working environment. The study on Aquistore tiltmeter array reservoir surveillance project has two main focuses. One focus is to construct an effective and efficient tiltmeter array through good design and installation. The other focus is to acquire an understanding of noise signals through baseline study.

The objective of this research program is to provide a comprehensive understanding of tiltmeter array performance for monitoring CO₂ storage under the existing installation scenario in Aquistore and to capture sufficient surveillance information to assess the feasibility of utilizing this technology in the long term at commercial scale.

1.3 Scope and methodology

The present research describes the design phase, installation phase and baseline phase of the tiltmeter array project. This thesis will present the design thoughts for the array, techniques applied during the installation, and methodology in analyzing baseline data to reduce noise-signal ratio for the monitoring phase. The scope of this research does not include the evaluation of general tiltmeter technology, which has been applied to a variety of engineering fields and served broad purposes. This research targets the adoption of tiltmeter array in CO₂ reservoir surveillance level. As a wide range of tiltmeter configurations and array designs exist, methodology and conclusions from this research may not necessarily transfer to another tiltmeter array project.

The research objective will be achieved by understanding the role of tiltmeter array in monitoring geologic CO₂ storage, characterizing site conditions, applying the technology in an effective, efficient and economic approach, analyzing baseline data and proposing modelling methods of several noise signal. The following research tasks will be undertaken:

1. Provide an overview of tiltmeter array technology and its role in monitoring geologic CO₂ storage;
2. Design and deploy STA for the optimized performance;
3. Interpret baseline reading for noise factors that obstruct performance;
4. Propose methodologies to quantify and remove noise patterns from monitoring data.

1.4 Organization of thesis

Chapter 2 presents an overview of carbon capture and storage technology and components of MMV program. An introduction is given to tiltmeter array technology and its adoption in the reservoir surveillance field.

Chapter 3 introduces the Aquistore project, the integrated surface surveillance system, and details of the surface tiltmeter array program.

Chapter 4 presents the design guidelines and installation details of tiltmeter array. A description of all instruments, supplemental equipment is presented. The general operation performance is also summarized in this chapter.

Chapter 5 introduces noise signals that are present in baseline tiltmeter readings. This chapter is focused on characterizing noise signals and modelling individual tilt patterns, including those of earth tide, barometric pressure, precipitation, thermal and seismic origins.

Chapter 6 evaluates and quantifies in details the noise effect of rainfalls through numerical modelling.

Chapter 7 presents the conclusions from this research and recommendations for future work.

CHAPTER 2 Overview of Monitoring Geologic CO₂ Storage

The tiltmeter array is one of surface deformation monitoring technologies applied in Aquistore geologic CO₂ storage project. As part of the measurement, monitoring and verification program, it provides near surface displacement during the injection of CO₂. A brief introduction is given to the carbon capture and storage (CCS) projects and MMV technologies in general, followed by a detailed review of utilization of tiltmeter array in monitoring surface displacement. This review will outline the role of tiltmeter array in a structured MMV program. It will rationalize the expected functionality and accuracy of tiltmeter array adopted in a CCS project.

2.1 Carbon capture and storage

Carbon capture and storage is the process designed to capture CO₂ from large source of emission, transport through pipeline and store permanently in secure geologic formations. CCS is a promising component of international strategies to reduce greenhouse gas emissions. A complete CCS project involves three stages: capture, transport and storage. CO₂ capture usually takes place in large CO₂ emission sources such as coal power plants, oil and gas operations (including oil sands in Canada). The most commonly used capture method separates CO₂ gas from combustion exhausts using chemical solvent [1]. In the transport stage, CO₂ gas is dehydrated and pressurized to a “dense phase” that allows it to flow in pipelines like liquid to the storage site. Small amount of CO₂ can also be transported using tankers by road or rail [2]. The final stage is storage or sequestration, where CO₂ is injected to underground geologic formations, as known as geologic CO₂ storage.

Geologic CO₂ storage is the process of injecting CO₂ underground before permanent sealing the site after capacity is reached. The storage site should exhibit the geologic conditions that ensure CO₂ can be retained for a long period of time. Deep saline formations, although not well characterized, are much more extensive and have enormous storage potential [3].

CCS is a viable option to reduce greenhouse gas emission. CCS projects have been operating successfully across the world since the mid-1990s. As of January 2013, there are 8 commercial scale CCS projects in operation in the world and more than 60 projects in development [4]. Because of the high cost and few regulation incentives, CCS projects are often tied with value-added components such as enhanced oil recovery (EOR). The world’s first commercial-scale CCS project was initiated in Sleipner, Norway in 1996. Up to 2006, more than seven million tons of CO₂ had been captured and injected to a deep saline formation under the North Sea [5]. In Canada, CCS will be the single largest greenhouse gas reduction sector by 2050 according to government greenhouse gas reduction target [6]. Canada has the world’s largest monitored geological CO₂ storage project, the IEAGHG Weyburn-Midale CO₂ storage project in Saskatchewan, which captured 2.7 million tons of CO₂ a year since 2000 [7].

2.2 Measuring, monitoring and verification

Measurement, monitoring and verification, or MMV in short, is the process where an operator of a CCS storage site measures the amount of CO₂ sequestered, monitors the site to ensure storage integrity and verifies that the stored CO₂ is acting as predicted without adverse effects to the surrounding environment. MMV is related to process and efficiency measurement as well as regulatory monitoring and reporting under various environmental legislations; therefore it is a critical part of CCS project that ensures its safe, effective and environmentally acceptable implementation.

Table 2-1: A summary of common technologies utilized in MMV (After Plasynski et. al [8])

Category	Method
Remote Sensing	LIDAR
	INSAR
	Hyperspectral Imaging
	GPS
Atmospheric Monitoring	Eddy Covariance
Methods for Monitoring Processes at Surface and Near Surface	Soil Gas Sampling
	Surface Flux Emissions
	Vehicle Mounted CO ₂ Leak Detection System
	CO ₂ Wellhead Monitoring
	Borehole Tiltmeters
	Ecosystem Studies
	Groundwater sampling
	Piezometers
Method for Monitoring Subsurface Phenomena	InSitu P/T Monitoring
	Fluid Sampling
	Crosswell Seismic
	Wireline Tools
	Downhole Microseismic
	3D Time Lapsed Seismic
	2D Time Lapsed Seismic
	Vertical Seismic Profiling
	Crosswell Resistivity
	Long Electrode Electrical Resistivity Tomography
	Permanent Seismic Sources/Receivers

MMV involves a board range of technologies and covers the entire production cycle of a geological CO₂ storage project, including site selection and characterization, site preparation and construction, site operation, project closure and post-closure surveillance. Spatially, MMV technologies can be classified according to monitoring zones (i.e. atmosphere, near surface and deep surface). Table 2-1 is a list of common monitoring techniques. These technologies serve various purposes from

monitoring physical properties and behavior of the CO₂ plume to detecting and quantifying leakage. New technologies are evaluated along with new CCS projects. An efficient suite of MMV tools will be the key to successful implementation of CCS on a commercial scale and will have a significant impact on the development of legal and regulatory protocols covering the geologic storage of CO₂ [8].

2.3 Surface deformation monitoring

Surface deformation monitoring (SDM) is an essential part of MMV program in geological CO₂ storage. At the reservoir level, CO₂ injection and storage bring pore-pressure change and fluid movement that create perturbation in stress and strain field. SDM technologies can detect surface displacement that radiates from the reservoir. In some cases, geomechanical inversion processes can be used to derive reservoir-level volumetric and strain changes from surface deformation. SDM can provide accurate and continuous observation that can be turned into actionable information. By monitoring ground deformation, the movement of CO₂ plume can be inferred. Surface deformation is also a quick indication of potential sequestration hazards.

Most common technologies applied in SDM include InSAR, DGPS and tiltmeter array, which have been used extensively for decades in EOR projects and have recently been successfully deployed in commercial scale CCS projects. Table 2-2 compares the strength and weakness of the three monitoring technologies.

Table 2-2: A comparison of three surface deformation monitoring technologies

Technology	Sensitivity	Advantage	Disadvantage
InSAR	~10 ⁻² m	<ul style="list-style-type: none"> • Broad coverage • Cost effective 	<ul style="list-style-type: none"> • Low resolution, • Long sampling interval • Signal decorrelation (due to vegetation, rainfall)
GPS	~10 ⁻³ m	<ul style="list-style-type: none"> • High resolution • Good reliability • Continuous data acquisition 	<ul style="list-style-type: none"> • High hardware cost
Tiltmeter Array	~10 ⁻⁶ m	<ul style="list-style-type: none"> • High sensitivity • Continuous data acquisition • Near real-time reporting 	<ul style="list-style-type: none"> • Sensitive to background noise • Mapping resolution depends on density of array

Interferometric synthetic aperture radar (InSAR) is a radar technique used in geodesy and remote sensing. It combines two or more synthetic aperture radar (SAR) scenes taken by satellite or aircraft and uses the differences in the phase of waves present in those images to generate surface deformation or digital elevation maps. InSAR is a highly cost-effective technology that can monitor a large area with monthly intervals. Disadvantage with InSAR includes limited resolution (in centimeter range for a single interferogram) and that surface vegetation may impact results.

Differential global positioning system (DGPS) technique uses a network of fixed, ground based reference stations to broadcast the difference between the positions by GPS and use the difference to create surface deformation map. Because of high hardware cost, DGPS is used to supplement tiltmeter array and InSAR technologies by providing a long-term stable point of reference [9]. Tiltmeter array is a highly precise tool to detect ground movement. The above technologies are often integrated in SDM for the best monitoring results.

2.4 Tiltmeter and tiltmeter array

Tiltmeters, also known as inclinometers, are used to monitor the change in inclination (rotation) of two points in ground surface or structure. A tiltmeter consists of a gravity-sensing transducer within an appropriate housing and that can be installed either on or below ground surface or within a structure. Earlier tiltmeters used mechanical transducers such as pendulum to reflect and measure tilt with a precision of $10^{-4} \sim 10^{-5}$ R. With the invention of electrolytic level transducers, the precision has been greatly improved. Electrolytic tiltmeters operate on the same principle as a carpenter's level. Each tiltmeter houses two orthogonal sensors with a precise curvature. Electrodes detect angle movements of the gas bubble above a conductive fluid as the fluid seeks the lowest spot in the sensor (illustrated in Figure 2-1). Modern tiltmeters can resolve tilt changes as little as one billionth of a radian (10^{-9} R). With the advancement in sensor and housing materials, modern tiltmeters are less sensitive to temperature and comes with a field ready package. Customized electronics built inside tiltmeters can measure and digitalize the information from the sensors and store data in an internal memory. Built-in compass and re-leveling motor greatly reduce complication during field installation. With the above advancements, the applicable areas of tiltmeters have been greatly expanded. Tiltmeter is used extensively in the study of volcano eruption prediction as the induced tilt pattern indicates the movement of magma chamber (e.g. [10]). With the improvement in precision, tiltmeters begin to be adopted in engineering field. Tiltmeters have been used to monitor the filling response of dams by installing in the bank shell or dyke (e.g. [11]). Similarly it has been installed under slopes to monitor creep and predict landslides (e.g. [12]).

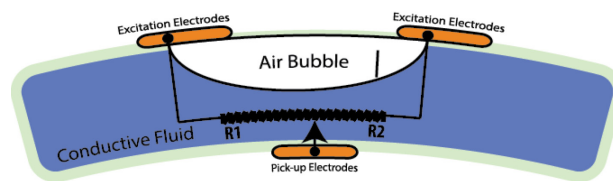


Figure 2-1: Schematic diagram of an electrolytic level sensor

Combing multiple tiltmeters into an array can further expand their functionality. From a network of tilt vectors, displacement can be interpreted. Surface tiltmeter array has a horizontal network of tiltmeters and can be used to deduce surface deformation as shown in Figure 2-2. Vertically

distributed downhole tiltmeter array can be very useful in measuring displacement radiates from a single source of stress field as shown in Figure 2-3. The resolution of the mapped deformation is determined by the density of tiltmeters. Tiltmeter deployed in borehole can minimize the disturbance from surface and therefore has higher accuracy while the accuracy of measurement is closely related to the installed depth.

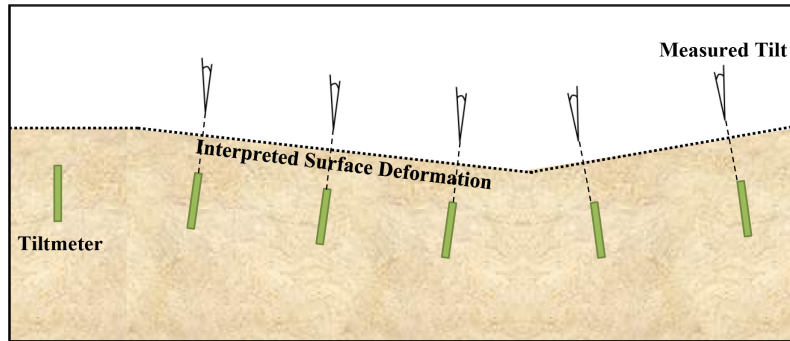


Figure 2-2: Interpreting horizontal surface deformation from surface tiltmeter array

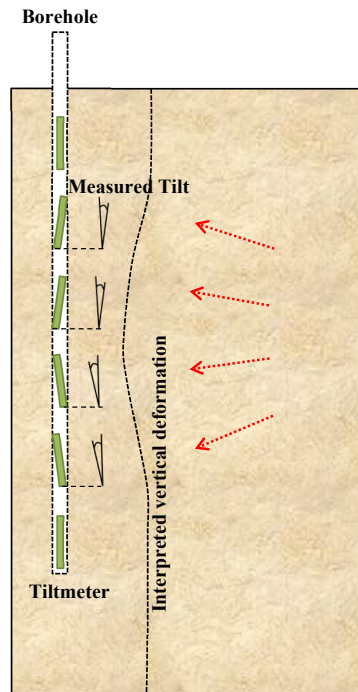


Figure 2-3: Interpreting vertical deformation from downhole tiltmeter array

Fracture mapping is an area that has seen extensive adoption of tiltmeter array. The principle of tiltmeter fracture mapping is to infer hydraulic fracture geometry by measuring the fracture induced rock deformation using tilt (e.g. [13]). The induced deformation field radiates in all directions and can be measured either downhole with wireline-conveyed tiltmeter arrays or with a surface array of

tiltmeters. Tiltmeter fracture mapping is currently utilized on more than 2000 fracture treatments per year to measure fracture orientation, volume, complexity and approximate location [14]. Application of tiltmeter array in monitoring geologic CO₂ storage is similar to that of fracture mapping. Tiltmeter array is deployed above injection zone. Tilt readings are taken every few minutes and collated by a data acquisition computer to produce near real-time surface deformation during the injection. In addition, time-lapse deformation videos are published every hour for review. Tiltmeter array has greatly helped the monitoring and verification process during the movement of CO₂ plume. The nanometer sensitivity of tiltmeter allows displacement measurements on the order of one billionth of a millimeter. Data from tiltmeter array can be used to calculate tiny reservoir-level stress and strain changes. Tiltmeter array allows for near real-time mapping of CO₂ plume movement. As shallower strain can create larger surface deformation, Tilt readings can be used to quickly detect out-of-zone fluid migration and cap rock integrity issues, which are the main focus of MMV programs [9].

The limitation of tiltmeter technology is mostly related to the influence of external noise. Tiltmeter sensor is sensitive to environmental and cultural activities. To minimize this error tiltmeter is usually deployed in an insulated downhole environment. Also the density of tiltmeters in the array determines the spatial resolution of deformation mapping. To provide reliable monitoring results, the distribution of tiltmeters has to be systematically designed before implementation.

CHAPTER 3 Project Descriptions

Saskatchewan is leading the world in CCS demonstration projects. The Weyburn-Midale Carbon Capture and Storage Project (2000-2011) [15] studied CO₂ storage in two depleted oilfields in southeastern Saskatchewan. Starting in 2011, Aquistore Project has dedicated to demonstrate the safety and workability of permanently CO₂ storage in deep saline formations. This chapter will provide the details of Aquistore Project, including the supplementary surface deformation monitoring component. In particular, this chapter outlines the tiltmeter array reservoir surveillance study conducted in Aquistore.

3.1 Aquistore project

Aquistore project is a fully integrated demonstration of CO₂ sequestration, transportation and storage within a deep, brine-bearing geological formation. It will launch with 550 tonnes CO₂ per day captured from SaskPower's Boundary Dam Power Station in the northeast of Saskatchewan, compressed on site and transported approximately 2.8 km by pipeline before injected into a deep, highly saline clastic formation (location as shown in Figure 3-1). Aquistore geologic CO₂ storage site sits on Williston Basin, a sedimentary basin spans from southwestern Manitoba to southern Saskatchewan. With the two deepest wells in the province of Saskatchewan, Aquistore will be injecting 3.4 km deep into the Winnipeg and Deadwood formations [16]. In overall, the targeted formations can be viewed as major geologic packages forming an alternating sequence of aquifers and aquitards and have been proved to exhibits excellent injectivity and storage capacity potential.

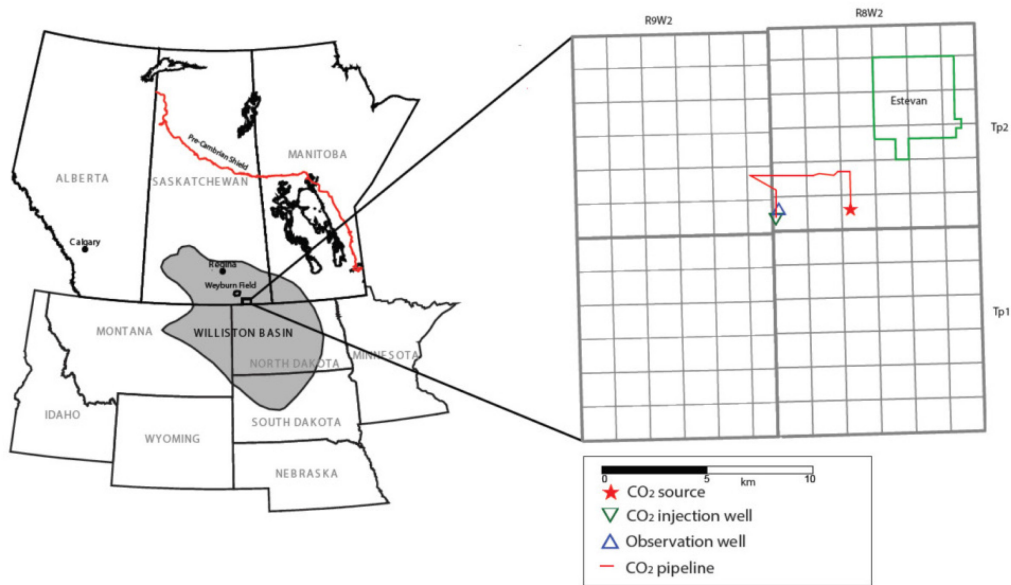


Figure 3-1: Location Map showing the Williston Basin and the enlarged area with the CO₂ source and Aquistore's injection and observation wells (After Worth et. al [16])

Aquistore Project includes a comprehensive MMV program consisting of surface, shallow subsurface, and deep subsurface monitoring components. Surface monitoring technologies target groundwater, air and ground surface and provide leak detection, risk control and public assurance. Downhole and casing-conveyed monitoring technologies take account of downhole pressure, downhole temperature, formation fluids and seismic activities. These technologies ensure safety and integrity during injection and contribute to the understanding of CO₂ movement in the reservoir. The MMV program in Aquistore aims at minimizing the leakage associated risks through early detection and providing conformance of the storage process through continuous monitoring. The program has an added focus on integration of monitoring methods to boost efficiency and accuracy for long-term CO₂ reservoir monitoring. Aquistore will provide an efficient, cost effective, and field-tested basis for designing effective MMV programs for other similar projects worldwide [16].

Aquistore has a suite of technologies installed across the storage area to monitor ground deformation. Injection-related surface deformation monitoring is provided by tiltmeter array, InSAR and GPS technologies. In an effort to minimize the impact of surface and landscape, the project co-located these monitoring stations together into 18 sites across Aquistore, as listed in Table 3-1.

Table 3-1: Distribution of surface deformation monitoring instruments in Aquistore

Site Name	Tiltmeter depth (m)	GPS Depth (m)	InSAR Depth (m)
SITE		30	4.5
NE01		30	4.5
NE02	30	30	
NE03	30	30	
NE04	30	30	
NW01	30	24	4.5
NW02	20~30	20~30	
NW03	20~30	20~30	4.5
SE01	30	30	4.5
SE02		30	
SE03	30	30	
SW01	30	30	4.5
SW02	30	30	
TL05	30		
TL06	30		
TL08	30		
TL11	30		
TL15	30		

InSAR technologies deployed in Aquistore has the potential to determine surface changes related reservoir-level fluid distribution and pressure changes. Used during ascending and descending imaging, corner reflectors are installed at each location to mitigate temporal de-correlation and the impact of snow cover in winter months. A total of 13 paired corner reflectors will be deployed in Aquistore that covers a surface area of 6.5 km². Since the commencement of the project in early 2012, SAR images had been collected to provide baseline information over Aquistore site (as shown

in Figure 3-2). Over the project life, the addition of more sources of SAR images should allow ground deformation measurement with a precision of a few mm/year [17].

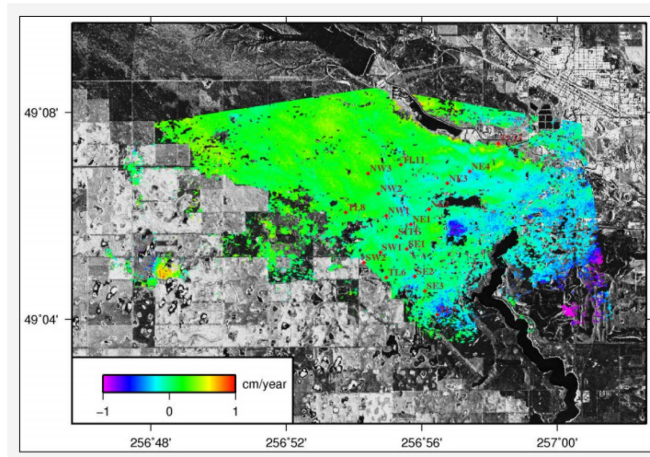


Figure 3-2: Baseline vertical ground displacement obtained from InSAR data in Aquistore (after Francisco et. al [18])

In conjunction of InSAR, 8 dedicated GPS stations have been installed in Aquistore. Each station includes a continuous-operating geodetic-grade GPS receivers and antennas, which are mounted on a steel well casing anchored to a depth of 30 m. GPS data will be transmitted on a daily basis to servers for processing and analysis [18]. GPS technology is also used as a reliable reference for tiltmeter array and InSAR. It provides a stationary reference location for the other two surveillance systems.

All three monitoring instruments are collocated to the same stations and are solar powered during operation. Figure 3-3 shows a completed surface deformation surveillance station.

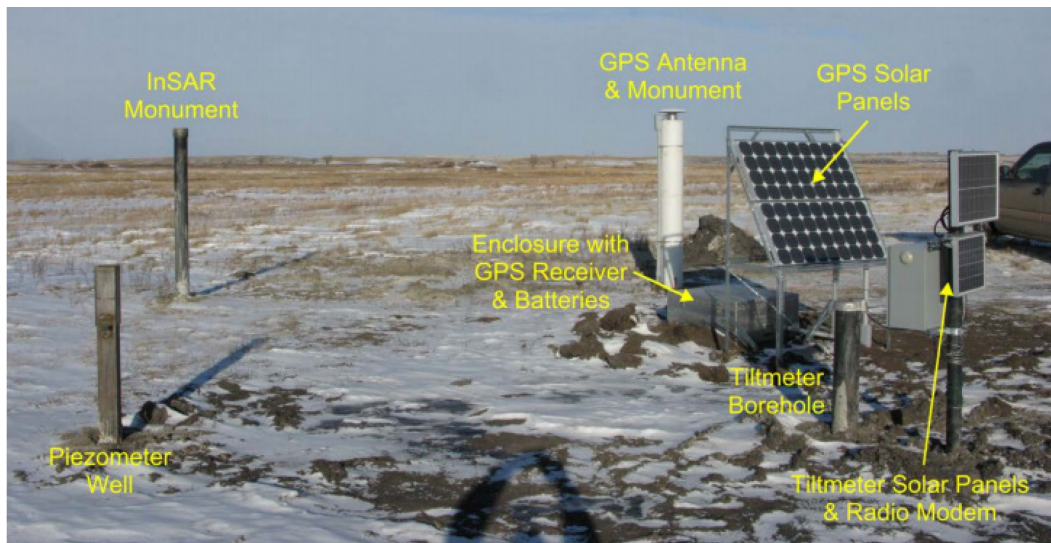


Figure 3-3: An Aquistore ground station showing surface instruments from different surveillance systems

3.2 Tiltmeter array reservoir surveillance study

Tiltmeter array reservoir surveillance study is part of the monitoring program in Aquistore that utilizes surface tiltmeter array to assess near surface displacements during the injection of CO₂. The scope for this study is to provide a sufficient tiltmeter monitoring program for the initial CO₂ injection plan for Aquistore to measure ground displacements and to capture sufficient surveillance information to assess the feasibility of utilizing this technology for the long term at commercial scale. Initially, an array of 15 surface tiltmeters combined with supplementary environmental monitoring (precipitation, wind velocity, temperature, etc.) will be deployed. This will be accomplished through design, installation, baseline, and monitoring phases. Below is a brief description for each phase of the study. The scope of this thesis covers the design, installation and baseline phases, as they will be expanded in details in the following chapters.

3.2.1 Design phase

Design of a suitable long-term monitoring tiltmeter array involves forward modeling using models ranging from simple analytical approximations to a full non-homogeneous three-dimensional finite element/difference model. The prediction of CO₂ plume movement determines the optimal tiltmeter locations above the injection site. The design of the surveillance program also includes adding supplementary monitoring plans and conducting specialized environmental calibrations on individual tiltmeters to minimize potential environmental and cultural noise impacts during the monitoring phase.

3.2.2 Installation phase

The University of Alberta team coordinates the schedule of all field activities during the installation phase. Tiltmeters are deployed in insulated boreholes of 30 m depth. The drilling of the holes is subcontracted to local company under the supervision of the University of Alberta. The installation also includes adding communication components to the tiltmeter array and deploying the dedicated weather station for environmental monitoring purpose.

3.2.3 Baseline phase

Before the injection of CO₂ starts, baseline tiltmeter data are collected on a regular basis. The initial data are analyzed to understand the natural signature lease. Furthermore, mathematical or numerical models are proposed to quantify any noise pattern should it affect interpretation during the monitoring phase.

3.2.4 Monitoring phase

After the injection of CO₂ starts, monitoring data from tiltmeter array will be downloaded and analyzed frequently. The result of this data acquisition services, quality assurance, quality control,

and analysis of collected data will provide surface deformation results to Aquistore project to work in combination of InSAR and GPS for interpretation.

CHAPTER 4 Tiltmeter Array Design, Deployment and Operation

Designing and deploying tiltmeter array is a critical step that sets the foundation of the reservoir surveillance system. An effective tiltmeter array structure will cover the disturbed surface area over the CO₂ reservoir with adequate resolution while maintaining a low noise-signal level during operation. This chapter introduces the design and deployment phases of tiltmeter array in Aquistore. The emphasis on both phases is to maximize the operational performance within the scope of Aquistore project.

4.1 Tiltmeter array design

The core elements in tiltmeter array design include aerial distribution of the array and burial depth of individual tiltmeter. For the surveillance program to be effective, the tiltmeter array must be reasonably distributed so that both desired spatial resolution is reached and the specification of the CO₂ reservoir are covered. This requires proper instrument spacing and aerial extent. Deeper burial depth of tiltmeter greatly mitigates its vulnerability to surface noise, while also greatly increases the hardware cost.

4.1.1 Array aerial distribution

Spatial distribution of tiltmeter array should accommodate the specification of the potential disturbed area. The movement of injected CO₂ is estimated from simple analytical approximations and simulated with a full non-homogeneous three-dimensional finite element/difference model in Aquistore. Results indicate the plume diameter to be approximately 1 km after 5 years of injection and approximately 3 km after 25 years at the end of injection (Figure 4-1). The plume will also elongates towards the northeast consistent with the regional dip [19]. Based on the estimated plume specification and number of stations available, spatial distribution and coverage of the array is designed as shown in Figure 4-2 and Figure 4-3 with 15 tiltmeter sites in total. 10 tiltmeter sites are aligned in two axes centred at the injection site, covering an area of approximately 5 km by 5 km. There are two more sites planned in the northeast direction in order to cover the possible elongation of the plume. Three sites are planned in between the axes to help refine the mapping results.

Instrument spacing determines the spatial resolution of deformation mapping from tiltmeter array. Higher density of tiltmeters increases resolution, but also increases the cost of the system. Optimum spacing is typically 1/3 depth of the layer requiring monitoring [20]. As CO₂ is injected at 2200 m depth in Aquistore, the designed spacing of about 0.7-1 km between the nearest boreholes is adequate for effective monitoring of reservoir level displacement radiance.

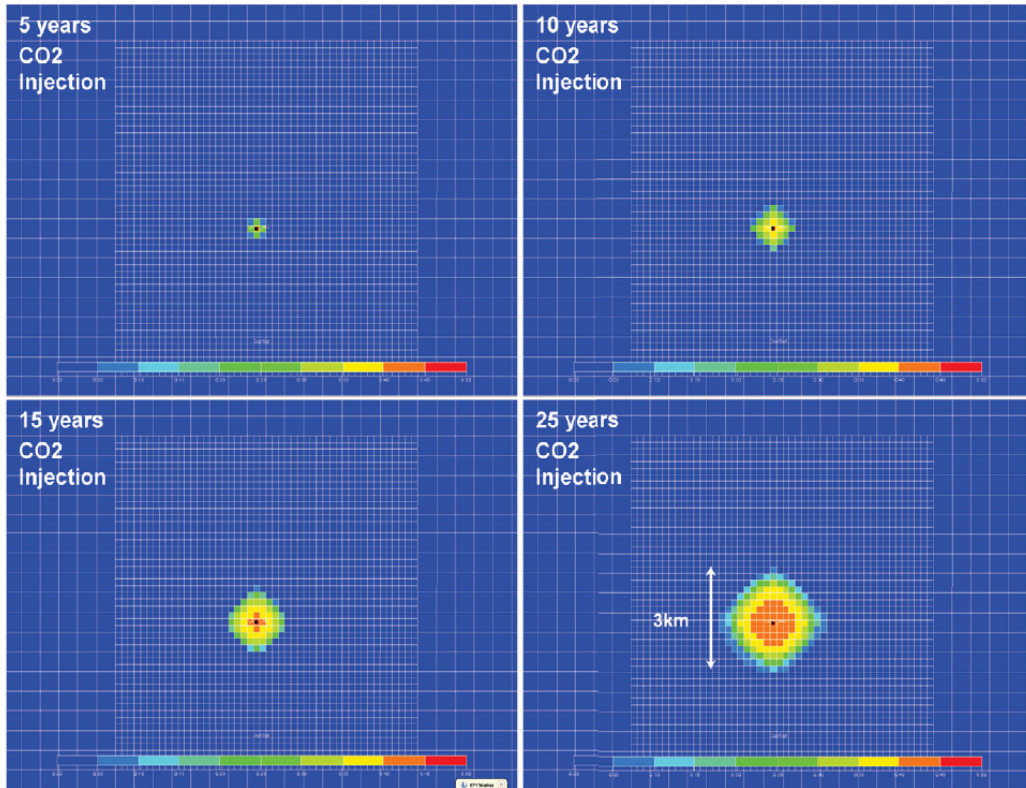


Figure 4-1: Preliminary simulation results of CO₂ footprint after injection (Whittaker and Worth, [19])

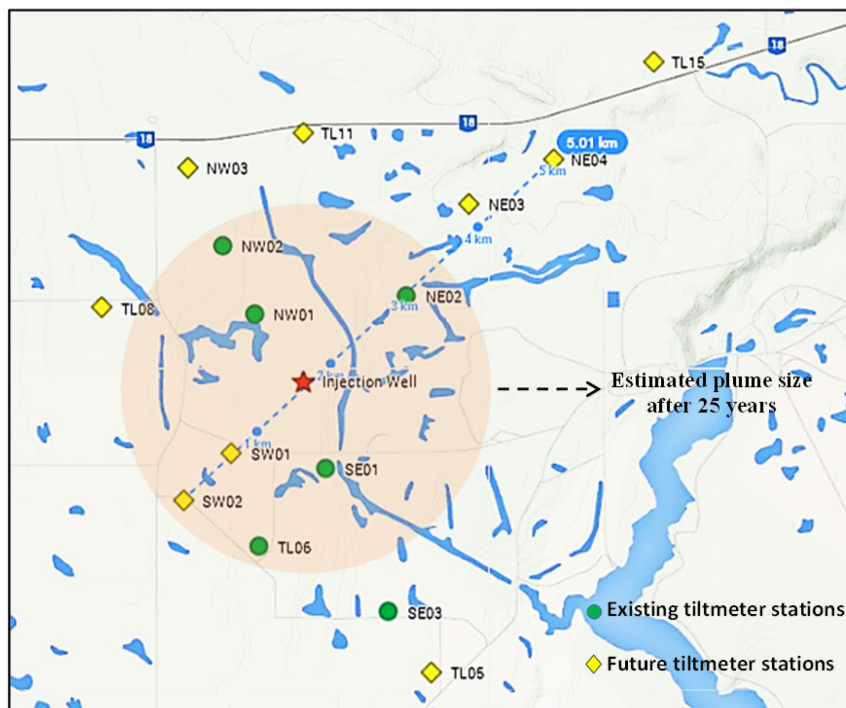


Figure 4-2: Tiltmeter array distribution map

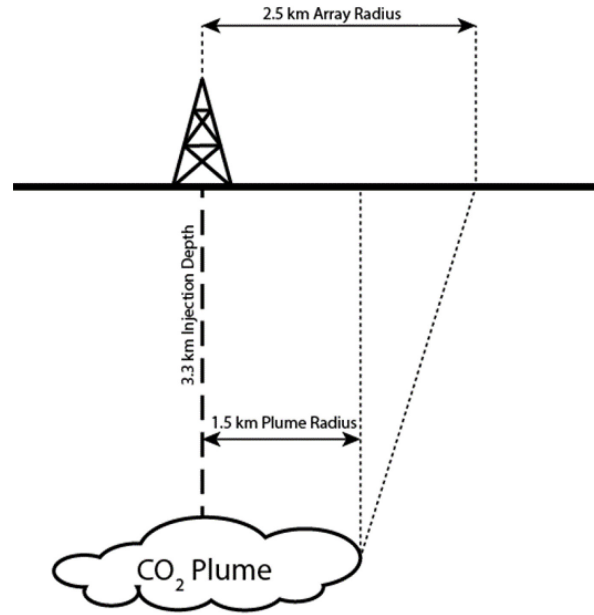


Figure 4-3: Coverage of tiltmeter array in Aquistore

4.1.2 Burial depth

Installing tiltmeter in boreholes can minimize environmental and cultural noise from surface. Greater burial depth can exponentially decrease the scale of most noise signal, but also requires more expensive construction cost. Under this balance, conventional tiltmeter installation usually has a burial depth of 3-10 m for most applications.

In Aquistore, tiltmeters are installed in 30 m boreholes, which is a deep burial design compared to conventional practice. This design is based on minimizing surface noise and consideration of site condition, as the Aquistore site is located on reclaimed land which underwent long-period of surface mining. The mining operations stopped in 1956 and the site was reclaimed back to a natural landscape [21]. Burying tiltmeter at 30 m depth not only reduce noise effects from surface substantially, but also avoids the uncertainty from the surface reclamation.

The design of the borehole casing system is shown in Figure 4-4. The borehole casing system used in Aquistore consists of an outer steel casing (OD: 12.85 cm) and an inner PVC casing (ID: 7.62 cm). The steel casing is installed to isolate the PVC casing (which contains the tiltmeter) from surface noise and to allow dry storage of tiltmeter cables. After drilling, grout is pumped into the bottom of the borehole. Steel casing is sealed with a bottom cap and dropped into the grout. The steel casing should be firmly grouted outside with native soil at bottom and backfilled near surface. After grout outside the steel casing is dry, it is pumped inside the steel casing. PVC pipes are assembled with couplings at joints and attached with a sealed cap at bottom. Plastic hoses are tied to joints to keep the PVC casing completely vertical. The PVC casing is dropped into the grout

inside the steel casing until it is firmly sitting on the bottom. More grout is pumped until it reaches the last PVC joint. The casing installation process is documented including any problems occurred during the process, which will help determine the quality of tiltmeter data.

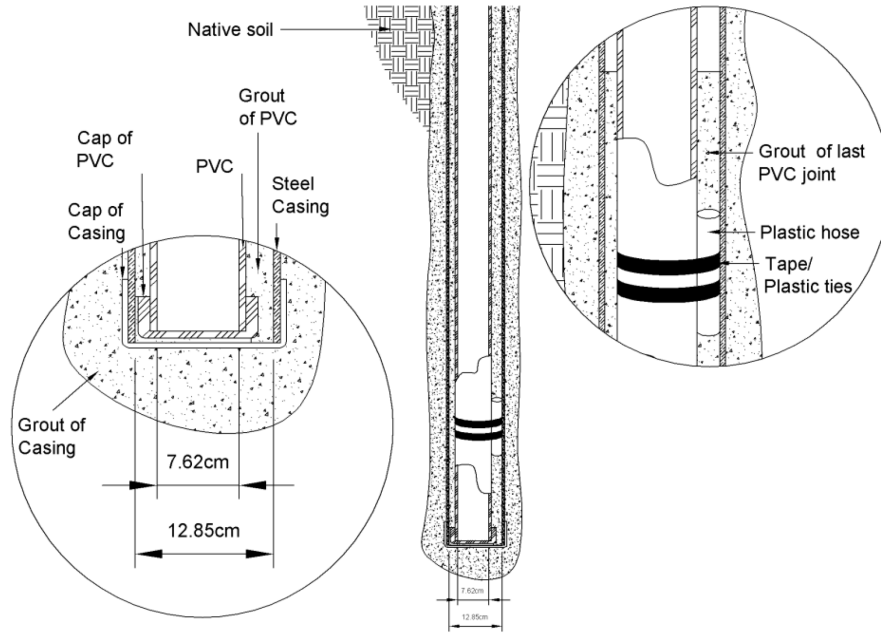


Figure 4-4: Tiltmeter borehole design in Aquistore

4.2 Field instrumentation

In Aquistore, 15 tiltmeter stations are the core instruments that constitute the tiltmeter array surveillance system. In order to obtain data simultaneously during the injection, a supplementary wireless data acquisition system is built into the tiltmeter array. In order to exclude the noise effect from environmental, a supplementary weather station is built along the tilt meter array to provide environmental monitoring including temperature, wind and precipitation.

4.2.1 Tiltmeter

Tiltmeter model used in Aquistore is Series 5000 manufactured by Pinnacle. This model of tiltmeter has a minimal resolution of 30 nR. A brief technical specs is provided in the follow Table 4-1. The internal of the tiltmeter is shown in Figure 4-5. On top the tiltmeter has a built-in compass to provide the heading direction of the marked axis (X-axis in output data). The digital data storage and communication unit obtain data after the analog amplification convert raw voltage readings to tilt. Tiltmeter has an internal memory of 512kB, which can store more than half a million data entries. Located at the bottom of the housing are the key sensing elements: two orthogonal bubble levels. Electrodes detect movements of the air bubble within a conductive fluid as the fluid seeks the lowest spot in the sensor and produce a voltage signal to the analog amplification. The two bubble levels sit on a steel plane, which can be rotated by leveling motors. The leveling motors are able to re-level

the sensing bubbles back to horizontal within 10° leaning angle of the entire housing. This enables the tiltmeter to expand beyond the range of level itself for much broader application.

Table 4-1: Tech Specs for Pinnacle Series 5000 Tiltmeters

<i>Model</i>	Series 5000 from Pinnacle
<i>Range</i>	±3000μR
<i>Resolution</i>	1nR
<i>Output</i>	RS232
<i>Temperature Range</i>	0.1°C to +60°C
<i>Power Requirement</i>	10.5V to 13.9V
<i>Dimensions</i>	51 mm dia. x 915 mm
<i>Housing</i>	Stainless Steel

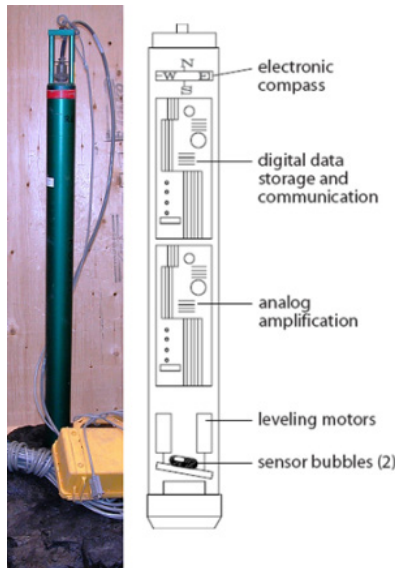


Figure 4-5: Pinnacle series 5000 tiltmeter utilized in Aquistore

At each tiltmeter station, downhole tiltmeter is connected to a 12V lead acid battery. The battery is charged by a 17.5V solar panel. Tiltmeter is linked to a RS232 port at surface through a 19-pin data cable, which provides both data transfer and power. Tiltmeter is attached to surface through an aircraft cable during installation. This aircraft cable is also used to hold the weight of the 19-pin data cable from its own weight for protection. Both cables are 31 m long. At each tiltmeter site, an aluminum enclosure is fastened on a pole. This enclosure protects the tiltmeter battery, provides the RS232 port to tiltmeter, and also contains a data acquisition unit. Figure 4-6 the surface enclosure at one tiltmeter site.



Figure 4-6: Tiltmeter station surface enclosure

4.2.2 Data acquisition system

In order to obtain tiltmeter data simultaneously during the surveillance program, a data acquisition system is installed alongside the tiltmeter array. This system includes individual radio units at each tiltmeter location, a central radio unit and an internet communicator at the center of the site. The system allows radio transmissions between tiltmeter sites to the central communication station, where data will be transferred to remote computers via satellite telemetry.

Each radio unit includes a transmitter, a battery, and a solar panel installed within the aluminum container (as shown in Figure 4-7). The antenna of the radio transmitter is located on top of the container. Tiltmeter is connected to the radio transmitter through a RS232 port at the bottom of the container. The radio transmitter relays tiltmeter data simultaneously to the central communication station.



Figure 4-7: an individual radio unit contained within a completed tiltmeter station

The central communication station is located near tiltmeter station TL06. It contains two main surface structures (Figure 4-8). Master radio unit includes an aluminum container and a solar panel. Inside the container are a radio transmitter, an internet modem and a battery. Solar panel is installed on top of the container to provide power. The nearby mast holds two antennas, one for radio transmission and one for satellite transmission.



Figure 4-8: Master radio unit and antennas

Tiltmeter data collected from downhole tiltmeter are processed by a surface radio unit before being relayed to the master communication station where connection to remote computer is established through satellite telemetry. Figure 4-9 illustrates the on-site data transmission map. This instantaneous data acquisition scheme enables continuous monitoring and quick interpretation during the monitoring phase.

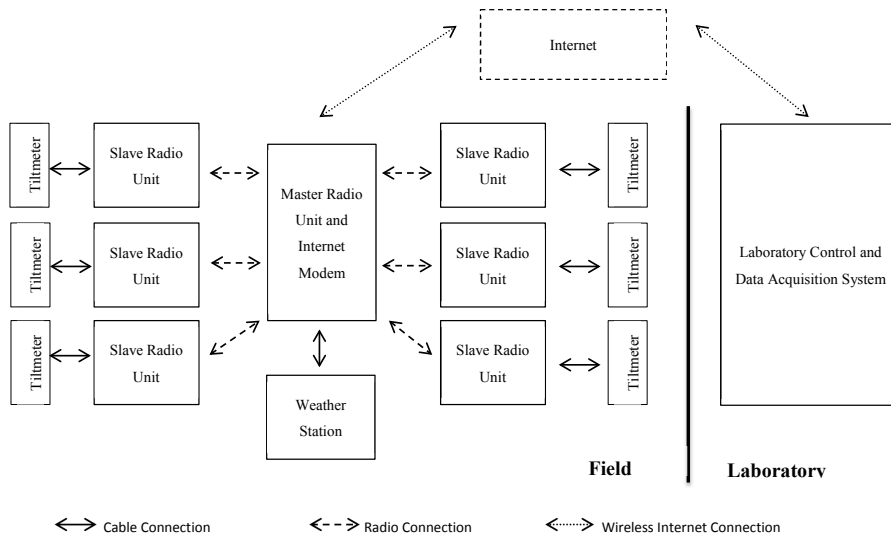


Figure 4-9: Tiltmeter data transmission diagram

4.2.3 Weather station

A dedicated weather station is built alongside the tiltmeter array to provide supplementary environmental monitoring. The weather station is provided by Campbell Scientific. It includes an air temperature sensor (Model 109), a rain gauge (Model TE505), and a wind monitor (Model 05103). The station takes readings of temperature, rainfall, wind speed and direction every 4 minutes and stores the data in a datalogger (CR200X). The data logger is connected to the internet modem in the central communication station through Ethernet cable. This weather station is installed alongside the central communication station in tiltmeter station TL06 (Figure 4-10). Wireless data collection is established with remote computer using the same method as tiltmeters.

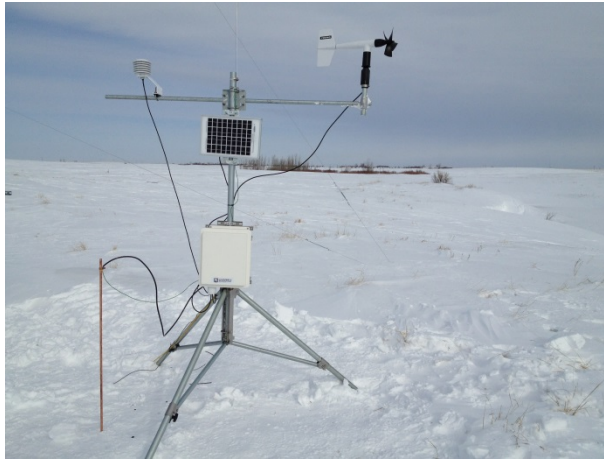


Figure 4-10: Dedicated weather station for surface tiltmeter array

4.3 Installation procedures

Tiltmeter can be installed in the borehole after the grout is completely dry. Tiltmeter is connected to a data cable and tied to an aircraft cable at top. Data cable is tied to the aircraft cable every 5 m that prevent it from straining by its weight. The aircraft cable is used to lower the tiltmeter to bottom until it sits on the PVC cap and surrounded by 1.5 L of silicon sand. The amount of sand will lock tiltmeter firmly in borehole while still making it retrievable. The surface opening of the steel casing will be locked with a cap to reduce further disturbance from the surface. Figure 4-11 shows the completed tiltmeter station TL06 alongside the master radio station and weather station. A complete working procedure for tiltmeter station is presented in Appendix A. The field trip logs describing the fieldwork are presented in Appendix B.

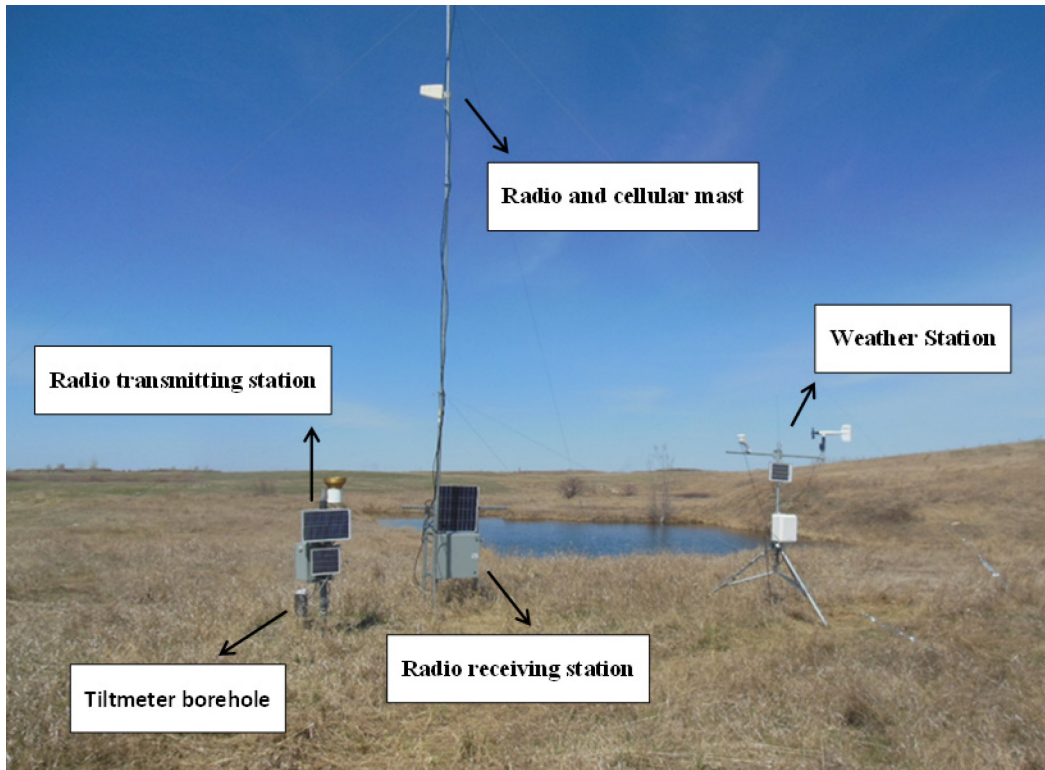


Figure 4-11: Photo of a completed tiltmeter station alongside the central communication station and the dedicated weather station

4.4 Data collection and system performance

Two tiltmeter stations have been in continuous operation in Aquistore since December 2012. Two years of data in the baseline phase have been collected as of the writing of the thesis. Baseline data are used to analyze the composition of noise patterns. This section provides an overview of the data that tiltmeters have collected.

4.4.1 Data management

Tiltmeter data is collected remotely from the field using the radio and satellite telemetry. The software used for data acquisition and management is TiltTalk Pro provided by Pinnacle (Figure 4-12), the manufacturer of tiltmeters. TiltTalk supports communications with up to 300 tiltmeters in the same array system [22]. Tiltmeter can be configured remotely. For each tiltmeter, working parameters including sampling rates, sampling resolution, and data collection scheme are configured right after installation. Tiltmeter data can be obtained in batch using scheduled pooling options as well as manually. New data collected from each tiltmeters are automatically appended to the same data file. TiltWatch functions of TiltTalk can wake or sleep tiltmeters at intervals to preserve battery life when long data sampling intervals are expected.

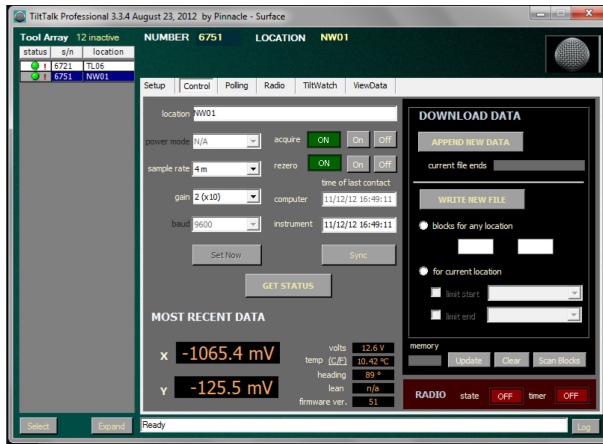


Figure 4-12: TiltTalk interface used to manage tiltmeter array

For tiltmeters in Aquistore, field sampling rates are set to every 4 minutes. At this sampling rate, the internal memory of tiltmeter can hold up to three months of new data without overwriting existing data. The sampling resolution is set to 1 nR, which gives a total range $\pm 300 \mu\text{R}$ before releveling. Since installation, tiltmeter data have been downloaded manually every week. The downloaded data includes time, downhole temperature, battery voltage, two sensor voltage readings (and converted tilt value), and tiltmeter configuration information. Data file can be viewed using TiltTalk and can be exported to Excel for further processing.

4.4.2 Baseline performance

Three years of tiltmeter data in the baseline phase have been collected in the time scope of the thesis. Figure 4-13 and Figure 4-14 presents the data set from two tiltmeter stations TL06 and NW01 between February 2013 and August 2013. Both sets of data will be used primarily in this study to understand the signature of noise signals.

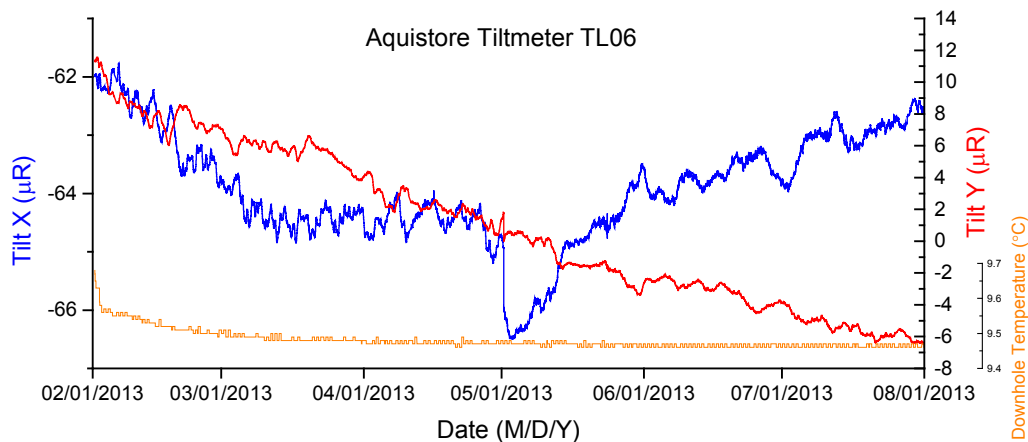


Figure 4-13: Baseline tiltmeter data from site TL06 between February 2013 and August 2013

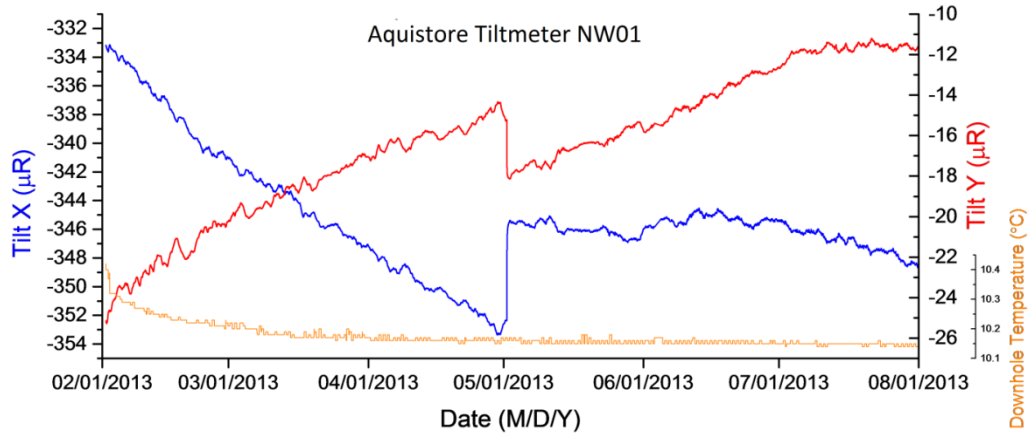


Figure 4-14: Baseline tiltmeter data from site NW01 between February 2013 and August 2013

4.4.2.1 Level sensor reading

Each tiltmeter has two orthogonal tube sensors in which an air bubble within the conductive fluids seeks the highest position and conductive plates mounted inside the tube gives voltage readings representing the position of the air bubble. The voltage reading can therefore be converted to tilt using a scale factor provided by tiltmeter manufacturer, which can also be refined through calibration test. The range of the sensor is further expanded through the leveling motor attached below the sensor that can re-level the sensor once the tilt limit is reached. Figure 4-15 shows the level sensors and the leveling motor inside the tiltmeter housing.

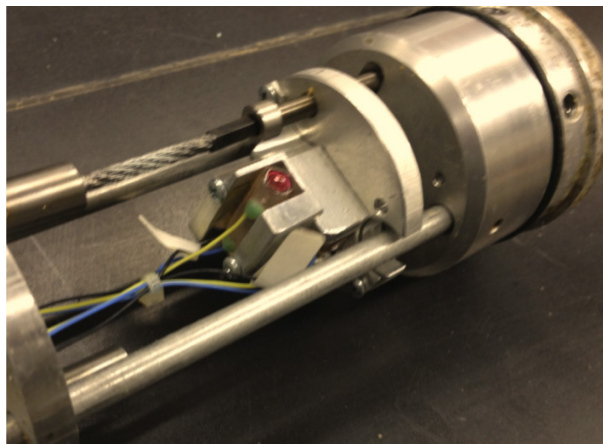


Figure 4-15: Two level sensors and a re-leveling motor contained inside a tiltmeter housing

In eight months of baseline readings, tilt series from four tilt sensors show different patterns. In overall, fluctuations are commonly present in all short, medium and large intervals. Tilt reading from TL06 has a relative small range of 20 μR . There are huge changes immediately after the installation, probably because of the cavity effects of the borehole. Then tilt readings gradually go smooth. X-axis data show a U-shaped trend with a flat period in the middle sandwiched by periods of rapid changes. Y-axis data show a steady downward trend with a consistent slope throughout the

year. Tilt data from NW01 have a much larger yearly range of 100 μ R. Both axes share a similar L-shaped trend with tilt goes quickly in the beginning and gradually flattens at the end of the year.

4.4.2.2 Temperature sensor Reading

Downhole temperature reading from both tiltmeters shows a similar trend. Temperature drops quickly in the first three months before it stabilizes. TL06 becomes stationary around 9.455 $^{\circ}$ C with 0.005 $^{\circ}$ C daily variance. NW01 stabilizes around 10.145 $^{\circ}$ C with daily variance of 0.004 $^{\circ}$ C. The difference between two tiltmeter sites (0.69 $^{\circ}$ C) is probably due to the difference in borehole depth and surface topography. Figure 4-16 shows the temperature readings from both tiltmeters.

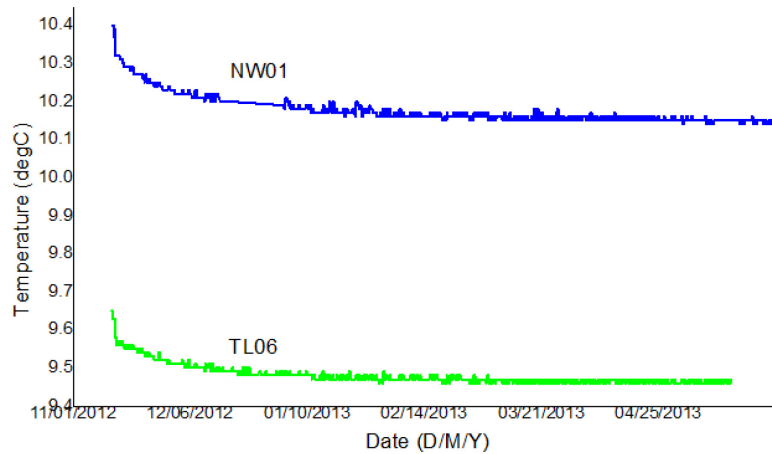


Figure 4-16: Tiltmeter temperature sensor reading in the first six months

4.4.2.3 Compass reading

Each tiltmeter has an internal compass that can detect the heading of the X-axis from north. This reading is refreshed by tiltmeter every six hours. Heading indicates the orientation of the instrument in degrees east of magnetic North. As expected, the headings of both tiltmeters are unchanged since installation. Heading for Tiltmeter TL06 is 93 $^{\circ}$ and for tiltmeter NW01 is 155 $^{\circ}$. Figure 4-17 below shows the orientation of tiltmeter sensors. In some cases the heading information can be used to standardize tilt readings to north and east directions for processing.

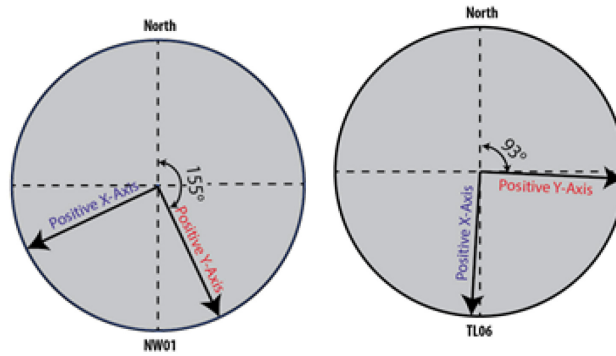


Figure 4-17: Initial compass reading from two tiltmeters

Combining tilt and heading readings, the tilt vector at each tiltmeter location can be visualized by in planar view over time as shown in Figure 4-18. With additional tiltmeters to be installed in Aquistore, a resolution can be reached where ground deformation can be interpreted.

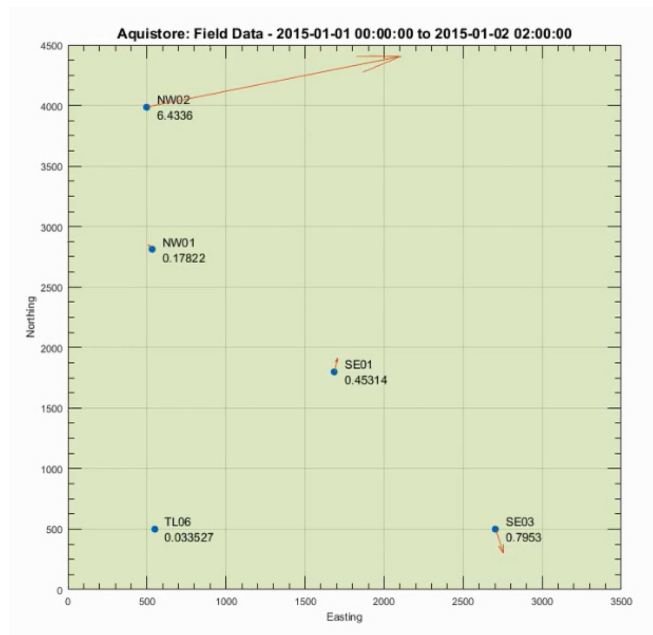


Figure 4-18: Combined vector map with existing tiltmeters in Aquistore in 2015

CHAPTER 5 Baseline Tilt Pattern Characterization and Modelling

5.1 Overview

Two (TL06 and NW01) of Aquistore’s six installed tiltmeter stations have been in continuous operation since November 2012. As CO₂ injection has not started, tilt data collected during this time period reflect baseline ground motion. Baseline tilt data are composed of patterns induced by multiple external factors, including earth tides, rainfall, groundwater tables barometric pressure fluctuations, thermoelastic deformation, borehole cavity effects, tectonic movements, and human activities. A list of major sources of baseline ground motion is presented in Table 5-1.

Table 5-1: Major sources of baseline ground motion

Category	Source
Tidal Factors	Earth tides
	Loading effect from ocean tides
Environmental Factors	Rainfalls/Snow
	Atmospheric pressure
	Temperature
	Wind
Tectonic Factors	Seismic events
	Global Tectonic Movement
Cultural Factors	Traffic/Production etc.

Noise patterns from these external factors are greatly influenced by installation depth and environment. Tiltmeters installed at shallow depths are predominantly affected by surface disturbance and temperature fluctuations, which can create strong signals. Deeply buried tiltmeters can reveal less subtle signals such as earth tides, and are less sensitive to surface rainfall. Those installed in bedrock are more sensitive to subtle earth motion such as tectonic movements. Figure 5-1 shows baseline differential tilt data collected from station TL06 since December 2012, revealing several patterns at different time scales. Figure 5-1 (a) presents the typical long-term response of tiltmeters in Aquistore. The maximum differential tilt in 18 months was approximately 38 μ R in the east-west direction. It is suspected that this initial response was related to ground disturbances due to installation as tilt measurements were more stable in the last 9 months. The long-term trend could also be related to ground thermal deformation or tectonic movement. Figure 5-1 (b) presents weekly and monthly tilt patterns, which include large episodic fluctuations possibly related to rainfall and barometric pressure conditions. Figure 5-1 (c) presents tilt patterns on a daily scale, which clearly shows the existence of semidiurnal earth tides.

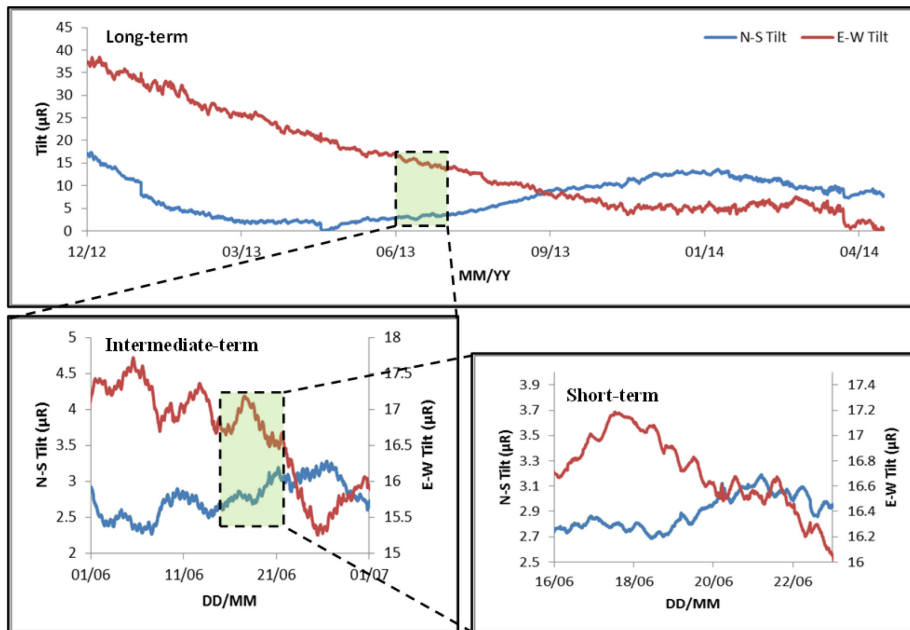


Figure 5-1: Baseline Tiltmeter reading showing short, intermediate and long term fluctuations

Baseline tilt patterns are regarded as noise signals during injection monitoring, as they could obscure or even alter the real signals from deep CO₂ distribution. The expected surface deformations have been estimated to be in the millimeter scale. The measurements of surface displacement on this scale can be significantly impacted by noise effects. When noise patterns overlap injection signals in comparable scales and time frames, deformation interpretation becomes biased or even invalid. For the best performance of surface tiltmeter arrays, the characterization and removal of noise signals become critical.

Aquistore site locates on a dedicated field without traffic and far from nearby production activities. Tiltmeters are deployed at 30 m deep boreholes, making it isolated from most cultural disturbance. The only cultural noises discovered on tilt readings are some dynamite shooting tests conducted within Aquistore project. Meteorological factors such as rainfall, snow, barometric pressure, temperature can create tilt patterns of varying scales. In Aquistore, the deep and isolated burial design of tiltmeter can minimize impact from surface disturbance. Site tests indicate vibration of surface casing and cable has no effect on tilt readings. Therefore the effect of wind can be neglected. The investigation of environmental noise should focus on mass distribution phenomena including rainfall and atmosphere loading other than that of direct surface vibration. The scale of temperature fluctuations which a tiltmeter is exposed to determines the scale of thermal noise. A measurement of downhole thermal profile is essential to estimate the impact of thermal effect. Tidal noise applies to tiltmeter regardless of the installation geometry. At practise it is used as an indication of installation quality of tiltmeters. As the location of Aquistore is far from ocean and large lakes, only

solid earth tides contribute to the recorded signals. Tectonic noise should impact tiltmeter array far beyond the time scale of the monitoring activity, except the rare occurrence of seismic activities. Therefore the study of tectonic noise should focus on understanding existing seismic noise signature. Five significant types of noise signals are analyzed in the scope of this paper: earth tides signals, barometric pressure signals, rainfall signals, thermal signals and seismic signals. These patterns are either well revealed in obtained baseline data, or incorporable with relevant site data. In order to remove the influence of noise signals, three general methods are proposed based on the revealed signal characteristics. Statistical regression method is used to quantify linearly-provoked noise such as that from earth tide. For complex process such as the impact of rainfall, a numerical modelling approach is adopted. As temperature fluctuations disturb tiltmeter sensor directly, a calibration method is proposed. Table 5-2 summarizes expected characteristics of noise signals to be analyzed in Aquistore tiltmeters. Figure 5-2 illustrates the general methodology used in quantifying the noise effects.

Table 5-2: Characteristics of captured noise signals in Aquistore

Origin	Pattern	Periodicity
Earth tides	Sinusoidal wave	Semidiurnal
Barometric pressure	Random fluctuations	Aperiodic
Rainfalls	Random fluctuations	Aperiodic
Thermal deformation	Sinusoidal wave	Annual
Seismic events	Spikes	None

A Methodology Flow-Chart

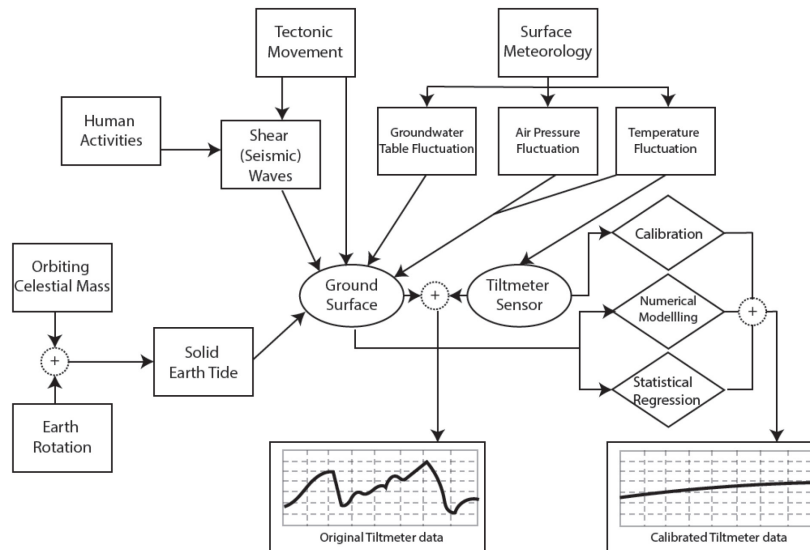


Figure 5-2: General mechanism of noise signals and methodology in removing their effects

5.2 Earth tide signal

5.2.1 Introduction

Short-term tiltmeter data from Aquistore exhibit clear semi-diurnal fluctuations. This tilt pattern reflects the harmonic movement of the earth created by the gravitation pull of the Moon and the Sun, referred to as earth tide signal in this thesis.

The gravitational attraction of the extraterrestrial mass (predominantly the Moon and the Sun) creates the periodic bulge and depression in the earth crust, in the same mechanics as ocean tide. The amplitude of earth crust distortion is determined by its relative position to the extraterrestrial mass, therefore it exhibits a composition of harmonic constituents because of the pattern of earth rotation and earth orbit as shown in Figure 5-3. The largest earth tide constituent is semi-diurnal, which is produced by the orbiting Moon. There are also insignificant diurnal, fortnightly and semi-annual contributions of earth tide. Each constituent force of earth tide acts on the surface of the earth and create 3-dimensional deformation with spatial variations. Tidal tilt is created along with the spatial displacement variations.

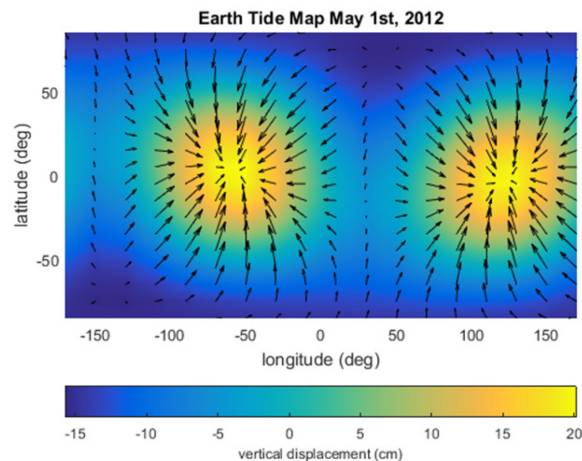


Figure 5-3: Earth heave and depression under solid earth tide

The observed amplitude of earth tide signal in Aquistore is less than 100nR. The pattern of tidal signal follows a sinusoidal waveform with a slightly inconsistent period (~12h). Earth tide noise only becomes significant in hourly-sampled tiltmeter data. While in long-term monitoring plans the signal will cancel out, earth tide signal will impose on tilt pattern induced by CO₂ injection its hourly output. Earth tide signal has the smallest scale among the observed noise signals, which essentially defines the detection threshold of reservoir surveillance program [23]. On the other hand, the revelation of tidal signal in the overall pattern is an indication of tiltmeter performance. The detection of earth tide signals can be regarded as a validation that tiltmeter is fully coupled with the ground. The presence of smooth tidal signal indicates minimal background noise, which is the desired working environment for tiltmeter. The measurement of the earth tide signal can be used to

study spatial variations in the elastic properties of the materials near the surface, as well as indicating discontinuities near the fault zone [24]. For the above purposes, tidal signal in tiltmeter has been characterized in a few case studies.

5.2.2 Literature review

Levine et al. [24] installed seven tiltmeters in 30 m boreholes in Colorado and Wyoming to evaluate secular tilt, earth tides and the coherence between tiltmeters. In order to analyze tidal signals unbiasedly, they separated secular signals from tidal signals using digital filtering and spline fit techniques. Digital filtering technique removes all non-tidal frequency secular data and spline fit technique is used to remove secular drift of longer periods. Amplitudes and phases of tidal lunar and solar components are estimated using least square methods with estimated theoretical tidal admittances. Levine proposed two methods to produce the fitting function, either by using spherical harmonics of lunar and solar positions or by summing up frequencies. Levine summarizes the tidal amplitude and phase shift for each site in different periods and results shows good unity. Good agreement is found between tiltmeter tidal measurements and with theoretical results from simple, first-order model with 2% error range. In their approach to evaluate tiltmeter performance by examining tidal response, Levine first filters non-related noise signals, then estimating theoretical tidal admittance and at last using statistical method to evaluate tiltmeter tidal records and proves the agreement.

Wyatt, Cabaniss, and Agnew [25] compare the readings from several types of tiltmeters at tidal frequencies to evaluate their performance. Tiltmeter that shows less deviation from theoretical tidal tilt is better at providing accurate information, i.e. monitoring tectonic movement. Spectral analyses are conducted for a 149 day period tilt data to evaluate the response of tiltmeters at tidal frequencies and resolve noise-signal ratio. Power density spectrums of the tilt data highlight the difference in instrument noise levels as higher noise level has a profound influence on tidal tilt measurements. They also analyzed the tidal data by fitting 13 sinusoids at the frequencies of the largest tidal harmonics to the observed series and express the observed phases to local tidal potential.

The adopted approach for analyzing earth tide signal in Aquistore follows a methodology as combined by the above two studies. First tilt data recorded by tiltmeters will be analyzed for tidal constitutes. A tidal tilt model will be constructed based on a simplified earth model and compared with observed data. This will indicates the general site condition and installation quality of tiltmeter. Tiltmeter performance will be evaluated based on the agreement between the two and tidal signal reduction method will be proposed.

5.2.3 Statistical analysis

Baseline data recorded by tiltmeter station TL06 between June 1st and November 1st 2013 is shown in Figure 5-4. Power spectrum analysis is conducted for the data set and the breakdown frequency

bands are presented in Figure 5-5 and Figure 5-6. The frequency band clearly shows a large semidiurnal component and a smaller diurnal component. The capture of both tidal constituents indicates that tiltmeters are well coupled with the ground. The clear measurement of both tidal constituents indicates that tiltmeter is adequately coupled with the ground.

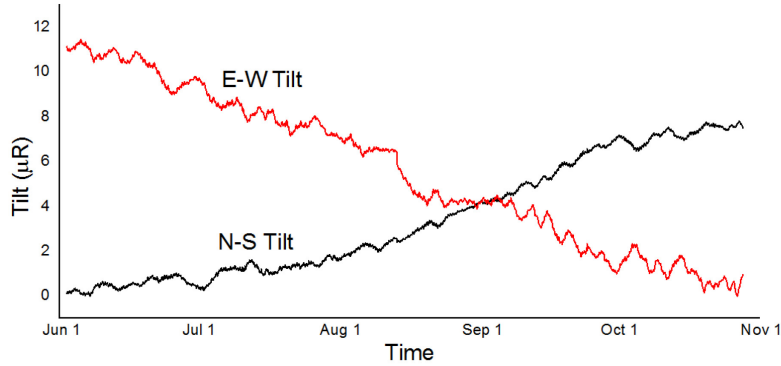


Figure 5-4: Tilt time series from tiltmeter station TL06 during 2013

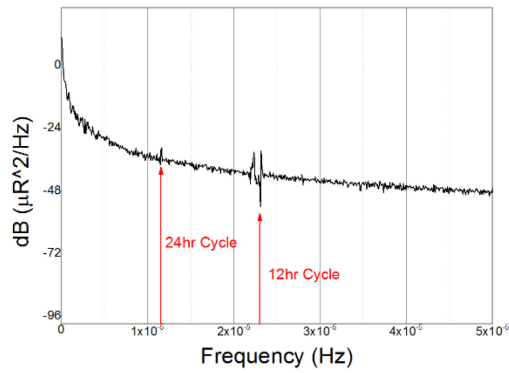


Figure 5-5: Power spectrum of N-S tilt reading from tiltmeter station TL06

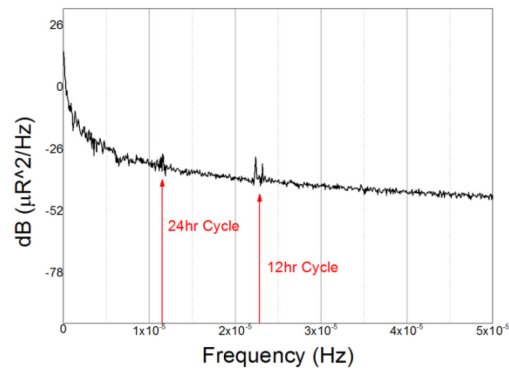


Figure 5-6: Power spectrum of E-W tilt reading from tiltmeter station TL06

5.2.4 Modelling

Baseline tidal signals can be estimated by fitting a theoretical solid earth model with existing data. Assuming an elastic, spherical, isotropic, non-rotating, and oceanless earth, tidal acceleration at a point in the earth's surface is determined by its relative position to the Moon and Sun. Tidal tilt is

essentially the horizontal gradient of tidal acceleration. Earth tide data processing codes SOLID [26] is used to calculate theoretical tidal amplitude with the coordinates of Aquistore. Three-dimension earth tide amplitude (north, east and vertical) is calculated for Aquistore site (49.09596N, 103.09005W) between September 1st and September 7th 2013 as shown in Figure 5-7.

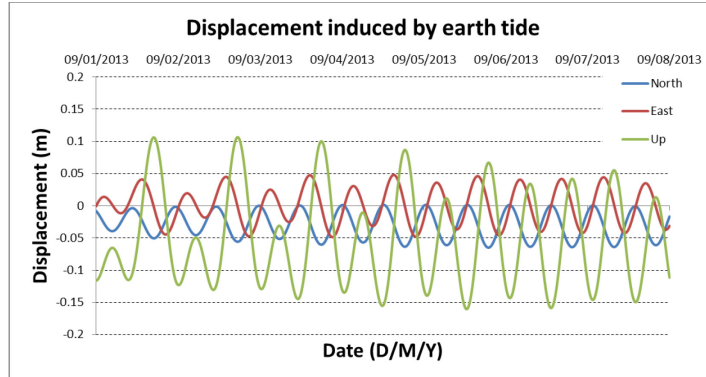


Figure 5-7: Tidal amplitude calculated for Aquistore using program SOLID

Since tilt is just the change in slope of an equipotential surface, it can be calculated for north-south and east-west directions using reference points. In this calculation, reference points are selected 1000 m away from base point and tilt calculated for N-S and E-W directions are shown in Figure 5-8 and Figure 5-9. In our analysis, positive tilt indicates tilting towards east and south.

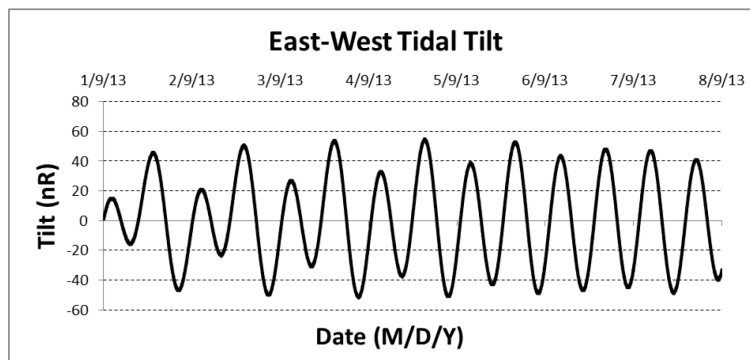


Figure 5-8: Calculated East-West tidal tilt in Aquistore

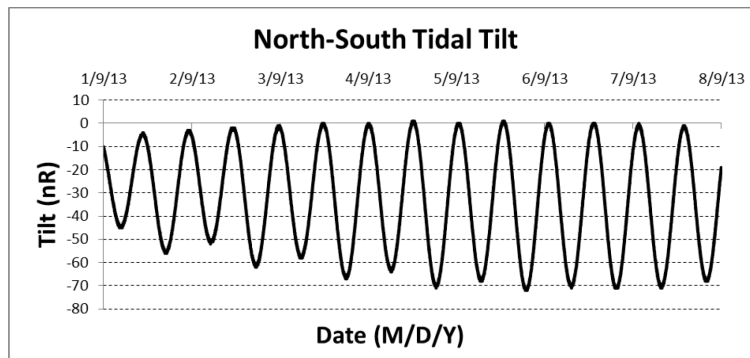


Figure 5-9: Calculated East-West tidal tilt in Aquistore

After theoretical earth tide tilt is calculated based on site location and time, it is compared with tiltmeter reading using coefficient of correlation. Figure 5-10 shows the tiltmeter reading of tiltmeter TL06 during September 1st and 7th 2013, the same time frame with calculated tidal tilt.

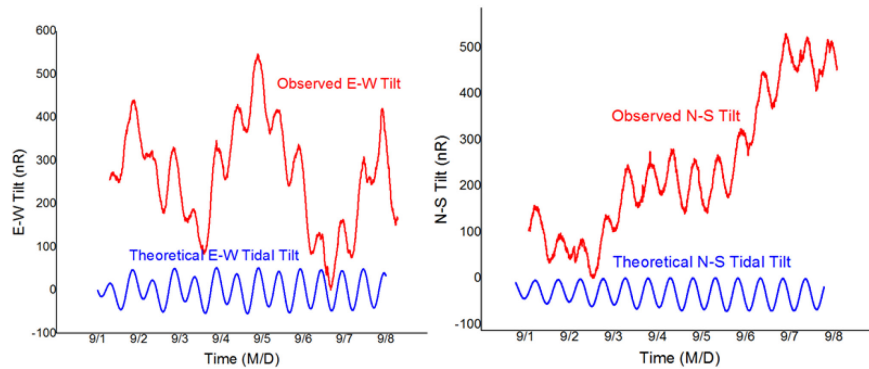


Figure 5-10: Observed tilt signal from TL06 station and theoretical earth tide tilt

Besides obvious earth tide signals, tilt data also show strong secular trend unrelated to the tidal frequency. These signals may be produced by surface rainfall, thermoelastic deformation etc. To remove the strong discrepancy created by these external noises, tilt data are detrended using polynomial fitting method. The detrended data is analyzed with theoretical tidal tilt using cross correlation method and are shown in Figure 5-11.

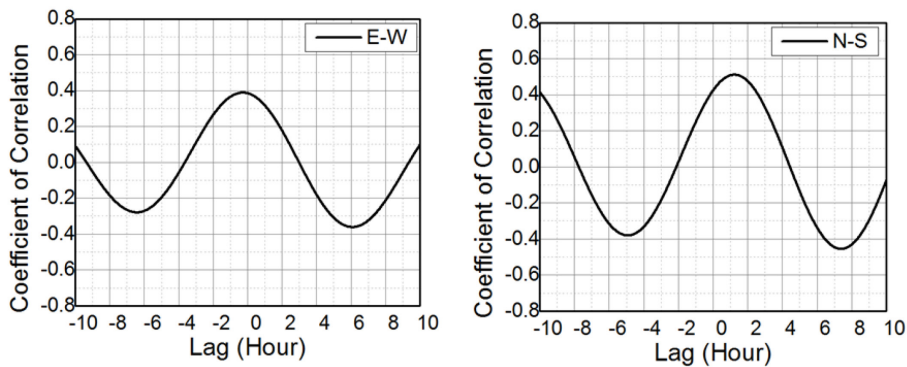


Figure 5-11: Cross-correlation plot for both directions of tiltmeter data

Tilt readings of both directions are in good agreement with theoretical tidal tilt for the time frame. A phase lag of 1.2 hours is found in the N-S direction as the tiltmeter response is lagging behind the earth tide tilt. For E-W sensor the tiltmeter is not showing an obvious phase difference. The phase difference can be explained as tidal response the earth is not perfectly following a simplified body tide with discontinuous elastic parameters. The amplitude of observed tilt is larger than the theoretical earth tide tilt by the factor of 1.41-1.43, which is calculated using least square fitting. The additional tilt maybe generated by the tidal effects of rivers, lakes and ocean as they respond dynamically to the tidal force and give periodic loads on earth surface with the same frequency with earth tide. Table 5-3 shows the tidal amplitude and phase for the observed and modelled response.

Table 5-3: Summary of tiltmeter response to earth tide compared to modelled results

	Observed Amplitude (Average)	Calculated Amplitude (Average)	Factor of difference	Phase
E-W	~110nR	~80nR	1.41	0°
N-S	~110nR	~75nR	1.43	20°

5.2.5 Discussion

Earth tide tilts, especially the semidiurnal component, are clearly observed in most short-range tiltmeter data. Although the complete tidal signal could be diverted or masked by the presence of other secular tilts from surface rainfall and thermoelastic deformation, long term tiltmeter data exhibits clear fluctuations at tidal frequencies. Therefore the successful coupling of tiltmeter to its surroundings can be verified, enabling effective long-term reservoir level monitoring.

After calculating theoretical earth tide deformation and tilt in Aquistore, the observed tilt signals from tiltmeter on site is compared with the results and shows high agreement with coefficient of correlation reaching 0.6 during a low noise period. The amplitude discrepancy between observed and theoretical tidal tilt is the N-S and E-W directions are factors of 1.41 and 1.43 respectively. Nearby water tide may result in this factor. A phase shift of 20° is found in the N-S direction. The phase shift could be the result of the non-linearity of downhole elasticity parameters.

The amplitude of earth tide tilt, being the smallest continuous tilt signals found in tiltmeters, could define the minimum detection limit of the tiltmeter as the fluctuating signal could obscure and alter any other signal of the similar magnitude. Smaller signals from the reservoir could be completely biased unless the earth tide signals are completely removed. The high correlation factor between theoretical and observed tilt signal offers an approach to reduce the earth tide noise. By using the factor of amplitude difference and adjusting phase difference one can estimate the actual weight of tidal signals in tiltmeters and eventually subtract it when necessary. The following Figure 5-12 exemplifies such an approach by reduce the E-W earth tide noise in tiltmeter data. After removing earth tide signals, tilt data is smoother and clearly showing secular tilt of longer wavelength.

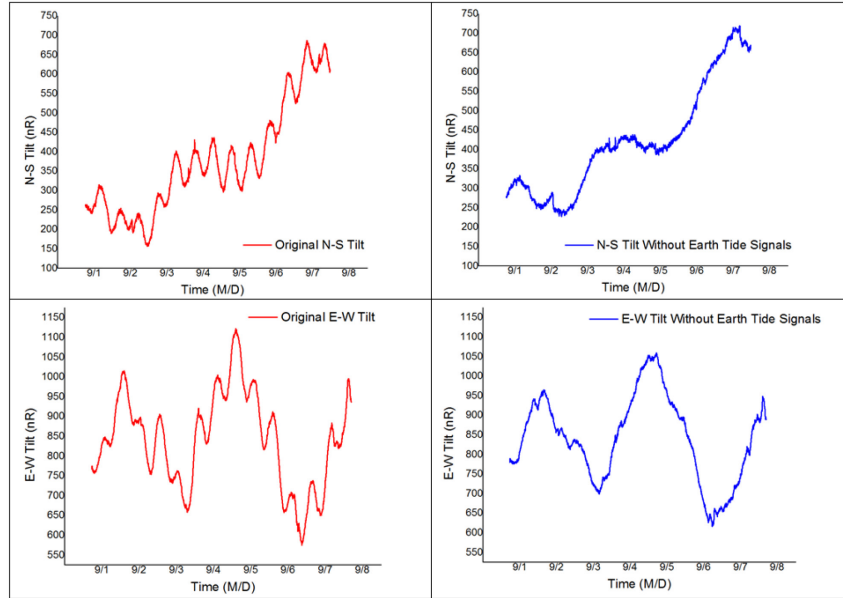


Figure 5-12: Tiltmeter data before (Red) and after (Blue) removing earth tide signals

Earth tide signals are dominant in tiltmeter readings in the short range. In the longer range tidal signals will cancel out and noise signals of longer wavelength will become the issue. Depending on the monitoring purpose, earth tide signals can be either analyzed as an evaluation of tiltmeter performance or can be removed to reveal small and unbiased signals from the reservoir.

5.3 Barometric signal

5.3.1 Introduction

Barometric signal refers to the tilt pattern induced by atmospheric pressure. It is part of environmental noise that has large impact on tiltmeter. The typical atmospheric pressure at surface has variations at the level of 20-50 mbar. Redistribution of air masses due to atmospheric circulation causes loading deformation of the earth. And barometric tilt is the manifestation of this loading effect. The modelling of barometric signals can be straightforward one signal variant (air pressure) and can be linearly deducted. The reduction of barometric signal is the first step in analyzing rainfall signals in the following section.

Barometric signal is recognized in several studies about geodetic techniques including tiltmeters. Petrov and Boy [27] introduced a procedure to calculate three-dimensional displacements using a 6 hourly pressure field. Results from their model fell within acceptable error budget and can be used for routine data reduction of space geodesy observations. This method is simplified from rigorous study by considering the mass loading of adjacent area but still requires a large amount of weather data which cannot be obtained in the scope of Aquistore project. Dal Moro and Zadro [28] analyzed the correlation between crustal deformation data and precipitation/pressure variations and offered physical explanation in the frame of the elasticity theory. In their case the induced tilt by

precipitation is one order of magnitude stronger than that induced by barometric pressure. They determined the orientation of major and minor axes of deformation but claimed that there is a threshold of precipitation and pressure before a linear regression coefficient can be used. This method can be adopted for analyzing the influence of barometric signals in Aquistore.

5.3.2 Statistical analysis

The presence of strong signals from barometric pressure is statistically verified using the cross-correlation function. Baseline tilt data are processed through a band pass filter that removes both high (>1 cycle per day) and low (<0.05 cycles per day) frequency signals unrelated to atmospheric patterns. The filtered data are then organized in hourly averages and analyzed with barometric data from a weather station about 15 km from Aquistore. Figure 5-13 presents the cross correlation function between tilt and barometric pressure data from site NW01. Data analysis reveals a high correlation factor of above 0.5 in both directions, and an almost linear relationship between barometric pressure and tilt.

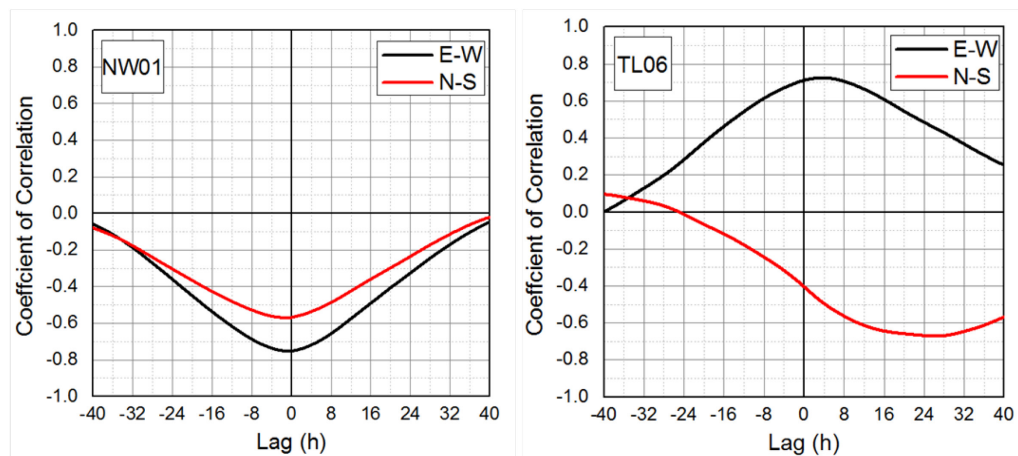


Figure 5-13: Cross-correlation analysis between tilt and barometric pressure

5.3.3 Modelling

Rigorous modelling of barometric tilt pattern requires knowledge of regional earth crust strength data as well as aerial distribution of atmospheric mass. The scope of this study does not include a direct geophysical modelling method, but propose using history data to produce an empirical regression coefficient. The statistical regression method is used to quantify the barometric pattern in Aquistore. Constant regression coefficients are found for both directions, as shown in Table 5-4. Fixed tilting plane are determined based on two orthogonal tilts for each tiltmeter and the angle of this plane implies the distribution of the earth crust strength. With additional barometric pressure data, barometric signals can be removed from the baseline pattern (Figure 5-14).

Table 5-4: Tilting angle and regression coefficient determined for barometric pressure signal

	Plane Angle (degree to N)	Regression Coefficient ($\mu\text{R}/\text{kPa}$)
NW01 East-West	229°	-0.31
NW01 North-South		-0.42
TL06 East-West	114°	0.50
TL06 North-South		0.31

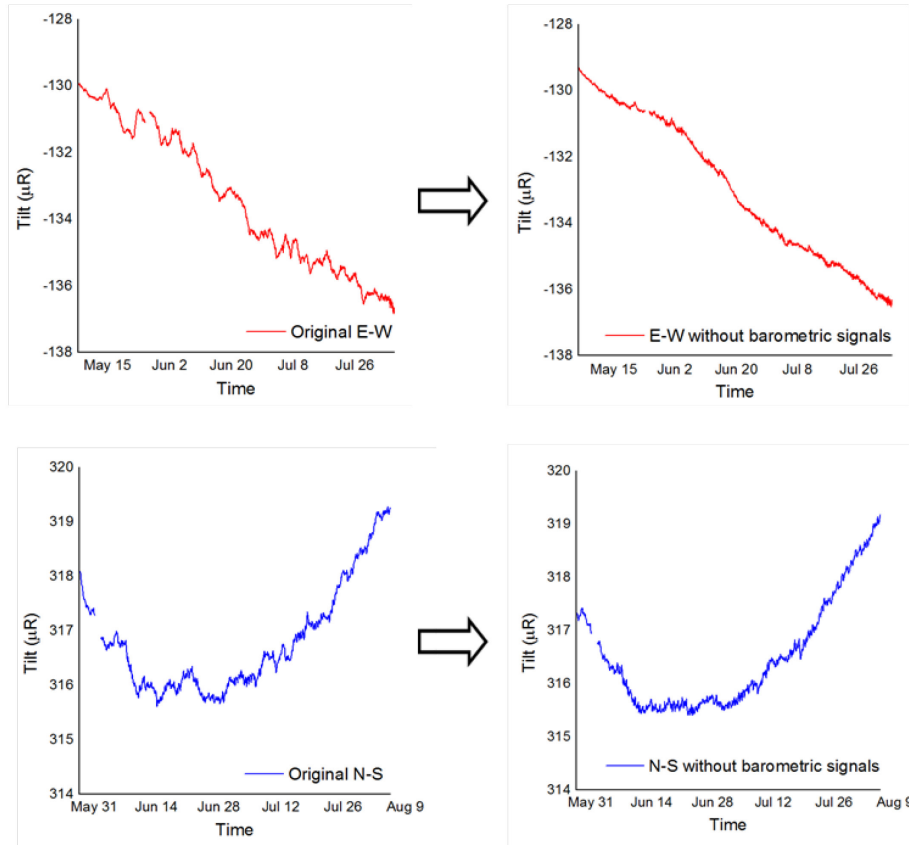


Figure 5-14: Subtracting barometric signals from baseline tiltmeter data

5.3.4 Discussion

In Aquistore the appearance of barometric pressure signal is significant and consistent. As the statistical analysis shows a linear correlation between tiltmeter reading and barometric pressure. The most likely explanation of barometric pressure signal is the loading effect of atmosphere mass over the region. The distribution of barometric pressure over the area is regarded as uniform. With the possible inhomogeneity in regional earth crust strength, atmosphere loading creates a horizontal stress variation when air pressure changes. This explanation can be supported that for both tiltmeters, a fixed direction exists that tiltmeter will tilt towards when air pressure changes. This direction indicates the overall declining direction of earth crust strength in that area.

5.4 Rainfall signal

5.4.1 Introduction

Rainfall signal refers to the tilt pattern created primarily by surface precipitation, as well as concurring evaporation and runoff. Rainfall signal is a major type of noise constituting the baseline tiltmeter data. The exact pattern of rainfall signal varies in shape and in a broad band of frequencies. For shallower tiltmeters the pattern consists of more an instantaneous spike whereas for deep tiltmeters it shows more of a delayed response. Closely related to groundwater table, the scale of rainfall signal ranges from short term (days) to long term (months). The episodic appurtenance of rainfall signal is difficult to predict and insulation of tiltmeter has no effect towards its attenuation.

The episodic appearance and broad frequency band of rainfall bring huge uncertainty to reservoir surveillance. In order to improve the accuracy of deformation interpretation, the nature of rainfall signal has to be understood. With the additional meteorological monitoring plan in Aquistore, It is possible to quantify the occurrence of rainfall signal and construct a reduction model for better data interpreting during period with heavy rainfalls.

Unlike previous types of noise signals, statistical methods prove to be difficult to concisely describe the appearance of rainfall signal. A rainfall data series consists of only zero and positive values, therefore make any correlation coefficient with tilt series to be low. A simulation approach is necessary to quantify rainfall tilt. The following section provides a literature study and a statistical analysis related to the topic of rainfall signal and the simulation part is detailed Chapter 6.

5.4.2 Literature review

The study into explanation and quantification of rainfall-induced tilt has been conducted by some researchers. The applied fields in these studies range from seismicity monitoring to volcano predication and the installation geometry of tiltmeters ranges from deep bedrock environment to shallow unconsolidated ground. Even though their conclusions may not apply well into reservoir monitoring in Aquistore, the theory and methodology is a very valuable reference.

The noise pattern exhibited from deep and shallow tiltmeters are different. For insulation purposes, tiltmeter is barely installed above groundwater table to avoid the high environmental noise. Shallow tiltmeter is subject to more direct loading effect and larger force of groundwater flow. In the case presented by Westerhaus and Welle [33], tiltmeters are installed at 3-4 m near an active volcano to detect the possible chamber movement for eruption predict. With adequate insulation, meteorological noise exists. The author proposes three mechanisms behind rainfall signal, including loading effect of rainwater, pore water induced deformation, and inertia force of groundwater flow. They suggest that the eventual noise pattern is the combined effects of the three mechanisms and propose a rain function method as the evaluation of rainwater mass on the earth. By comparing with actual observed tilt pattern, the result correlates quite well, indicating that loading effect is the

primary physical factor. The author suggests that with limited knowledge of subsurface, the optimum fit of rain function with tilt pattern using the proposed method could only last for a short period of time, while long term interoperation requires a sufficient characterization of the site condition. The methods introduced in the present study to predict rain induced ground deformation and tilt covers the all basic mechanisms. The physical explanation of rainfall tilt is valid in their case and supported by their observation. For shallow tiltmeter, the amplitude of rainfall signal is more prominent given high lateral movement of seepage flow. The loading model, the infiltration model and the seepage model all largely depend on the slope of the surface as well as the projected groundwater table. As in this case, tiltmeter are installed on a hill with a slope of 20° and at a shallow depth of 3-5 meters. All these factors contribute to their high relevance for shallow buried tiltmeters.. However for deeply buried tiltmeter, the sensitivity of tilt becomes much less dependent on the geometry. While mechanism such as inertia force of groundwater seepage can be neglected, more site characterization efforts are required to propose an accurate model.

For deep burial tiltmeters, visual inspection of rainfall tilt becomes less obvious and statistical analysis is required to characterize the observed rainfall signal. Dal Moro and Zadro [28] present their tiltmeter and strainmeter measurements in seismic area to monitor tectonic movement. The instruments are installed at 60 m depth. As their first step, the authors analyze tilt and strain data to find the correlation coefficient with surface precipitation. Tilt and strain time series are filtered to remove high frequency noise and earth tide signals before performing a normalized cross-correlation analysis with rainfall time series. A strong correlation coefficient is found between strain and rainfall while that between tilt and rainfall is weak. Dal Moro explains the difference with the more complicated influence of the water table variations on tilt. Through statistical analysis, a non-linear correlation is discovered with a detecting threshold of about 30-40 mm per day and a coefficient of -1.91 nstrain/mm after that. As for physical explanation of rainfall signal, the authors propose the elastic loading model of the rainfall mass on a homogeneous media with different orientations of the rock discontinuities. In this paper, the author acknowledges the hydraulically induced deformation through a filtering and correlation approach and explains the physical origin as the elastic loading process as both activities occur contemporarily. Dal Moro ignores the pore pressure effect which may result in a lag. Their choice can be justified by the deep burial depth of tiltmeter which may not be in phreatic water system that responds quickly to the surface precipitation. The authors do not provide a physical model of the process but the back regression approach is effective in quantifying the noise signal.

Rainfall signal is closely related to the projected groundwater table. In the study of Edge, Baker, and Jeffries [29], they present the dependency of tilt pattern and groundwater level. Their data are obtained from tiltmeter installed at 12 m depth covering 9-months period. Significant correlations are found between tilt reading and groundwater table level. Seasonal groundwater table variations create the largest tilt that can be observed at both depths. Heavy rainfalls introduce additional tilt

that creates onset lasting one day followed by a decay lasting more than 10 days. The amplitude of tilt is also clearly dependent on geographical azimuth. However this study does not offer an explanation of why tilt in certain direction is more prominent and no physical model is proposed.

Following up on the impact of groundwater on tilt pattern, Kümpel, Peters, and Bower [30] provide both an empirical and a deterministic approach to calculate the tilt induced by groundwater table variation. In their case tiltmeters are installed at 47m and 110m depth in granite. The empirical method first uses cross correlation technique to determine both azimuth of the strongest tilt signals and the time lag between rainstorms occur and tiltmeter registers the signal. Least square method is used to find the best regression coefficient for the tilt signals. Through empirical approach, non-tidal noise is reduced at the same level as the least sensitive azimuth, however residual signals still shows fluctuations. The deterministic approach uses Biot's consolidation theory to explain the mechanism behind deformation induced by groundwater variation. Tilt is created by a lateral non-uniform change in groundwater table, which may from due to surface topography, anisotropic permeability, surface runoff conditions, etc. Kümpel create a basic finite element model to calculate tilt under a defined uniform groundwater slope. They also test the parameters to find the deciding factors in the amplitude of tilt. They explain that the porewater pressure gradient, together with Young's modulus and Poisson's ratio, determined the amplitude of tilt. One of the disadvantages of their model is that the model always assumes a steady state condition, which is unlikely given that rainfall, one of the main driving factors in groundwater table change, needs time to change the water table. The whole process is a transient instead of steady state. However, their model systematically describes the physical process of the hydraulic tilt.

Installing tiltmeter deep in bed rock can further decrease the direct of surface precipitation, but tilt reading still show the impact through changes in pore water pressure. Longuevergne et al. [31] investigate the deformation induced by water pressure variations in hydraulically active natural fractures. The author first set up a mechanical model using FEM method to determine the magnitude of tilt and strain near a dipping hydraulic fracture with regards to geologic parameters like root depth, base, water height and dip. A second hydrogeological model is set up based on meteorological data to predict water height variation in the fracture. The two models are coupled with the best fit parameters to simulate the tilt time series under water pressure variations near the fracture. Result from the coupled mechanical and hydrogeological modelling show a good agreement with observed tilt from tiltmeter. The results can be used to remove the hydraulic signals, In addition, more parameters about the fractured can be obtained by a reversing process. This study also offers suggestions in tiltmeter installation environment based on the modelling process. The highlight in this paper is the coupling of mechanical and hydrogeological modelling, which simulates the two process of between rainwater entering the ground and groundwater produce tilt. This method provides transient simulation of the total process.

5.4.3 Statistical analysis

With the deep burial design in Aquistore, tiltmeter is around 10 m below the groundwater table. The isolation effect of groundwater should keep the amplitude of rainfall signal small. In order to identify the tilt pattern, both visual inspection and statistical analysis are conducted. In this section, baseline tiltmeter data from Aquistore are analyzed for the occurrence of rainfall signal between May and August 2013. The starting month of May excludes the infiltration of melting snow and the following time period includes frequent precipitation events.

Visual inspection of rainfall signal is inconclusive for the baseline data. Tiltmeter reading usually exhibits a short-term drift following the rainfall event. However this pattern is not consistent, possibly due to overlapping of other noise signals. The observed tilt drift occurs after the rainfall event, following a downward or upward trend and gradually recovers back to the baseline level. Figure 5-15 below shows tilt data from one tiltmeter station with significant noise from frequent rainfall events during the period.

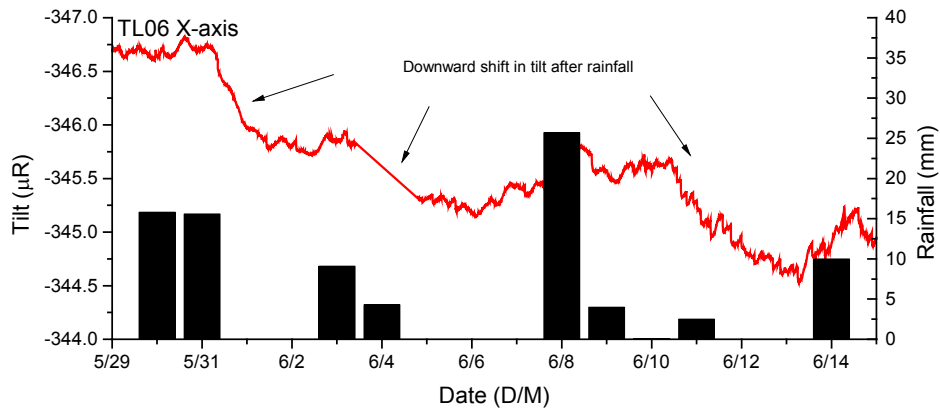


Figure 5-15: Baseline tilt pattern during a period of heavy rainfalls

In order to quantify the occurrence of rainfall tilt in Aquistore tiltmeters, a statistical verification process is implemented. This analysis compares 3 months of tilt and precipitation data to determine the correlation coefficient. Before statistical correlation, tilt data is filtered to reduce other type of noise signals as much as possible. High frequency noise including that from semidiurnal earth tide is removed by resampling tilt readings in daily readings. Then resampled data then passed through a low band filter (<0.05 cycle per day) to remove high wave length noise including possible tectonic drift, seasonal groundwater and temperature variations. To remove the highly coupled air pressure signals from the data series. The regression coefficient determined from the previous chapter is used. Daily derivatives of the processed data are analyzed with daily precipitations for cross correlation function. The processed daily derivative tilt data and daily precipitation data from weather station are represented in Figure 5-16 below.

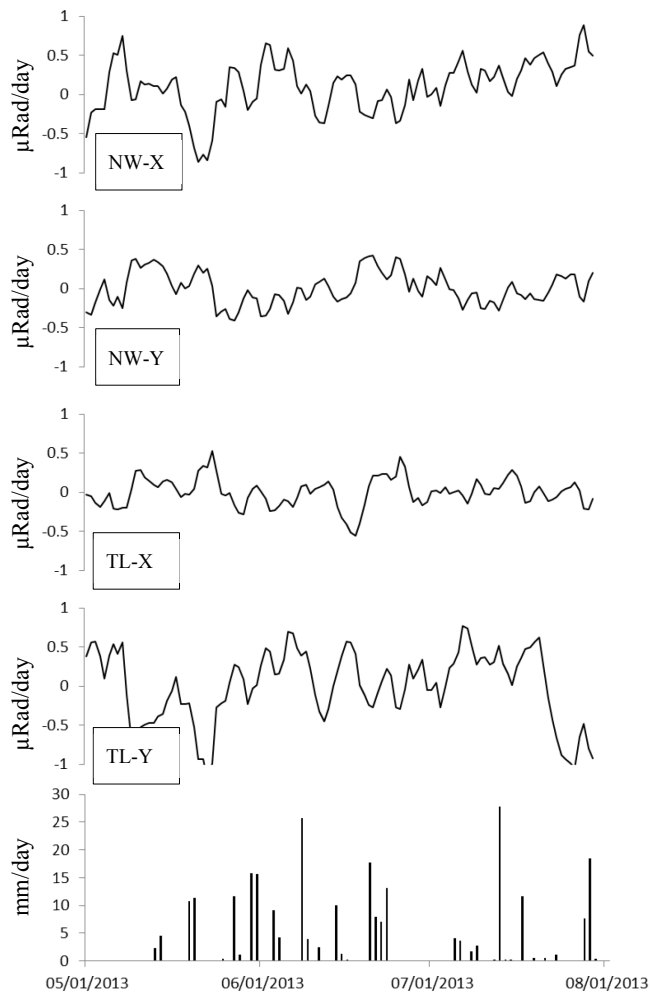


Figure 5-16: Daily variation tilt data from two tiltmeter in Aquistore and daily precipitation data

The dependency between daily tilt and precipitation is determined by their correlation coefficient. Normalized cross-correlation function (coefficient) $\rho_{ij}(t)$ with variable time lag (t) between the daily varied tilt data (i) and daily precipitation data (j) can be calculated as follows:

$$\rho_{ij}(t) = \frac{C_{ij}(t)}{\sqrt{C_{ii}(0)C_{jj}(0)}}$$

where

$$C_{ij}(t) = E\{[i(t) - \mu_i][j(t) - \mu_j]\}$$

and E is expected value and μ is the mean value of the data series. Correlation coefficient ranges from -1 to 1 where 1 and -1 implies perfectly linearly dependent and 0 implies no dependency. Results are plotted in Figure 5-17.

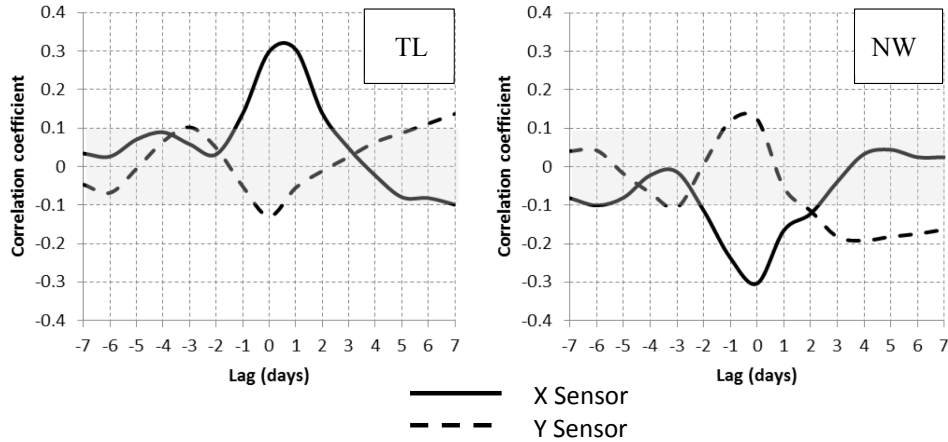


Figure 5-17: Cross-correlation function between daily tilt data and daily precipitation

The cross-correlation results indicate apparent correlation in both directions of TL06 and N-S direction of NW01. The E-W direction of NW01 only has noise-level oscillation. For tiltmeter TL06 a peak coefficient of 0.20 is reached with a lag of 1 day, indicating most correlated tilt pattern occurring one day after the rainfall. For N-S direction in tiltmeter NW01, a peak coefficient of 0.25 is reached with one day lag, indicating a stronger induced pattern than that of TL06.

It is noteworthy to point out that the peak correlation coefficients are low in a statistical point of view. This can be explained by the poor representation of rainfall series in statistics. As precipitation level is sampled at episodic time steps, grouping the data by daily steps is not a reliable representation of the overall intensity pattern. However the possible tiltmeter response to rainfall is not instantaneously either. The overlying soil layer works like a sponge that dampens the impact of precipitation. Therefore it is practical to process the data with the proposed method.

5.4.4 Discussion

Results from statistical analysis indicate that rainfall induced tilt pattern exists in Aquistore and the response of tiltmeter is delayed around one day. Developing a regression coefficient for removing rainfall signal is not feasible due to:

1. The rainfall series is different from the tilt series from a statistical point of view as the rainfall series only contains zeros and positive values;
2. Linear correlation between precipitation and tilt does not exist because the overlying soil layer is acting as a damping media for surface precipitation;
3. Precipitation is not the only factor that create the hydraulic signal tiltmeter receives, evaporation, surface runoff also contribute.

In order to quantify the tilt pattern induced by surface meteorological conditions, the above factors should be taken into account when developing a model. The key part of the model is to accurately

convert the input of meteorological factors into a time series of tilt signal. There are two approaches for the quantification, an empirical method and a defined physical approach. For the empirical approach, some previous studies have proved feasible through developing a rain function. After tweaking a few parameters of the rain function, the best-matched function will be used to quantify future rainfall signals. The limitation in this method is that it does not take into account any geologic settings (slope, soil type, groundwater conditions). With additional environmental and geological data available in Aquistore, a more refined empirical approach will be developed. For the deterministic approach, the physical mechanism of the rainfall signal should be first determined, then a model built upon the physical mechanism will be constructed to simulate the process. Both the empirical and deterministic approaches will be presented in the next chapter.

5.5 Thermal signal

5.5.1 Introduction

Noise signals created by environmental temperature fluctuations can be quite large for tiltmeters, depending on the installation geometry. Installing tiltmeters in boreholes can greatly minimize the thermal effects and it has become common for tiltmeter array installation when high accuracy is desired. Thermal noise still exists in borehole tiltmeters through damping effect of surface temperature fluctuations. Borehole tiltmeters are affected by downhole temperature variations in two mechanisms: sensor error and ground thermoelastic deformation. In this chapter both mechanisms are explained and analyzed for Aquistore tiltmeters. Temperature calibration test is proposed and conducted on all tiltmeters. Thermoelastic deformation is explained and briefly analyzed for the site conditions in Aquistore.

5.5.2 Temperature dependent behavior of sensor

5.5.2.1 Tilt sensor

Tiltmeter is sensitive to temperature. Surface tiltmeter is subject to the largest temperature change and therefore has the large noise effects. Tiltmeter installed in a borehole has a smaller response to temperature change due to the damping effect of the ground. The degree of sensor dependency is proportional to differential thermal dilation in the screws mounted at the base of the sensor as well as the overall steel housing of the sensors. The electrolytic transducer is subject to thermal fluctuations since the liquid is subjected to contraction and expansion. Borehole tiltmeters have a radial symmetry and are mostly affected by volumetric strain changes [32]. The following Figure 5-18 shows tilt reading exhibiting temperature-dependent trend in a stable tiltmeter setup in zero-vibration laboratory with fluctuating room temperature.

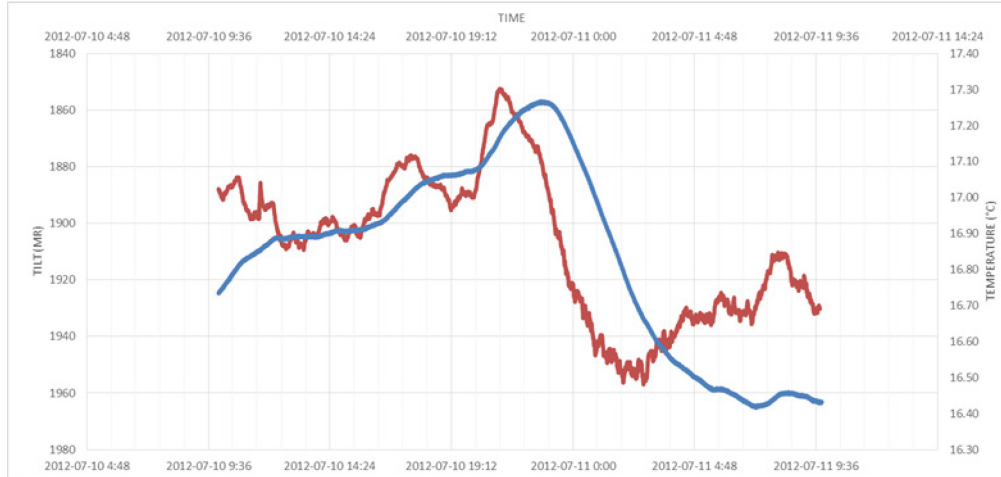


Figure 5-18: Tilt readings from laboratory zero-vibration temperature test

The effect of temperature reflects in tiltmeter reading as the change in scale factor (SF). Scale factor, expressed in $\mu\text{rad}/\text{mV}$, is the coefficient that is applied to raw voltage reading to get the tilt reading. Series 5000 tiltmeter has a factor default scale factor (SF_{def}) determined with calibration test by the manufacturer at a constant temperature (T_{def}). The thermal dilation of tiltmeter internal structure with fluctuating environmental temperature (T_{cal}) will lead to consequent change of scale factor SF_{cal} . Tiltmeter data processing software TiltTalk only considers the default scale factor and this will bring error to tiltmeter reading when temperature fluctuation exists. If the thermal effect on tiltmeter due to difference between environmental temperature and calibration temperature is not taken into account, the output tilt data will contain error. A thermal compensation test is proposed and conducted to all tiltmeter sensors that calibrate individual scale factors.

5.5.2.2 Thermal compensation test

Thermal compensation test calibrates the environmental scale factor that is related with environmental temperature. Figure 5-19 shows that a shift in temperature results in a shift in scale factor of a tiltmeter and a possible zero-shift. A dependency coefficient (D), which is the angle of the temperature-scale factor curve, is determined by combining multiple compensation tests.

$$D = \frac{\Delta SF_{\text{cal}}}{\Delta T_{\text{cal}}}$$

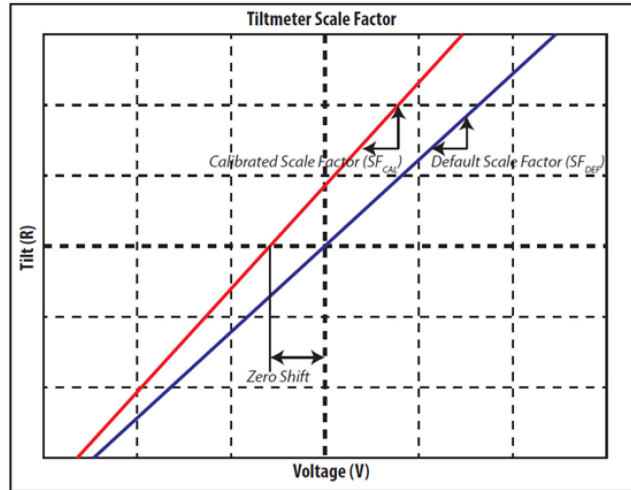


Figure 5-19: Shift in scale factor after a shift in environmental temperature

The calibration test is set up in an environmental chamber with controllable temperature. The detailed description of procedures of the test is shown in Appendix C. Figure 5-20 shows the setup of the test.

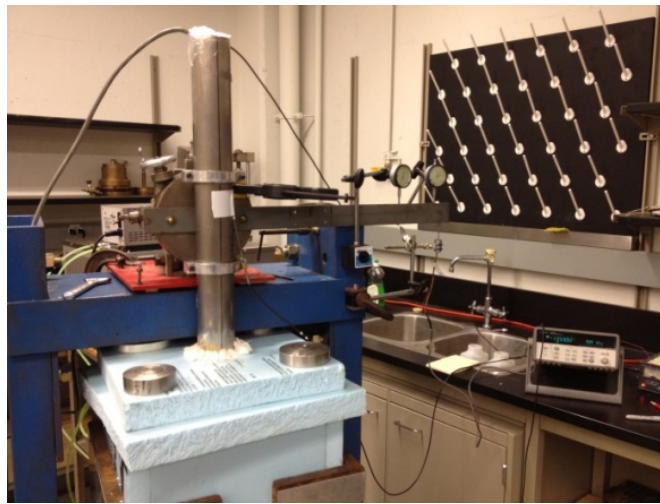


Figure 5-20: Thermal compensation test setup

The temperature trend of all calibration tests from different tiltmeters reveals the following characteristics.

Scale factors of most tiltmeters are linearly dependent on temperature (constant D) (Figure 5-21), while some (Figure 5-22) show a non-linear dependency. The linear dependency between the scale factor and temperature can be explained by the uniform dilation coefficient of the instrument as well as the conductivity change of the electrolyte fluid.

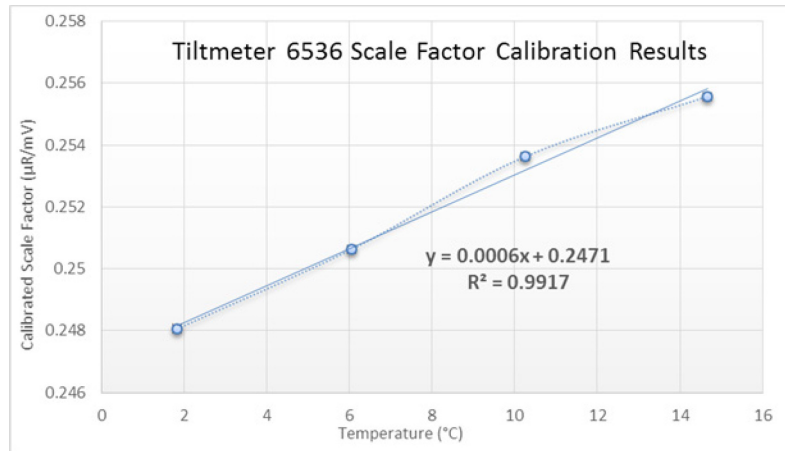


Figure 5-21: Tiltmeter 6536 showing a linear dependency between scale factor and temperature

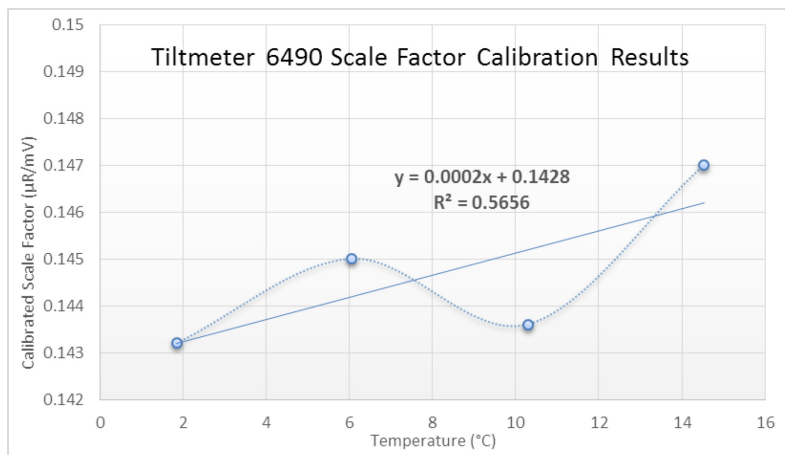


Figure 5-22: Tiltmeter 6490 showing a non-linear dependency between scale factor and temperature

Tiltmeters shows a positive dependency between scale factor and temperature, except one that shows a general negative correlation (Figure 5-23). Given the same internal structure of all 15 tiltmeter, this result is unexplainable.

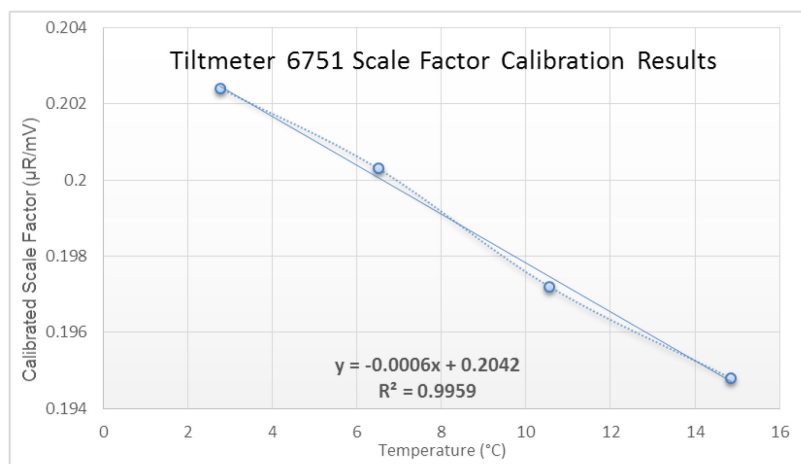


Figure 5-23: Tiltmeter 6751 showing a negative correlation between calibration factor and temperature

5.5.2.3 Conclusions

Sensor dependency is corrected by conducting scale factor calibration test on tiltmeters prior to field installation. With scale factor thermal dependency in $10^{-4} \mu R/mV \cdot ^\circ C$ range, downhole temperature fluctuations of less than $0.01 ^\circ C$ as observed by tiltmeter downhole sensor will not create enough noise signals (less than 1 nR) to be captured by tiltmeter. Therefore sensor dependency is not a source of noise signals in Aquistore field data due to the deep burial depth. However, this calibration method should be feasible for tiltmeter buried in shallow boreholes with more significant temperature change.

5.5.3 Thermoelastic tilt

The surface of earth is subject to thermal wave that follows the oscillation of solar radiation. Thermal wave damps in the soil and create a temperature field around tiltmeter borehole. Owing to the thermal expansion of soils, temperature oscillation will introduce thermoelastic deformation that produces tilt signals. These tilt signals can be considered as noise in tiltmeter recordings and the compensation of tilt signal using calibrated scale factor does not correct the thermoelastic tilt of the ground. In this section thermoelastic deformation is explained and the induced tilt will be estimated that offers a thermal noise interpretation for Aquistore tiltmeters.

5.5.3.1 Literature review

Tiltmeter reading is sensitive to temperature, as tiltmeter sensor is subject to thermal expansion, also because thermal fluctuation in the ground will cause thermoelastic deformation. Thermoelastic tilt refers to the signal created by temperature conciliation and the consequent ground deformation. Berger [33] introduced the formulation to calculate thermoelastic strain and tilt in an infinite and homogeneous half space, which laid the foundation for the later analysis of thermoelastic deformation for sensitive measuring devices, including tiltmeter.

Ricco, Aquino and Gaudio [32] presented the methodological approach to estimate thermoelastic signals for a tiltmeter monitoring system installed for volcano monitoring. They propose two methods to calculate the signal that can be used for thermal compensation. One general method is based on Berger's formula that introduce temperature field in the ground and tilt is created by the spatial variation of the field. A more specific method based on the method of Harrison and Herbst [34] method that estimate thermoelastic tilt under a long uniform slope, which essentially simplify Berger's temperature field into realization that is created by topography. The authors did not bring the two methods to practice though. Berger's solution is fundamental equations for thermoelastic deformation in any space. Harrison and Herbst's method do simplification to Berger's method that considers subsurface deformation under topography that defines the temperature field. However topography is not the only factor that controls subsurface temperature regime, therefore this method

is limited. And the equations for an infinite slope is unrealistic but can be easily adopted to take 2D and 3D situations.

Prawirodirdjo et al. [35] used a model to predict seasonal variations observed in interpreted GPS network. This model consists of an unconsolidated upper layer and an underlying elastic half-space. On the elastic layer a single standing wave of temperature is applied that introduce thermoelastic deformation in the elastic layer. They compare the computed thermoelastic strain to observed horizontal GPS series from three regions. The predicted thermoelastic strain fit well with observed data, that they conclude that the model captures the key first-order ingredient of thermoelastic strain in that area. The results can be used to reduce signal/noise ratio in GPS data. Their model is simplified from Ben-Zion and Leary [36], which assumes that variation in temperature field and thermal diffusivity creates a set of harmonic thermal waves and combining the solution of each single wave can provide the entire response of thermoelastic deformation in the elastic layer. They authors make the simplification due to limited information to describe the set of harmonic waves but their results still validate the successful prediction.

5.5.3.2 Downhole temperature profile

The thermal wave oscillation at surface has two main periods that follows solar radiation: a daily period and a yearly period. Surface ground temperature oscillation can be expressed in a sinusoidal wave

$$T_0 = A \cos(\omega t)$$

Where A is amplitude of wave, ω is angular frequency and t is time.

Thermal wave is attenuated and delayed when conducting to subsurface. Assuming the subsurface as a homogeneous half space with horizontal parallel thermal isotherms, according to heat conductivity equation, at a given depth z, the wave becomes:

$$T_z = A e^{-ky} \cos(\omega t - ky)$$

where $k = \sqrt{\frac{\omega}{2D}}$ the attenuation factor and D is the thermal diffusivity. According to the above equation, thermal wave decreases exponentially with depth according to k and is subject to a time delay that causes a phase shift compared to the surface thermal wave.

Theoretically, applying a typical soil thermal diffusivity of 0.0018 m²/h to Aquistore, a yearly thermic excursion of 30 degrees will be reduced to 0.00005°C at 30m, which is below the sensitivity of tiltmeter temperature sensor. In fact, subsurface environment for tiltmeter is not homogeneous, especially when considering that steel casing in the borehole has a much higher thermal diffusivity and that heat conduction in air is much faster than in soil, therefore the downhole temperature oscillation should be higher.

Figure 5-24 below shows the temperature readings in 2013 obtained from two downhole tiltmeter sensors. It is noted that temperature gradually decreases right after installation and remain stable after about three months. There is a recorded daily fluctuation of around 0.008°C and no clear yearly cycle during the one year range. The daily fluctuation recorded by tiltmeter sensor is unlikely from the surface heat wave as it is not proportional to the observed annual temperature fluctuation. The likely explanation is that the daily temperature fluctuation is produced by internal tiltmeter electronics.

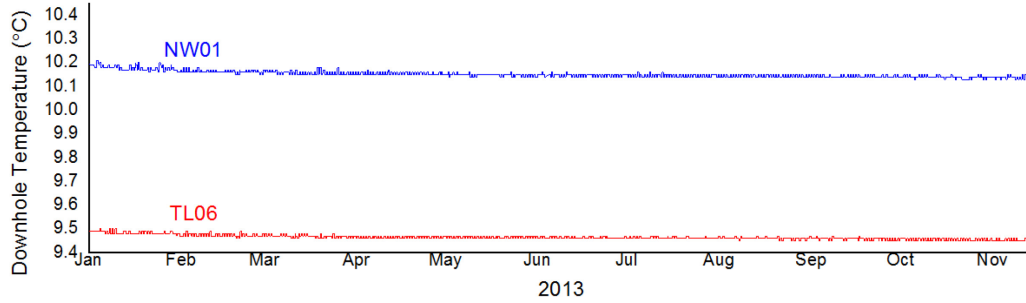


Figure 5-24: Downhole temperature record in 2013

5.5.3.3 Modelling

The surface of earth is subject to both temporal and spatial thermal waves. Propagation of heat wave will cause thermal deformation in the subsurface. Spatial thermal wave will create thermoelastic tilt in the ground.

According to two-dimensional model proposed by Berger (1975), consider a traveling temperature wave on an infinite homogeneous half space:

$$T_z = Ae^{-\gamma y} \cos i(\omega t - \kappa y)$$

Where $\gamma = \kappa \sqrt{1 + i\omega/D\kappa^2}$ is the attenuation factor and $\kappa = 2\pi/\lambda$ is the horizontal wave number.

Thermal dilation of the medium is:

$$\varepsilon = \beta T_z$$

Where β is the thermal dilation coefficient. At depth y , Berger's solution of horizontal plane strain gives:

$$\varepsilon_{xx} = \sum_{\omega} \frac{1 + \sigma}{1 - \sigma} \left(\frac{k}{\gamma + k} \right) \left(\left(2(1 - \sigma) + \frac{k}{\gamma - k} - ky \right) e^{-ky} - \left(\frac{k}{\gamma - k} \right) e^{-\gamma y} \right) (\beta T_{\omega} e^{i(\omega t + kx)})$$

$$\varepsilon_{yy} = \sum_{\omega} \frac{1 + \sigma}{1 - \sigma} \left(\frac{k}{\gamma + k} \right) \left(\left(-2\sigma - \frac{k}{\gamma - k} + ky \right) e^{-ky} + \left(\frac{\gamma^2}{k(\gamma - k)} \right) e^{-\gamma y} \right) (\beta T_{\omega} e^{i(\omega t + kx)})$$

The above solutions contain an equivalent thermal body force term falling off with depth as $e^{Re(\gamma)y}$, and an equivalent thermal surface traction term falling off as e^{-ky} . These two terms superposing as the thermoelastic strain at depth y .

Tilt can be derived from Berger's strain solution by $\Omega_y = \partial_x U_y$, where U_y is the y component of the displacement:

$$\Omega_y = i \sum_{\omega} \frac{1 + \sigma}{1 - \sigma} \left(\frac{k}{\gamma + k} \right) \left(\left(\frac{k}{\gamma - k} - (1 - 2\sigma) - ky \right) e^{-ky} - \frac{\gamma}{(\gamma - k)} e^{-\gamma y} \right) (\beta T_{\omega} e^{i(\omega t + kx)})$$

It is noted that thermoelastic tilt contains the same two terms as the strain solution.

Starting from Berger's solutions and considering the horizontal wavelength of the temperature field to be very large and exclude the traction term (e^{-ky}), Harrison and Herbst (1977) gives the solution for horizontal strain and tilt on thermal isotherm of a given slope (α):

$$\varepsilon_{xx} = \frac{1 + \sigma}{1 - \sigma} \beta T e^{-\gamma y} \cos(\omega t - \gamma y) \sin^2 \alpha$$

$$\Omega_y = \frac{1}{2} \frac{1 + \sigma}{1 - \sigma} \beta T e^{-\gamma y} \cos(\omega t - \gamma y) \sin 2\alpha$$

As this model does not take the traction term into account, it underestimates the theoretical tilt.

To estimate the magnitude of thermoelastic tilt on Aquistore tiltmeter readings, Thermoelastic strain and tilt is predicted with local temperature record and is compared with field tilt data.

The calculation adopted for Aquistore is based on the model of Harrison and Herbst with the following assumptions: (1) a homogeneous subsurface environment, (2) thermal isotherms are parallel with topography, and (3) a surface topography with a uniform slope much longer than the thermal skin. Ideally observed temperature variations at given locations can be combined and create a spatial characterization of the temperature field (Linette Prawirodirdjo, 2006), however this approach requires additional data that are not currently available to us.

Using typical values of $\sigma=0.33$, $\beta=10^{-5}$, surface annual temperature oscillation of 20°C will create strain of $4 \times 10^{-4} \sin^2 \alpha$, and tilt of $2 \times 10^{-4} \sin 2\alpha$ at surface. Assuming a surface slope of 15° , tilt at surface will be $100 \mu\text{R}$. Tilt variation with depth is the same as temperature attenuation and at 30m tilt will be $1.67 \times 10^{-4} \mu\text{R}$. According to above prediction, no thermoelastic tilt would arise from surface temperature oscillations.

Although theoretically thermoelastic tilt at -30m will not be detected by tiltmeter, tilt data right after installation is following the trend of temperature (Figure 5-25 and Figure 5-26). It is not known what caused the declining temperature trend, as during installation the surface temperature is well below 0°C . But given that daily fluctuations in the same period does not produce any scalable tilt signals, the initial trend in tilt is therefore unrelated to the initial temperature trend.

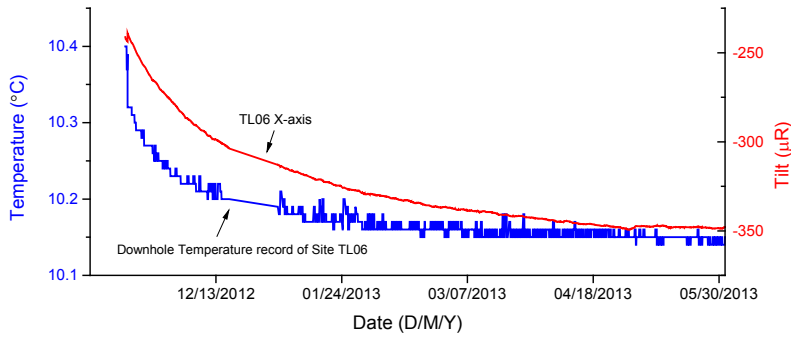


Figure 5-25: Downhole temperature and tilt reading after installation from TL06

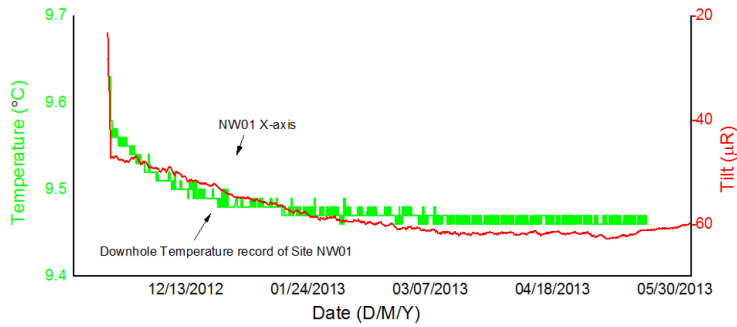


Figure 5-26: Downhole temperature and tilt reading after installation from NW01

A relocation of one tiltmeter at site NW02 provides an opportunity to investigate the influence of thermoelastic tilt in Aquistore, as shown in Figure 5-27. The tiltmeter is repositioned from 4.2 mbgs to 13 mbgs. Based on tiltmeter data before and after the event, two parameters are determined that can be used to calculate future thermoelastic tilt for this tiltmeter site (Table 5-5).

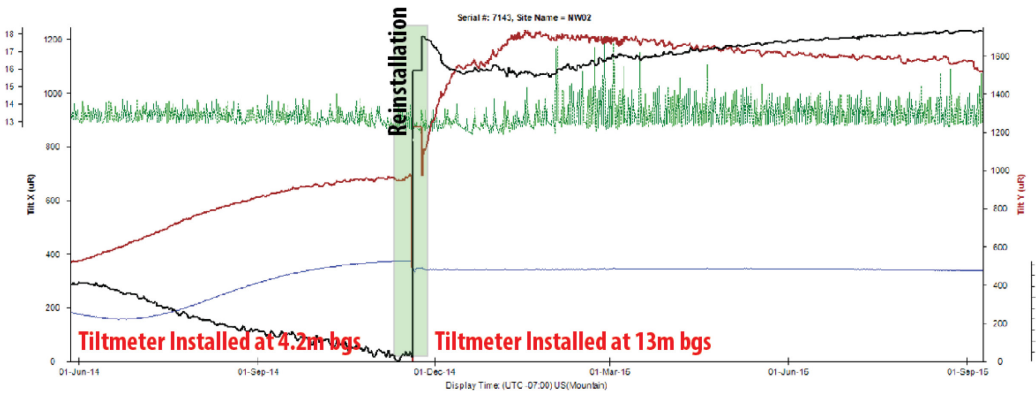


Figure 5-27: Tiltmeter data showing the impact from repositioning of the tool

Table 5-5: Back calculated Thermoelasticity parameters for site NW02

Depth	4.2 mbgs	13 mbgs
Theoretical temperature amplitude	-	0.81 °C
Observed temperature amplitude	10°C	0 °C
Back calculated thermal diffusivity	1.23 x10 ⁻⁶ m ² /s	
Theoretical thermoelastic tilt	-	23 μR
Observed thermoelastic tilt	290μR	0 μR
Back calculated βsin2α	29	

5.5.4 Discussion

Tiltmeter sensor is dependent on temperature though thermal dilation and conductivity change. Scale factor is used to convert voltage reading to tilt and can be calibrated according to temperature to offset this dependency. Laboratory testing shows a linear dependency between scale factor and temperature, which can be used to calibrate field data with downhole temperature record. But the change in coefficient of scale factor with the observed downhole temperature record will not create tilt above the detection limit of tiltmeter, therefore sensor-induced thermal signal does not exist in Aquistore.

Temperature change also creates thermoelastic strain and tilt in the ground. The scale of thermoelastic deformation is determined by both temporal and spatial temperature distribution of the thermal profile. Thermoelastic tilt, which can be registered by downhole tiltmeter, decreases exponentially with depth; therefore borehole tiltmeter can generally minimize the effects by installing at deep location. Theoretically, with the burial depth of 30m for Aquistore tiltmeters, temperature sensor should not register any change for the downhole temperature.

5.6 Seismic signal

5.6.1 Introduction

Seismic signal refers to the tilt pattern induced by seismic activity of both natural (i.e. earthquake) and man-made origins. Seismic activities generate compression and shear waves which will be captured by tiltmeter along its transmission. The pattern of seismic signals follows the nature of seismic shock waves. The amplitude of seismic signal is proportional to the energy level that tiltmeter receives.

5.6.2 Observed seismic signals

Multiple seismic events have been captured in baseline reading in Aquistore. In this section three incidences are reported. Figure 5-28 (a) shows the spike signal of a M7.7 earthquake centered 2269 km away in Alaska (55.368°N 134.621°W). Tiltmeters in Aquistore registered the signal of about 3 μR 5 minutes after the earthquake occurred on Jan. 5th 2013. On Sept. 3rd 2013 a series of three

major (M6.2, M4.3, M5.6) earthquakes occurred in British Columbia, Canada (51.05°N, 130.62°W), about 1923 km away. Both tiltmeters registered the M6.2 and M5.6 events with spikes of about 0.025 μR , as shown in Figure 5-28 (b). The seismic program in Aquistore was conducted with dynamite shooting investigations and seismic signals were also captured. In this case only nearby shootings created signals detected by tiltmeter with spikes between 2-5 μR , as shown in Figure 5-28 (c). The amplitude of seismic signals is proportional to the energy level that tiltmeter is exposed, determined by magnitude of seismic event and relative distance.

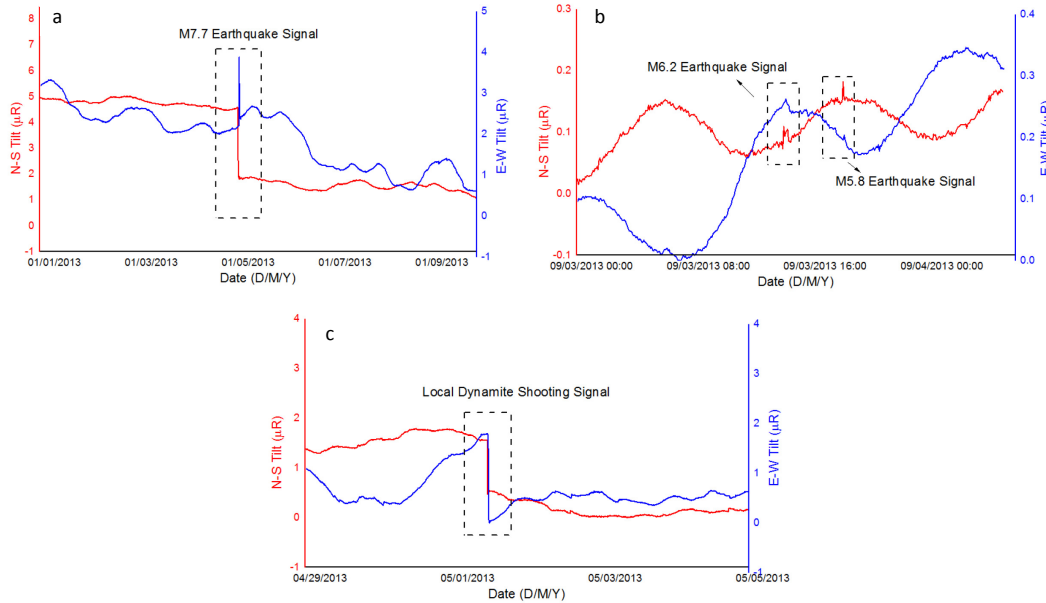


Figure 5-28: Tilt signals reflecting by seismic activities

5.6.3 Discussion

Based on analysis of three major earthquake occurrences in tiltmeter TL06, there is no clear relevancy between earthquake bearing and tiltmeter movement. Amplitude of tilt signal shows a positive relationship to earthquake magnitude and distance as shown in Figure 5-29.

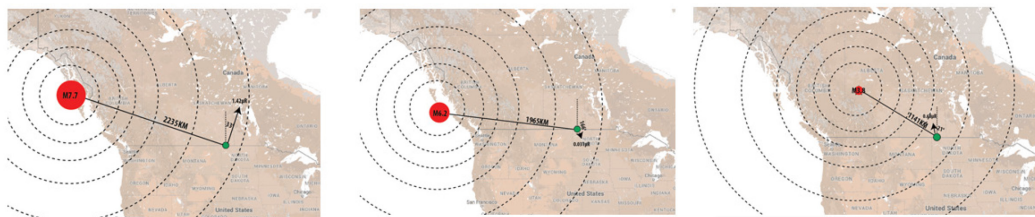


Figure 5-29: Illustrative figures showing magnitude distance of earthquake, and corresponding movement of tiltmeter TL06

Based on the time between earthquake occurring and tiltmeter register the signal (Table 5-6), tiltmeters may receive both compressional and shear waves of seismic activities. As tiltmeters respond to local manmade seismic activities during the baseline phase, it is very likely that tiltmeter will capture injection-induced microseismic signal during the monitoring phase. Therefore it is

recommended that origins of large spikes be verified by referencing Natural Resourced Canada earthquake records during reservoir surveillance.

Table 5-6: Calculated seismic wave speed compared to theoretical seismic wave speed

Earthquake Magnitude	Distance (km)	Tiltmeter responding time	Calculated seismic wave speed	Speed of Primary Wave	Speed of Secondary Wave
M7.7	2235	240s~360s	6200~9300	1000-8000-	1000-8000
M6.2	1965	360s~600s	3200~5500	14000	Loose
M3.8	1141	120s~180s	6300~9500	Water-Crust-Mantle	sediments-Mantle

CHAPTER 6 Numerical Modelling of Episodic Rainfall Tilt Pattern

In this chapter, a rainfall-tilt model is presented that simulates the movement of tiltmeter under surface precipitation events. This simulation consists of sequential modelling of surface infiltration, movement and distribution of rainwater, and the induced ground displacement. The derived tilt pattern from this model is compared to tilt signals captured by tiltmeter and will be used as a reference for quantifying rainfall signals in Aquistore.

6.1 Framework of modelling

Rainfall-tilt model is intended for the estimation of tilt signals captured by downhole tiltmeters. This model should combine the input of surface meteorological into the process of surface infiltration, which sequentially creates subsurface seepage that leads to altered distribution of groundwater. Ground deformation reflects on groundwater dynamic and can be used to obtain tilt pattern. The model is comprised of three sequential stages of modelling. Figure 6-1 and Figure 6-2 describes the framework of the rainfall-tilt model.

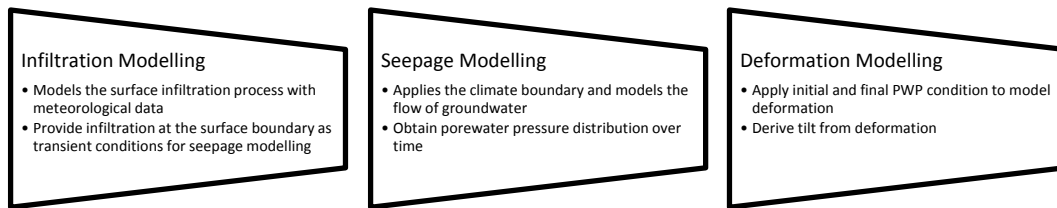


Figure 6-1: Framework of rainfall-tilt model

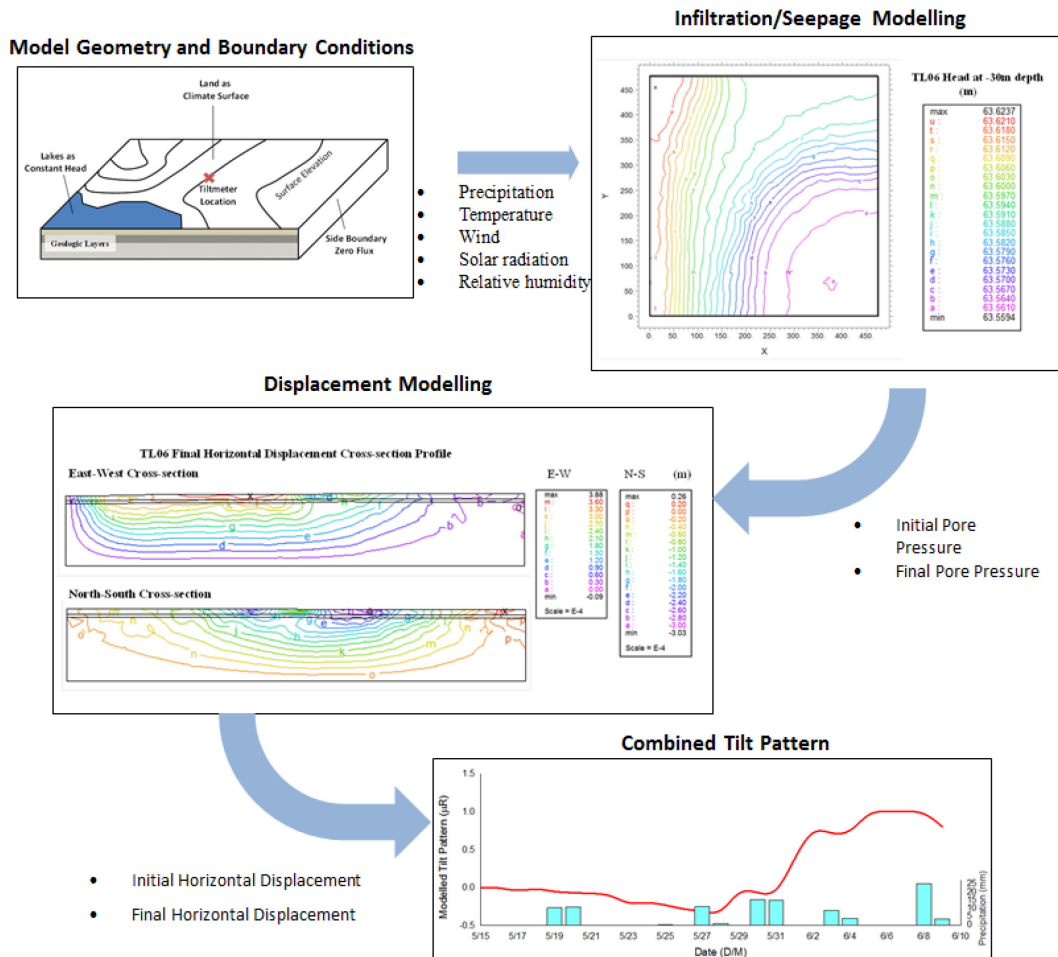


Figure 6-2: Flowchart of simulation components in the rainfall-tilt model

6.1.1 Infiltration modelling

Infiltration modelling is the first stage that simulates the atmosphere-soil interaction at ground surface. Infiltration is determined by three components that are present at ground surface: precipitation, evaporation and runoff. The output infiltration is a distribution of moisture movement rate applied as the upper transient boundary conditions in the second seepage modelling stage.

Precipitation is the downward flux, determined by the rate of rain volume. The snow melting in spring is also considered as infiltration, which accumulates through the winter season and release during thaw. Precipitation data is in the format of millimetres per unit area. Precipitation is the only add-on in infiltration calculation, which is limited by the saturated coefficient of permeability [37]. When the intensity of precipitation exceeds the capacity of infiltration, the excess precipitation will become runoff.

Evaporation is the upward flux, removing water from the soil. Evapotranspiration is the process of vegetation taken up moisture from surface that is often regarded as part of total evaporation. This

process is not considered in this modelling given the field is mostly covered in short grass. Evaporation is determined by atmospheric factors including temperature, wind speed, relative humidity and solar radiation and limited by soil conditions. Penman [38] proposed the equation to calculate potential evaporation based on atmospheric factors on a saturated surface.

$$PE = \frac{\Delta R_n + \rho_a c_p (\delta e) g_a}{\lambda_v (\Delta + \gamma)}$$

Where:

Δ = Slope of the saturation vapor pressure curve (Pa K⁻¹)

R_n = Net irradiance (W m⁻²)

ρ_a = density of air (kg m⁻³)

c_p = heat capacity of air (J kg⁻¹ K⁻¹)

g_a = momentum surface aerodynamic conductance (m s⁻¹)

δe = vapor pressure deficit (Pa)

λ_v = latent heat of vaporization (J kg⁻¹)

γ = psychometric constant (Pa K⁻¹)

The modified Penman's equation by Gitirana et al.[39] uses climate data for evaporative fluxes:

$$PE = \frac{\Delta Q_N + E_a \gamma}{\Delta + \gamma}$$

Where:

Q_N = heat budget (m*day)

$E_a = f(u) p_v^{air} (1-RH)$

$f(u) = 0.35(1+0.15U_a)$

U_a = wind spees

RH = relative humidity

p_v^{air} = vapor pressure above surface

Heat budget is determined by solar radiation, and the term E_a is calculated based on relative humidity, wind speed and air temperature.

A limiting function by Wilson [40] is used to account for soil unsaturation at surface of bare ground:

$$AE = PE \left(\frac{p_v - p_v^{air}}{p_{vsat} - p_v^{air}} \right)$$

Where:

p_v = vapor pressures (kPa) of the material surface

p_v^{air} = vapor pressures (kPa) of air near ground

p_{vsat} = vapor pressures (kPa) of under complete saturation

The above vapor pressures are calculated based on temperature and relative humidity, the vapor pressure above ground is also determined by moisture content of the soil at surface.

Infiltration is the net flux of the downward precipitation and upward evaporation, and lateral runoff if occurred. The following equation is used to calculate net flux on bare ground [39]:

$$NF = \begin{cases} P \cos \alpha - AE & : \text{when } u_{ws} < 0 \\ EF(0 - u_{ws}) & : \text{when } u_{ws} > 0 \end{cases}$$

where α is the angle of surface slope, u_{ws} is the porewater pressure at surface and EF is a large number. The condition of u_{ws} represent the saturation of surface. When suction exists in ground surface, no runoff would occur. When a positive water pressure is reached during extensive rainfall, the infiltration rate is limited and equals to maximum seepage velocity determined by the permeability and water head.

6.1.2 Seepage modelling

The second stage models the transient seepage conditions in the ground. This stage simulates the moisture flow in the soil system under from surface transient infiltration, where both precipitation and evaporation are involved. Surface infiltration is the variable in this modelling process, restrained by soil hydraulic properties. Porewater pressure distribution profiles are estimated and are varying with time. These profiles are imported to the deformation stage as variables.

Seepage modelling is the simulation of moisture flow in the model. Seepage flow is driven by water head difference, which is created by surface infiltration in this case. The flow is governed by the hydraulic properties as well as the storage coefficient of the soil. Assuming water is incompressible and deformation is incrementally infinitesimal, the water continuity equation is as follows [37]:

$$\frac{\partial \theta_w}{\partial t} + \nabla(v_w) = 0$$

where:

θ_w = water content

t = time

∇ = divergence operator

v_w = Darcy's flux

According to water phase constitutive relationship in unsaturated soil, water content θ_w can be expressed as [41],

$$\frac{d\theta_w}{\theta_w} = [m_1^w d(\sigma - u_a) + m_2^w d(u_a - u_w)] * \gamma_w$$

where:

m_1^w, m_2^w = coefficient of water volume change i with respect to net stress and matrix suction

$\sigma - u_a$ = net normal stress

$u_a - u_w$ = matrix suction

γ_w = unit weight of water

According to Darcy's Law, Darcy's flux in the I direction v_{wi} can be expressed as,

$$v_{wi} = -k_{wi} \frac{\partial h}{\partial i}$$

Where:

k_{wi} = hydraulic conductivity in the I direction

h = hydraulic head

Substituting θ_w and v_{wi} in the continuity equation and ignore the change in net normal stress, the differential equation for three-dimensional flow is:

$$\frac{\partial}{\partial x} \left(k_{wx} \frac{\partial h}{\partial x} \right) + \frac{\partial}{\partial y} \left(k_{wy} \frac{\partial h}{\partial y} \right) + \frac{\partial}{\partial z} \left(k_{wz} \frac{\partial h}{\partial z} \right) = m_2^w \gamma_w \frac{\partial h}{\partial t}$$

This equation applies for both unsaturated and saturated materials and for both transient and steady state flow. For saturated soil, water storage equal zero and only saturated permeability is required to solve the equation. For unsaturated soil, two soil properties (i.e. coefficient of permeability k_w and water storage coefficient m_2^w) are required to solve the transient seepage problem.

Water storage coefficient is the derivative of soil-water characteristic curve and it describes the ability of unsaturated soil to absorb water per unit change in matrix suction. Soil-water characteristic curve (SWCC) is a relationship between soil suction and moisture content. This curve is particular for each type of soil and it's a widely used property in unsaturated soil mechanics. SWCC can be determined experimentally and further fitted using empirical equations. SWCC can also be determined through grain size distribution (GSD) curve [42]. There are several equations proposed to fit existing SWCC data, e.g. Fredlund and Xing [43], Genuchten [44], Gardner [45]. In this case, the equation proposed by Fredlund and Xing is used and has the following form,

$$\theta_w = \theta_s \left\{ \frac{1}{\ln[e + (\frac{\Psi}{a})^n]} \right\}^m$$

Where:

θ_w = volumetric water content of

θ_s = volumetric water content at saturation

Ψ = soil suction

a = soil parameter related to air entry value

n = soil parameter that controls the slope at the inflection point in SWCC

m = soil parameter that is related to residual water content of the soil

This equation can either be used to fit existing SWCC points or apply a , n and m parameters to estimate the curve. Storage coefficient can be expressed as,

$$m^w = \frac{\partial \theta_w}{\partial \Psi}$$

Permeability indicates the ability for fluid to pass through porous. Permeability is determined by the intrinsic permeability of the material and the degree of saturation, which is a function of soil suction. For saturated material permeability is only dependent on intrinsic permeability and stays constant. Unsaturated permeability also depends on soil suction, which lowers the permeability below intrinsic value. The unsaturated soil permeability can be determined either experimentally or empirically. There are several methods proposed that express unsaturated permeability as a function of soil suction (Fredlund et al. [46], Gardner [45], Leong and Rahardjo [47]). These equations give the best-fit parameters which produce a curve fitting the measured data or data estimated from the soil-water characteristics curve. The method used in this case is modified Campbell method. This equation produces a curve between a constant saturated permeability and a constant residual permeability when soil suction reaches residual.

$$k = k_s \left(\frac{\theta_w}{\theta_s} \right)^{2b+2}$$

Where:

k_s = saturated permeability

b = empirical determined constant

With the continuum equation for seepage flow and the expression for storage coefficient and saturated/unsaturated permeability, porewater pressure distribution can be obtained with time and be used in the deformation analysis to provide deformation simulation.

6.1.3 Deformation modelling

The third stage model ground deformation under changing porewater pressure. Deformation is calculated with certain time interval by applying initial and final conditions of porewater pressure distribution obtained from seepage modelling. The modelling outcome is a dynamic deformation profile that can be used to resolve tilt.

This model only considers surface infiltration as the only source that creates porewater pressure variation. This simplification excludes other sources of groundwater replenishment including lateral flow, as the information is not available. The impact of other groundwater replenishment is in longer wavelength than that from rainfall, therefore the induced tilt may not in the same frequency domain. As the captured tilt series is a composition of various types of baseline signals, these effects, if prominent, can be added back to the modelled results through independent modelling when adequate data becomes available.

Deformation modelling is the simulation of soil matrix displacement due to change in stress state. For unsaturated soil, effective stress is the only stress state variable whereas for saturated soil, two stress state variables controls the final strain [48]. The change in stress state will induce deformation governed by the overall static equilibrium of the structure,

$$\frac{\partial \sigma_{ij}}{\partial x_j} + b_i = 0$$

Where:

σ_{ij} = net total stress tensor

b_i = body force vector

In this case, the body force tensor is unit body weight for the vertical direction and zero for horizontal direction. In order to obtain the differential equation for displacement, the net stress tensor can be expanded with stress-strain relationship and strain-displacement relationship.

The constitutive stress-strain relationship for soil structure can be expressed with elasticity parameters. For unsaturated soil with three phases (solid, water and air), the relationship can be expressed as an incremental elasticity,

$$d\varepsilon_{ii} = \frac{1}{E} d(\sigma_{ii} - u_a) - \frac{\mu}{E} d(\sigma_t - \sigma_{ii} - 2u_a) + \frac{1}{H} d(u_a - u_w)$$

$$d\gamma_{ij} = \frac{d\tau_{ij}}{G}$$

Where:

ε_{ii} = normal strain in the i-direction

τ_{ij} = shear strain ($i \neq j$)

E = modulus of elasticity or Young's modulus

G = shear modulus [$G=E/(2+2\mu)$]

H = modulus of elasticity for the soil structure with respect to change in $(u_a - u_w)$

σ_{ii} = total normal stress in the i-direction

σ_{ij} = shear stress ($i \neq j$)

$\sigma_t = \sigma_x + \sigma_y + \sigma_z$

u_a = pore air pressure

u_w = pore water pressure

Volumetric strain ε_v can be expressed as,

$$d\varepsilon_v = 3\left(\frac{1-2\mu}{E}\right)d(\sigma_{mean} - u_a) + \frac{3}{H}d(u_a - u_w)$$

Where:

$$\sigma_{mean} = (\sigma_x + \sigma_y + \sigma_z)/3$$

The strain can be expressed in displacement as,

$$\varepsilon_{ij} = \frac{1}{2}\left(\frac{\partial u_i}{\partial x_j} + \frac{\partial u_j}{\partial x_i}\right)$$

Where:

u_i = displacement in the i-direction

Combining structure equilibrium equation, stress-strain equation and strain-displacement equation we have the differential equation between change in stress state variable and the induced displacement [49],

$$G\nabla^2 u_i + \frac{G}{1-2\mu} \frac{\partial \varepsilon_v}{\partial x_i} - \beta \frac{\partial (u_a - u_w)}{\partial x_i} + \frac{\partial u_a}{\partial x_i} + b_i = 0$$

Where:

$$\beta = E/H(1-2\mu)$$

$$\nabla = \frac{\partial^2}{\partial x^2} + \frac{\partial^2}{\partial y^2} + \frac{\partial^2}{\partial z^2}$$

The equations are continuous for saturated soil, as positive porewater pressure is reached and pore air pressure becomes constant (i.e. zero).

The differential equation for displacement requires net normal stress and matrix suction (effective stress in saturated condition) as variable and elasticity parameters E , H and μ as constraints to solve (for the vertical direction, unit body weight is also required). The elasticity parameters E and H used in the analysis are functions of stress state. The coefficients can be expressed with either coefficient of volume change (m_1^s and m_2^s) or volume change index (C_s and C_m), which can be obtained experimentally. The expression is subject to loading conditions. For three dimensional loading,

$$E = 4.605 * \frac{(1 + \mu)(1 - 2\mu)(1 + e_0)}{C_s} (\sigma - u_a)$$

$$H = 4.605 * \frac{(1 + \mu)(1 + e_0)}{C_m} (u_a - u_w)$$

where e_0 is the initial void ratio.

C_s is volume change index with respect to net mean stress and C_m is volume change index with respect to matrix suction. For unsaturated soil, these two indices characterize the surface of void ratio with respect to matrix suction and matrix suction. For cross-section of the surface with a given matrix suction or net mean stress, the slope remains constant and equals to C_m and C_s . Gitirana describes the surface used in the analysis with the following equation,

$$e = e_{1kPa} - C_s (\log_{10}(\sigma_{mean} + \Psi \frac{C_s}{C_m} - 1))$$

The two Indices can be obtained experimentally, C_m can be obtained from shrinkage curve and C_s can be obtained from consolidation curve.

The detailed modelling description and procedures are explained in the following section.

6.2 Modelling description

Based on the modelling framework described in the previous section, two separate models are built and tested using SV Flux. The first is a simplified 2D model that aims to achieve the best fit to observed tilt pattern. The second is a 3D model based on site topographical and hydrogeological conditions that aims to simulate tilt in regional scale. Both models are used to estimate tilt pattern for the same tiltmeter site. Following the same simulation stages, two models differ on dimension, geometry and boundary conditions. Simulated with the same period of meteorological data, their results are presented and compared with observed tilt pattern.

6.2.1 Dimension and geometry

6.2.1.1 2D Model

2D model assumes the pattern of tilt is linearly dependent on the intensity of rainfall. This assumption requires a constant spatial distribution of rainwater across the region. This model presents a simplified scenario where groundwater recharge and discharge locations are constant and the intensity of rainfall is small. In the 2D model the spatial distribution of rainwater is not modelled, but a range of distribution scenarios are tested to find the best match with observed tilt pattern. The purpose of 2D model is to find a set of model dimensions and a correction coefficient to optimally fit modelling results to actual measurement and use this simplified model for further noise reduction.

In order to create a model that best fits with observed tilt pattern; a flat model is adopted (Figure 6-3). The model have a depth of 50m and a width of 600m. Three geologic layers exist according to the borehole log during construction. The top layer is 5 m of fissured clay, overlying a silt layer of 3 m. The bottom layer is 42 meters of till.

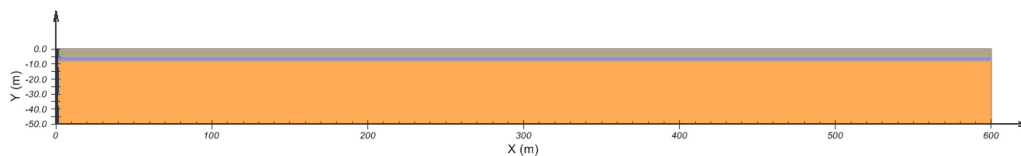


Figure 6-3: 2D model geometry

6.2.1.2 3D model

3D model simulates the distribution of rainwater by introducing topography and local discharge areas into the model. Therefore location and orientation becomes relevant when estimating tilt pattern. Theoretically 3D model is more accurate in representing the actual impact of rainfall in the area and has the advantage of explaining the difference displayed in the two axis of tilt. However a lack of comprehensive description of regional environment and the scale effect limits the accuracy of the model. For the modelling in Aquistore, the topography and existing groundwater discharges are incorporated into the model. However regional soil inhomogeneity and variation in groundwater regime will bring uncertainty to the model therefore 3D model is best worked with 2D model for validation and reference.

3D modelling introduces topographical and hydrogeological factors into the model by adopting the geometry from digital elevation map. The model is 475 m by 475 m in dimension. Elevation is based on the digital elevation grid (25 m by 25 m) with a resolution of 0.5 m. The model has a base elevation of 80 m. The geologic layer system is the same with the 2D model, overlying parallel to surface topography. Two locations are modelled in this study for two tiltmeter sites (TL06 and NW01). The regional overview of the two tiltmeter sites is shown in Figure 6-4.

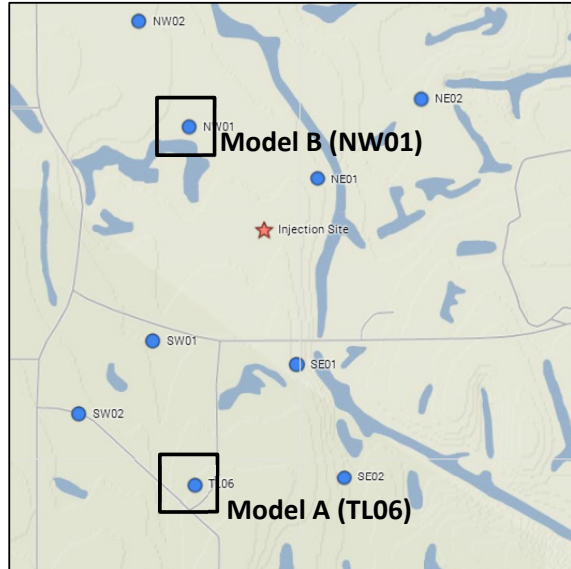


Figure 6-4: Planar view of modelling areas of 3D model

Model A for tiltmeter TL06 is a 3D model with only elevation as global constraints. This model can be used to quantify the influence of surface elevation on amplitude of rainfall induced tilt. The model is 475m by 475m in planar view, centered on the TL06 station. This area has a total elevation difference of 4m with the highest elevation in northwest and lowest elevation in southeast. The model is 66m to 70m tall, with three material layers parallel to ground surface. There is no surface water in this area. The initial groundwater table is set at static state at 62m elevation and climate boundary is applied uniformly across the surface. The surface contour of this model is shown in Figure 6-5.

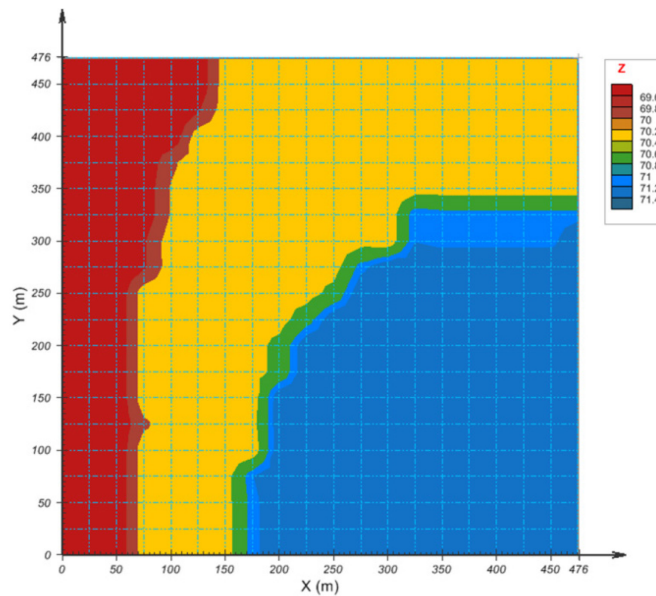


Figure 6-5: 2D surface geometry of Model A

Model B for tiltmeter NW01 is a 3D model with mild elevation change and a surface discharge area. This model can be used to quantify the influence of hydrogeological on rainfall tilt pattern. The model is 475m by 475m in planar, centered on the NW01 station. This area has a total elevation difference of 2 m that dips towards south. The model is 69 m to 70m tall, with three material layers parallel to ground surface. There is a surface lake in the southwest area. The lake is characterized in the mode with a depression covering an area of 100m by 350m. Lake water is static set at 66m in elevation, which is also the groundwater table initially for the model. The boundary condition above the lake area is set as static head of 66m elevation while climate boundary is applied uniformly across the rest of the surface. The surface contour of this model is shown in Figure 6-6.

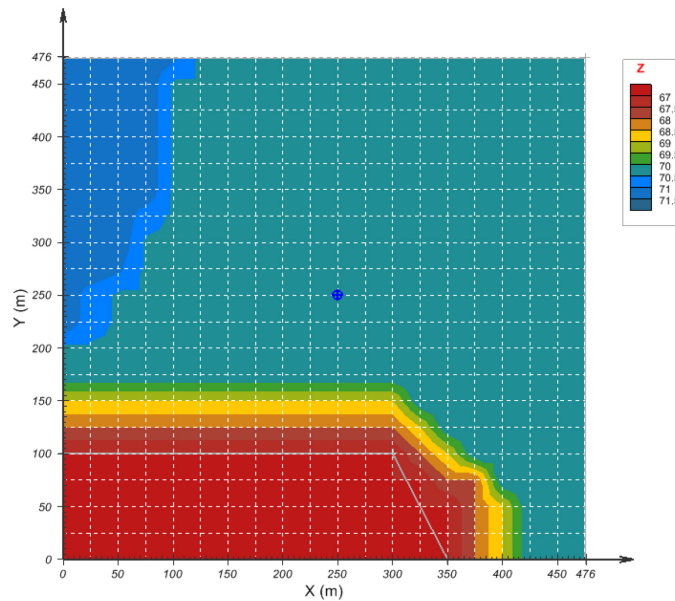


Figure 6-6: 2D surface geometry of Model B

The 2D model is used for quantitatively estimate the induced tilt by assuming a constant distribution of rainwater in groundwater table. The 3D model is a more realistic representation of field conditions with the actual topography and surface water bodies defining this distribution. With 2D model the match between theoretical result and observed data can be used to back deduct the actual slope of porewater pressure gradient. While in 3D model the gradient is modelled. However, these conditions are not adequate in defining the porewater gradient for field conditions. 3D model is best worked with 2D model for validation and reference.

6.2.2 Infiltration modelling

6.2.2.1 Modelling setup

Infiltration modelling is the first stage of rainfall-tilt model that simulate atmosphere-ground surface interaction that result in timely infiltration flux. Atmospheric factors are applied to the surface of

the model. The only geometric factor that has influence on the process is surface slope in 3D setup. Otherwise the simulation can be considered 1D.

This modelling stage is coupled with the seepage modelling as the change in surface suction will affect actual evaporation and runoff, although the deviation is small compared with potential evaporation and zero runoff conditions as the rainfall is mostly small. Material type at surface is fissured clay. The saturated permeability is 0.086 m/day, which set up a cap in infiltration once the surface soil is fully saturated. The detailed material information will be covered in the seepage section. As infiltration is coupled with seepage modelling, the initial condition is the same. Water table is set to be 8 m below surface and suction profile above water table is in hydrostatic condition.

6.2.2.2 Input

Climate data is applied above the surface and act as boundary conditions in this stage. Net flux is calculated as the sum of precipitation, actual evaporation and runoff. Precipitation data is collected by the rain gauge from the weather station. The weather station also provides air temperature and wind speed data for the calculation of potential evaporation. Other required data for evaporation include relative humidity and solar radiation. Relative humidity is obtained from nearby station in Estevan via Environment Canada website. Solar radiation data is not available for the proximity and it's set to constant of 20 MJ/(m²*day).

The following Figure 6-7 to Figure 6-10 shows climate data applied that simulates the infiltration flux between May 15th and June 15th 2013. The sampling rate is daily. Incremental and cumulative precipitation is presented in Figure 6-7. A total of 123.7mm for the study period is collected. A maximum daily precipitation of 25.7mm was measured on June 8th. Figure 6-8 shows the hourly and daily average temperature. Figure 6-9 shows the daily average wind speed data. Figure 6-10 shows the daily average relative humidity data.

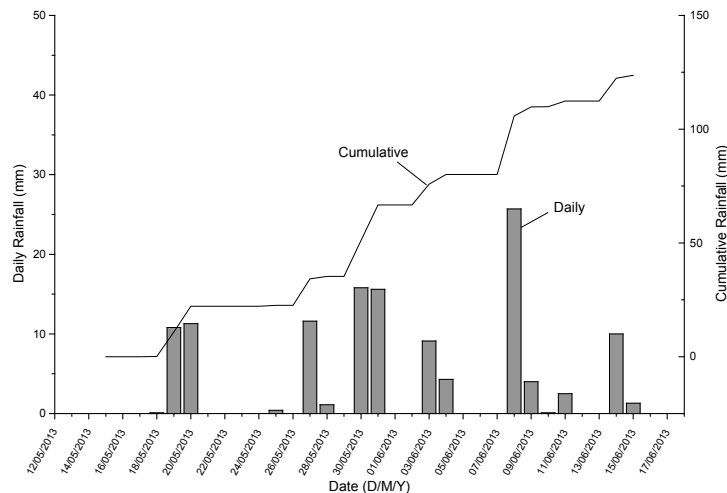


Figure 6-7: Daily and cumulative precipitation data used for modelling

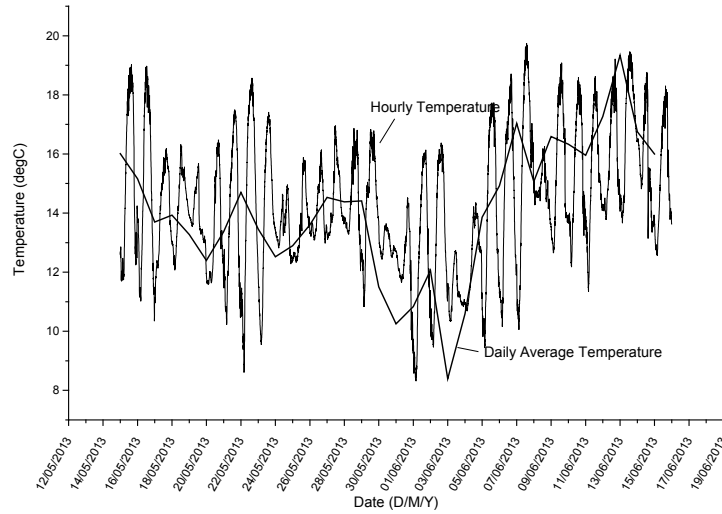


Figure 6-8: Daily air temperature data used for modelling

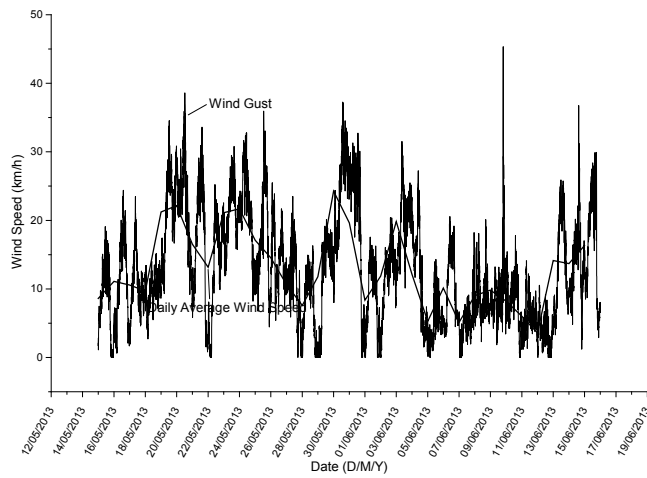


Figure 6-9: Daily wind speed data used for modelling

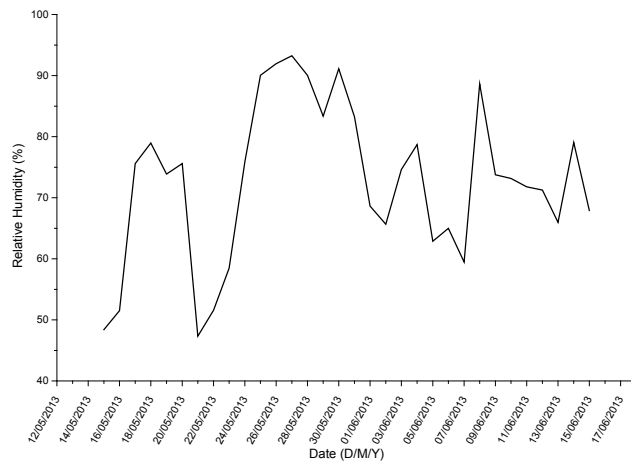


Figure 6-10: Daily relative humidity data used for modelling

6.2.2.3 Output

Results from infiltration modelling include daily net flux data as the sum of daily precipitation flux, daily actual evaporation flux and daily runoff. The net flux indicates that during the period total precipitation exceeds total evaporation and no runoff occurs, which leads to an overall downward flux of water into the ground. For a 25-day period, a 5 cm of water accumulates per unit area. Net flux will be applied as the surface boundary condition in the following seepage analysis.

6.2.3 Seepage modelling

6.2.3.1 Modelling setup

Seepage modelling is the second stage of the rainfall-tilt model. The first stage infiltration is coupled with seepage modelling as the boundary condition at surface. Seepage models the water movement from surface, going through the unsaturated soil layer, reaching and affecting groundwater. Seepage modelling is a transient process which gives the porewater pressure distribution with time. The movement of surface infiltration is governed by soil permeability and storage properties and will change porewater pressure distribution from the initial state. This modelling will provide transient pore water pressure data that will be used as initial and final conditions in the following deformation modelling.

Seepage modelling in 2D and 3D setup is basically using the same simulation codes. The difference lays in the choice of boundary conditions, as 3D modelling uses the boundary conditions from the field while 2D modelling uses simplified boundary conditions.

6.2.3.2 Material assignment

Seepage modelling requires material properties including hydraulic conductivity, volumetric water content. For saturated soil, both two parameters are defined as intrinsic properties. For unsaturated soil, both two parameters are also functions of soil suction. In this study soil property are chosen based on soil characterization using a soil database from SoilVision. The database gives field-tested data points, which are further smoothed using empirical equations.

Volumetric water content (VWC) has the maximum determined by porosity and reduces with increasing soil suction defined by SWCC curve. In this study Fredlund and Xing method (1994) were used to fit the existing data points. The following Table 6-1 summarizes the saturated VWC used in the model.

Table 6-1: Soil VWC and SWCC used in seepage analysis

Material	Saturated VWC	Fredlund and Xing Fit		
		Af (kPa)	nf	mf
Fissured Clay	0.492	13	0.73	0.32
Silt	0.4	65	0.85	1.46
Till (Saturated)	0.25	-	-	-

Hydraulic conductivity has the maximum determined by intrinsic conductivity when saturated and decreases with increasing soil suction defined by the unsaturated hydraulic conductivity curve. In this study the modified Campbell method is used to fit data points obtained for each material type. The following Table 6-2 summarizes the saturated hydraulic conductivity used in this model.

Table 6-2: Soil unsaturated permeability used in deformation analysis

Material	Saturated hydraulic conductivity (m/d)	Modified Campbell Fit	
		K minimum (m/d)	MCampbell p
Fissured Clay	0.072	0.01	5
Silt	0.89	0.000001	10
Till (Saturated)	0.068	-	-

The above soil parameters are selected and tested through the model and gives the best fit during deformation analysis. Volumetric water content and its derivative storage curve is the major factor in defining the rise of groundwater table (In this study the rise in groundwater table after rainfall is linearly proportional to the storage coefficient of the material, with 0.4 m increase when unsaturated material is filled with silt but 0.9m increase when unsaturated material is filled with clay. This ratio is identical with their ratio of storage coefficient (1.6/0.7). Soil permeability at unsaturated soil layer is the main factor that influences the temporal response of tiltmeter to surface rainfall as it defines the change in groundwater table. Low permeability will increase the delay between surface rainfall and groundwater table rise. In this study where initial groundwater table rests at -8m, one magnitude decrease in unsaturated soil permeability results in a three-day delay). Low permeability also makes the response of groundwater table change smoother, resulting in a smooth tilt response instead of a step-like response (Figure 6-11).

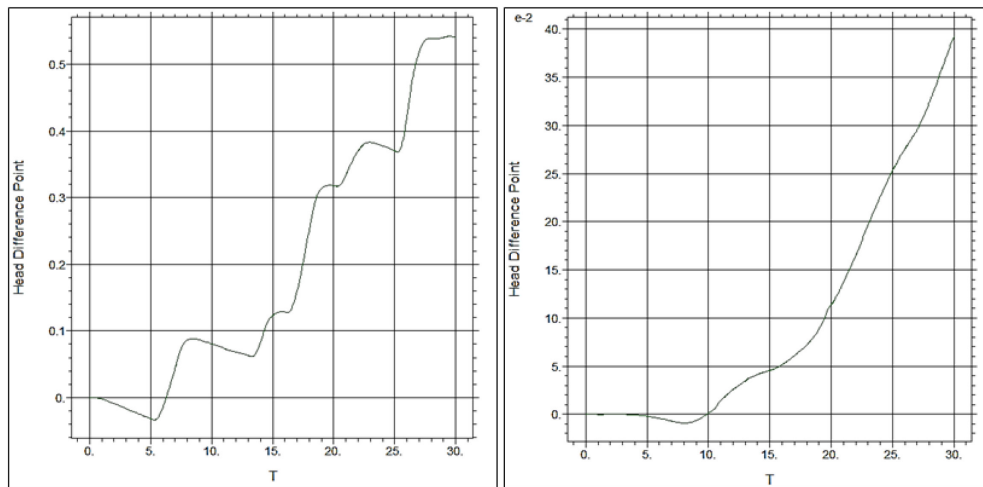


Figure 6-11: Saturated permeability 0.89 m/day (Left) and 0.089 m/day (Right)

6.2.3.3 Initial condition

Initial condition applied in seepage modelling mainly includes the initial groundwater table before the infiltration starts. Initial Porewater pressure profile is determined by the depth of phreatic water

surface in steady state. Although groundwater may be in a flow state in field condition, at the start of this modelling groundwater table is assumed to be in a static shape due to a lack of field data. This will bring a degree of uncertainty to the modelling results, however the impact on results should decrease with time as new infiltration quickly dissipates the initial influence. A continuous modelling of seepage can best reduce discrepancy and the results from an earlier modelling can be carried over to a new modeling period.

For this study the starting groundwater profile is chosen as a steady state, representing the groundwater table data collected from a nearby water wells. The initial groundwater table is set to be 8m below ground surface. The topography of the groundwater table is assumed to be flat in both 2D and 3D analysis. Porewater pressure and soil suction around the water table is in a linear relationship with depth. In 2D analysis groundwater table is set to be 8 m below the surface. In 3D analysis groundwater table is set to be 62 m in elevation.

6.2.3.4 Boundary conditions

Boundary conditions applied in seepage model consists of a surface boundary where infiltration is applied and side boundary which is set to be non-permeable. Surface boundary is used to introduce the flux from infiltration modelling to the seepage model. Side boundary conditions are used to confine seepage flow while reducing the boundary effect. The boundary conditions applied in 2D and 3D models are different based on the hypothesis of how rainwater is distributed across the area.

For the 2D model, a slope in groundwater table is introduced, as no tilt would arise from a uniform distribution of rainwater. Tilt pattern recorded by tiltmeter after rainfall is result of a horizontal gradient of porewater pressure. This lateral non-uniform distribution of rainwater can be induced by nearby discharge areas, surface topography, heterogeneous soil permeability, or variation in surface run-off conditions. The peak and trough of the induced groundwater table is fixed in the scenario and the slope can be regarded as a straight line when the total infiltration is small. In order to introduce this effect into the model, a declining infiltration surface boundary is adopted. This requires the surface climate conditions to be applied in a gradient. Different intensity of infiltration data is applied to the surface to produce the gradient. As limited by the software that no gradient can be applied to the infiltration modelling process, this lateral gradient is simulated with an infiltration factor. This factor is applied to the net flux and applied as a vertical flux boundary condition. The spatially constant distribution rainwater is represented as a declining rate of infiltration, as shown in Figure 6-12. Surface boundary is divided into six segments. From left to right each segment has a less infiltration flux by using an infiltration factor. For the 600m wide model, segments at two edges are 200m long each with full and zero infiltration to reduce the boundary effect. The length of the two segments is enough to maintain a horizontal porewater pressure gradient. The middle 200m of the model has four segments that have an infiltration factor

of 0.8, 0.6, 0.4 and 0.2 applied. A linear decline of porewater pressure is achieved in the middle of the mode where tilt will be measured.

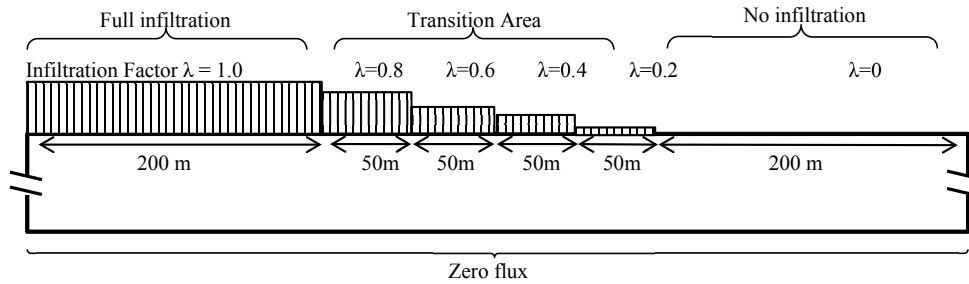


Figure 6-12: Surface boundaries with differential horizontal infiltration applied in 2D simulation

For the 3D model, the gradient in porewater pressure will be modelled based on site topography and local groundwater discharge areas (Figure 6-13). Boundary conditions are therefore defined according to digital elevation map and local surface water locations. For model without clear discharge areas, results from the infiltration will be applied equally throughout the surface boundary. Side and bottom boundaries are set to be impermeable. For model with local discharge, surface lakes will be represented in the model as a region with constant head condition. These regions are represented in map with the same elevation of groundwater table. On the other regions infiltration is applied equally on surface boundary. Overtime the distribution of rainwater will evolve according to surface elevation and fixed water level areas.

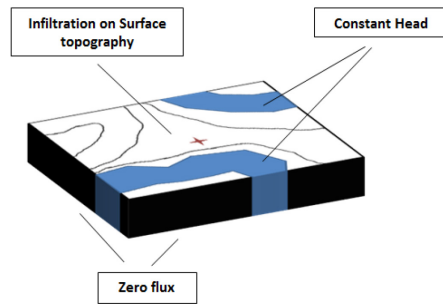


Figure 6-13: Schematic graph showing 3D spatial variation in induced groundwater table change after rainfall

During simulation, model mesh is generated automatically (grid density is related to magnitude of change in variables) as shown in Figure 6-14 and Figure 6-15.

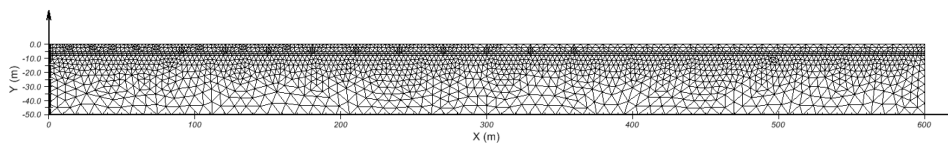


Figure 6-14: Grid distribution in 2D model

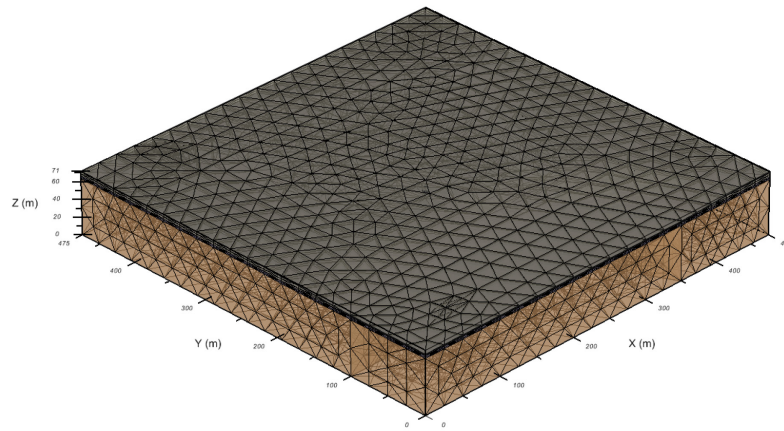


Figure 6-15: Grid distribution in 3D model

Transient seepage modelling has the maximum time step of 0.02 day. The basic reporting time step is one day, when pore water pressure distribution is generated and writes in a transfer file that will be used in the deformation modelling.

6.2.4 Deformation modelling

6.2.4.1 Modelling setup

Deformation modelling is the final stage of rainfall-tilt model that simulates ground deformation based on changes in porewater pressure from the previous seepage modelling. Displacement are obtained as results which will be used to deduce tilt, essentially the gradient of displacement in the vertical direction. Deformation modelling is the sequential stage of seepage modelling, as the previous passes porewater pressure as a variable within the same model geometry. For each iteration in porewater pressure profile, a steady state displacement analysis is done. Combining horizontal displacement results from continuous steps of deformation modelling, the tilt pattern can be revealed.

6.2.4.2 Material assignment

Soil properties required for deformation analysis includes elastic properties (swelling index with respect to net mean stress, swelling index with respect to matrix suction and Poisson's ratio), soil intrinsic properties (void ratio and dry density). These soil properties are chosen based on soil type and have been assigned common values. Soil properties used in the deformation modelling is summarized in Table 6-3 below.

Table 6-3: Soil properties adopted in deformation modelling

Properties	Fissured Clay	Silt	Saturated Till
Swelling index C_s	0.09	0.09	0.09
Swelling index C_m	0.1	0.08	0.04
Void ratio at 1kPa net stress and 1kPa matrix suction	1.2	0.9	0.7
Dry density (kN/m^3)	12	13.8	15.1
Poisson ratio	0.3	0.3	0.3

6.2.4.3 Initial and final conditions

Deformation modelling is a steady state displacement simulation for the change in pore water pressure between initial and final conditions. Initial conditions for deformation include both initial stress state and initial pore water pressure state. In this study initial stress state is set as K_o loading. Lateral earth pressure K_o is determined by Poisson's ratio γ using,

$$\gamma = \frac{K_o}{1 + K_o}$$

Initial and final conditions of pore water conditions use the transfer file from seepage modelling. To model the cumulative effective of rainfall tilt, the initial porewater pressure profile is fixed on the initial steady state seepage condition and final porewater pressure profile uses the distribution obtained from each period of seepage modelling.

6.2.4.4 Boundary conditions

For both 2D and 3D, boundary conditions for deformation modelling are identical. The surface of model is free; the bottom of the mode is fixed for both directions. The side boundary of the model is fixed in horizontal direction and free in vertical direction. The following Figure 6-16 shows the boundary conditions adopted.

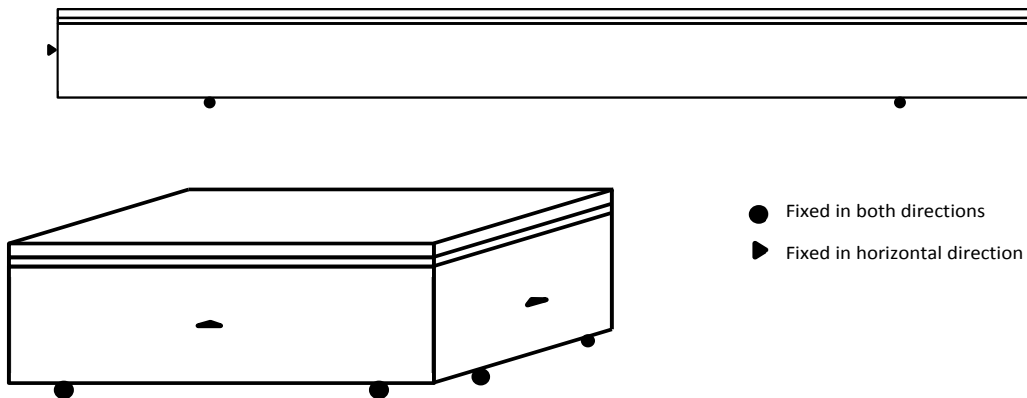


Figure 6-16: General boundary conditions adopted in deformation modelling

6.2.4.5 Output

During each iterative of the simulation, the mesh is generated automatically (grid density is related to magnitude of change in variables). Displacement can be obtained for the given location in the model. Horizontal displacement of two perpendicular directions (based on tiltmeter sensor) is obtained. Tilt is calculated based on two horizontal displacement data with 1 m (length of tiltmeter) of elevation difference. Tilt ϕ of a vertical subsurface location (x, z) and time t is obtained from:

$$\tan^{-1} \phi(x, z, t) = \frac{u(x, z_2, t) - u(x, z_1, t)}{z_2 - z_1}$$

Tilt pattern is the combination of each tilt iteration of modelling over one day time step. For each model location, two tilt patterns based on sensor direction are calculated and compared with observed tiltmeter data.

6.3 Results

6.3.1 2D model

In this section, a case study is presented that uses the 2D model setup to estimate the rainfall pattern in Aquistore for the period between May 15th and June 15th 2013. The 2D setup is used to simulate the tilt pattern by rainfall under a predetermined porewater pressure gradient, allowing for quantitatively evaluation of the effect of pore water gradient on amplitude tilt signals. The simulation results are compared with actual field data to validate and improve the overall modelling method.

Tilt is essentially the reflection differential horizontal displacement in the vertical direction. Differential loading and/or differential porewater pressure change create ground displacement. Difference in horizontal porewater pressure is the reflection of changes in groundwater table and groundwater flow, which are driven by surface infiltration. A uniform distributed surface infiltration will not create horizontal gradient in porewater pressure. The gradient is formed from the combined factors of surface topography, non-homogeneous permeability, surface runoff, as well as local hydrogeological conditions. The detailed characterization of these conditions could help physically explain the nature of the observed tilt. Modelling tilt pattern that match with observed data is an effective way to understand the gradient for each site and predict further tilt patterns. The 2D model uses this approach to estimate rainfall induced tilt for Aquistore.

6.3.1.1 Results

Infiltration simulation on the surface boundary provides full daily infiltration to the model as shown in Figure 6-17. Infiltration factor is applied to net flux and re-apply to the segments of surface boundary is several segments.

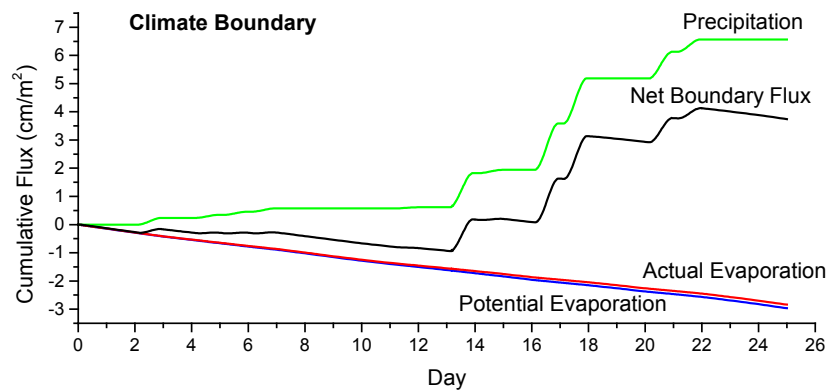


Figure 6-17: Full net boundary flux obtained from infiltration modelling in 2D setup

Seepage modelling in the model is governed by surface infiltration. Under full infiltration boundary, only vertical seepage flow exists. Lateral flow increases to maximum in the center of the model with the largest gradient in pore water pressure. The gradient decreases and maintain at zero at the right edge. After 30 day of surface climate, groundwater table rise 0.7 m at maximum under full infiltration conditions. Figure 6-18 and Figure 6-19 shows porewater head profile at the end seepage simulation.

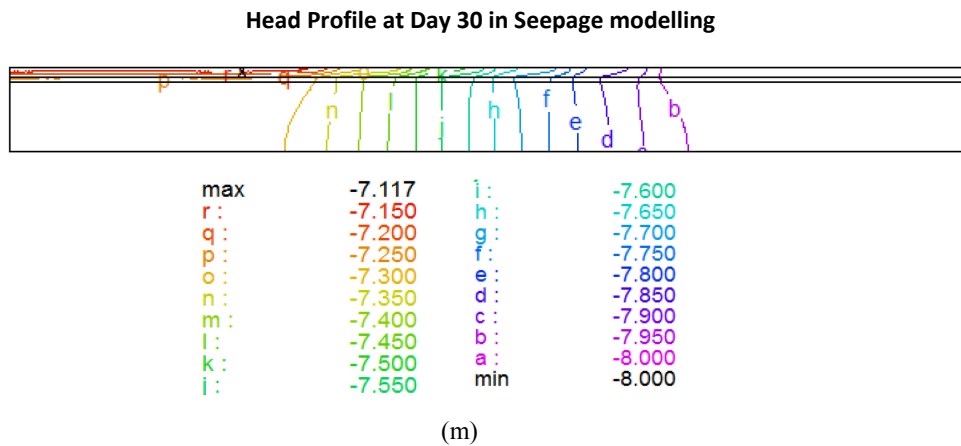


Figure 6-18: Head profile at the end of 2D seepage simulation

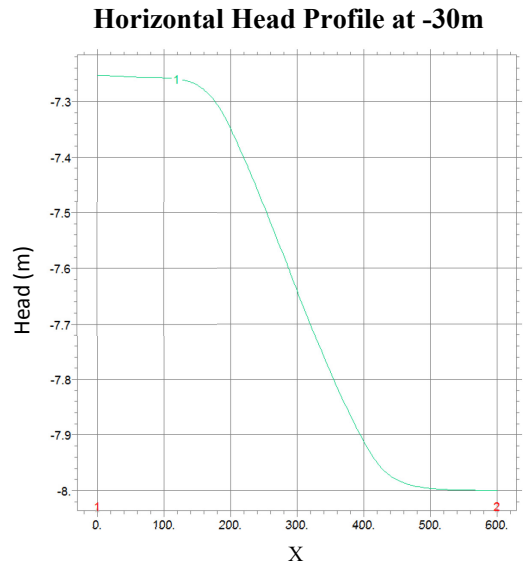


Figure 6-19: Horizontal head profile at -30m at the end of 2D seepage simulation

Incorporating porewater pressure profiles from seepage analysis, deformation analysis simulates deformation between two states of pore water pressure profiles. Displacement in horizontal direction can be obtained with depth across the horizontal profile. Figure 6-20 and Figure 6-21 shows the displacement profile at the end of the deformation simulation. Displacement reaches maximum at the upper left of the model as the region has the largest infiltration. At the right end of the model, displacement becomes minimal. Vertical displacement decreases from left to right with decreasing infiltration. Horizontal displacement is in a parabola curve that reaches highest in the middle of the model which has the largest horizontal gradient.

Displacement Profile at Day 30 in Deformation Modelling

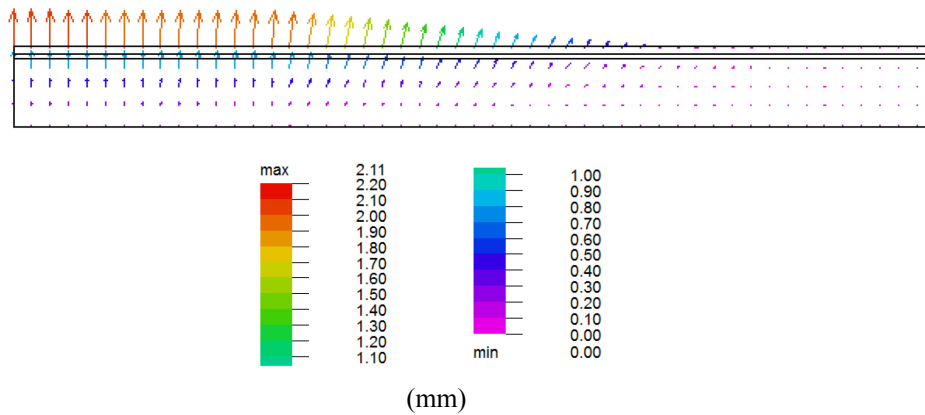


Figure 6-20: Displacement profile at the end of deformation analysis

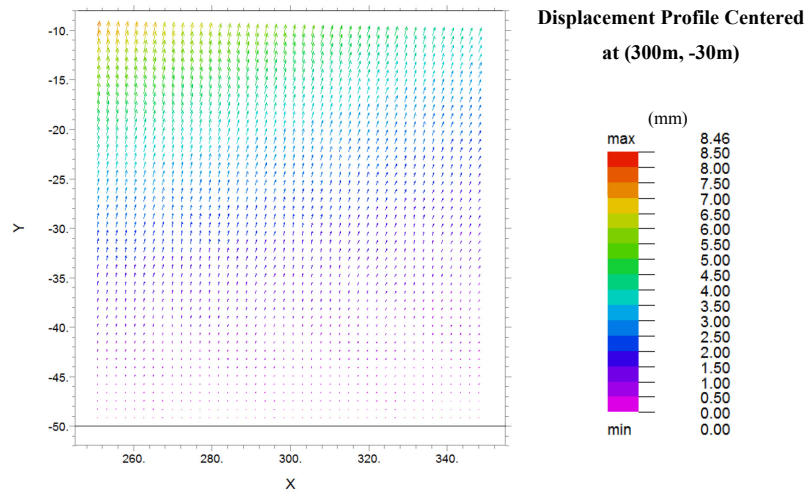


Figure 6-21: A zoomed view showing displacement vectors at the center of the model

Tilt is calculated from five sample locations from the model. For each location horizontal displacement at -30m and -31m is combined to a tilt angle using tiltmeter depth of -30m and base length of 1m. The five locations have the horizontal coordinates of 100m, 200m, 300m, 400m, 500m and 600m. Each step of modelling gives the cumulative tilting angle for the between initial condition and condition for that time. Combing tilt angles for the 30 time steps of simulation, tilt patterns can be plotted as shown in Figure 6-22. Similar to the parabola horizontal displacement curve, tilt rise from zero at the two edges to the maximum at the center of the model.

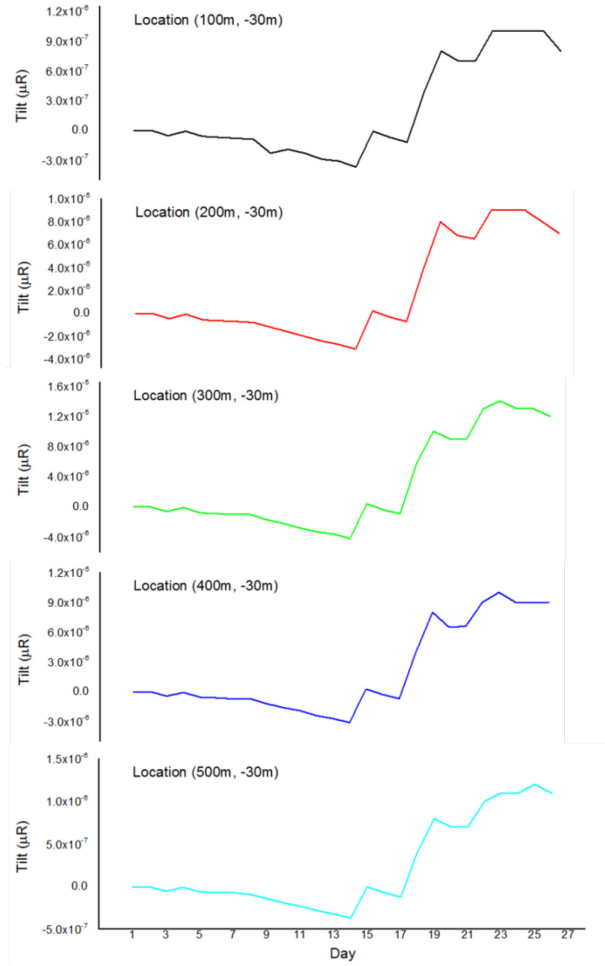


Figure 6-22: Tilt pattern from five locations from the 2D model

Tilt from location (100m,-30m) has the most same amplitude with both tiltmeter recordings. The observed and modelled tilt patterns are plotted together for each tiltmeter and for each sensor as shown from Figure 6-23 to Figure 6-26.



Figure 6-23: Modelled and observed tilt pattern for SW-NE sensor, NW01

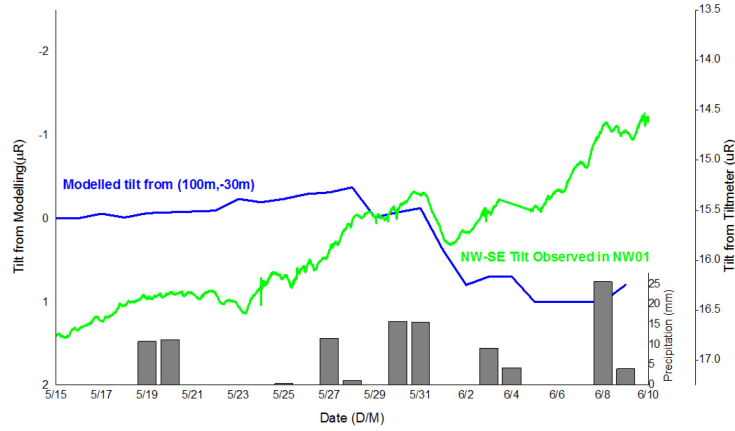


Figure 6-24: Modelled and observed tilt pattern for NW-SE sensor, NW01

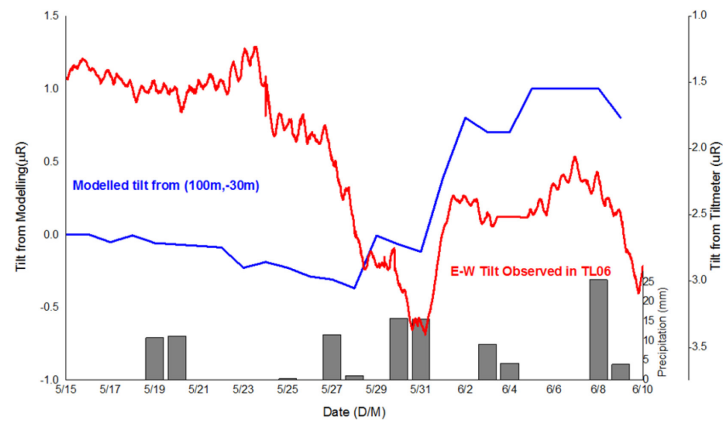


Figure 6-25: Modelled and observed tilt pattern for E-W sensor, TL06

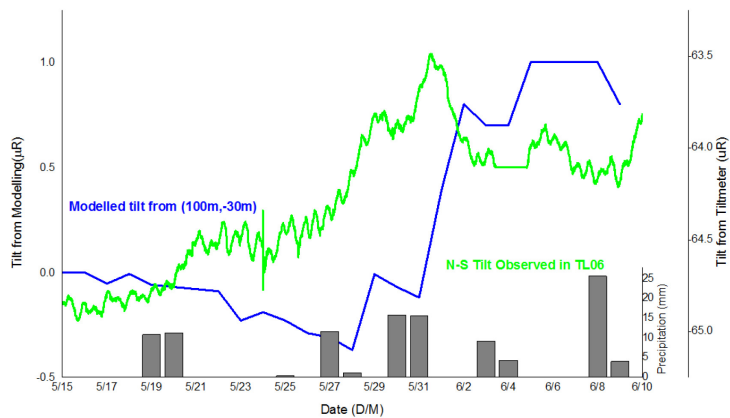


Figure 6-26: Modelled and observed tilt pattern for N-S sensor, TL06

6.3.1.2 Discussion

Tilt patterns from five model locations are identical and the pattern is in similar form with that actually observed by some tiltmeter sensors. Each major precipitation event creates a significant onset in tilt pattern that decays over time. The tilt pattern follows the trend with the porewater

pressure change at that location. And porewater pressure change is determined by the curve of infiltration, but delayed and smoothed. According to discussion from previous section, soil properties are the major factor that influence of change in porewater pressure at a certain location in the model. Therefore, a decrease in soil permeability will delay the response of tiltmeter on surface rainfalls and also result in a smooth curve. High permeability material above tiltmeter will bring quick response with a step-like pattern, as is the case for tiltmeters in Aquistore.

While tilt pattern from all five locations are similar, the amplitude increase zero at the two edges to maximum at the center, which resembles the gradient of porewater pressure. Porewater pressure gradient and the induced displacement at -30m depth are presented in a scatter plot as shown below in Figure 6-27.

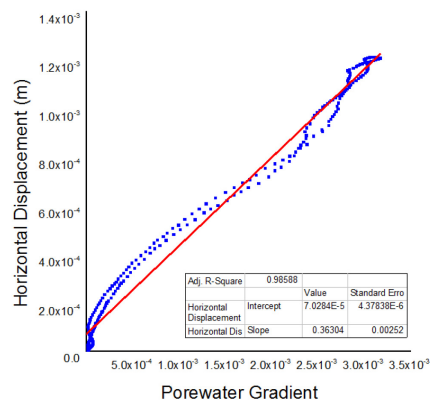


Figure 6-27: Scatterplot between porewater gradient and horizontal displacement

As shown in the figure, porewater pressure gradient and the induced displacement follows a near linear relationship, close to the situation where tilt is only dependent below an infinite gradient. The coefficient between gradient and horizontal displacement in this model is 0.036 m. Tilt at location (100m, -30m) is in a linear relationship with displacement at the same location, as shown in Figure 6-28. Therefore a coefficient of 1715 μ R exists between tilt amplitude and porewater gradient in the 2D model.

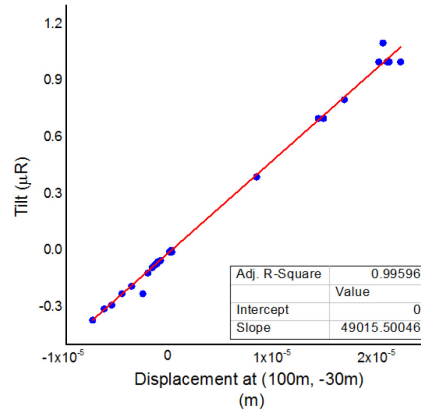


Figure 6-28: Tilt and displacement at (100m, -30m)

Tiltmeter readings from sensors of perpendicular directions do not show the same response. For tiltmeter NW01, tilt in NE-SW direction has a better match with modelled tilt pattern than NW-SE sensor. For tiltmeter TL06, Sensor in N-S direction does not correspond well the simulated pattern. Sensor in E-W direction shows the onsite following each rainfall, but is also subject to large drift not explained in this model. Sensor orientation is a major factor in the observed tilt pattern. Tiltmeter sensor in alignment with the maximum slope formed in groundwater table after rainfalls is possible give the best match in results. Also signal scales observed in different sensors may imply the direction of major porewater pressure gradient. The difference in sensor reading will be further explained by 3D models, which essentially applies different groundwater slopes to different sensors, according to site conditions.

6.3.2 3D model

Expanding upon the 2D model, 3D model simulates the distribution of rainwater with local topography and hydrogeological condition as constraints. This setus discards the general tilt pattern simulation and offers tilt patterns are specific with orientation and location. As a result this modelling methods gives explanation for the observed difference with regards to sensors of different azimuth as well as provides understanding regarding influential factors that controls the amplitude of rainfall tilt signals.

6.3.2.1 Results

Following the modelling procedures described in the previous section, both models configurations is simulated through coupled infiltration/seepage modelling and deformation modelling. For infiltration modelling, both models are subjected with the same boundary flux as shown in Figure 6-29.

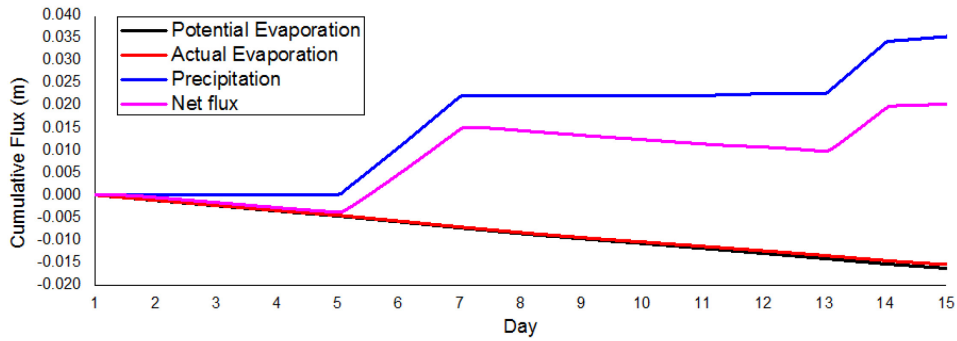


Figure 6-29: Boundary flux over time for both models

With infiltration as the only variables in seepage in Model A, seepage modelling gives porewater pressure distribution under surface topography (e.g. Figure 6-30, Figure 6-31). In Model B, the presence of constant head in the lake region is acting as a discharge area while the ground region is acting as recharge area. Groundwater interaction between the two areas defines the porewater pressure distribution (e.g. Figure 6-32, Figure 6-33).

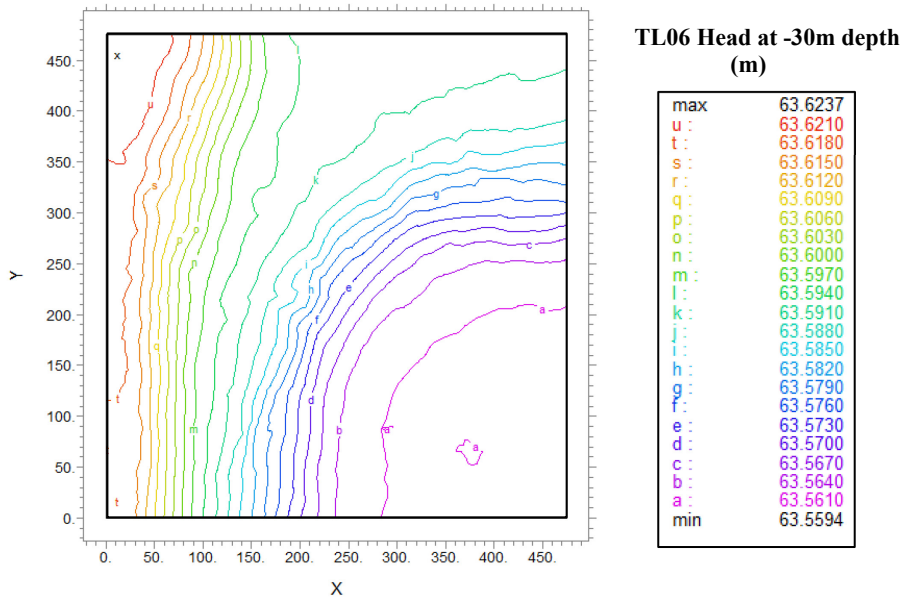


Figure 6-30: End of simulation porewater head contour at -30m depth for Model A

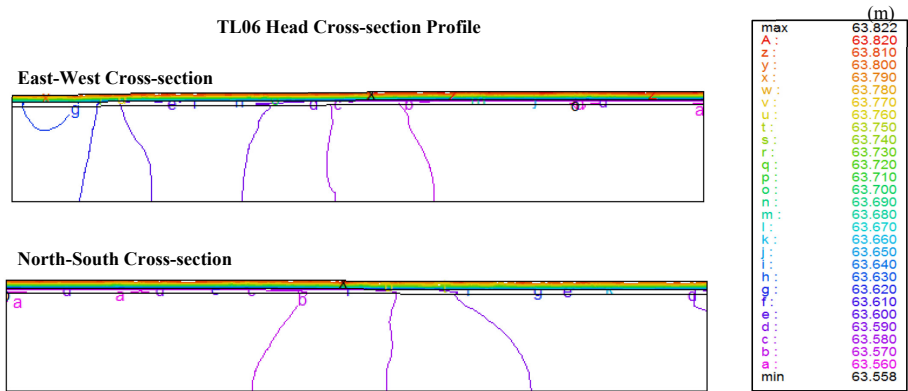


Figure 6-31: End of simulation porewater head profile for model A

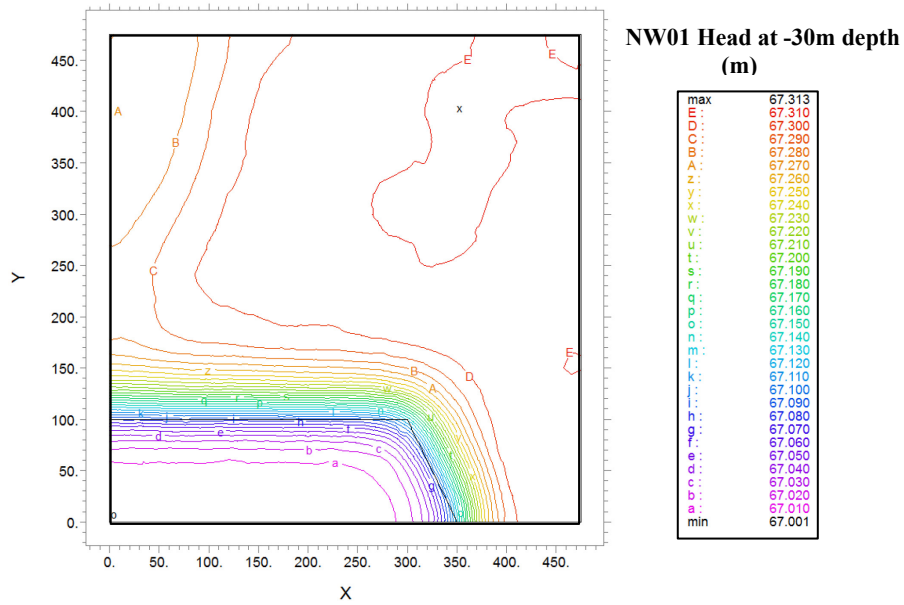


Figure 6-32: End of simulation porewater head contour at -30m depth for Model B

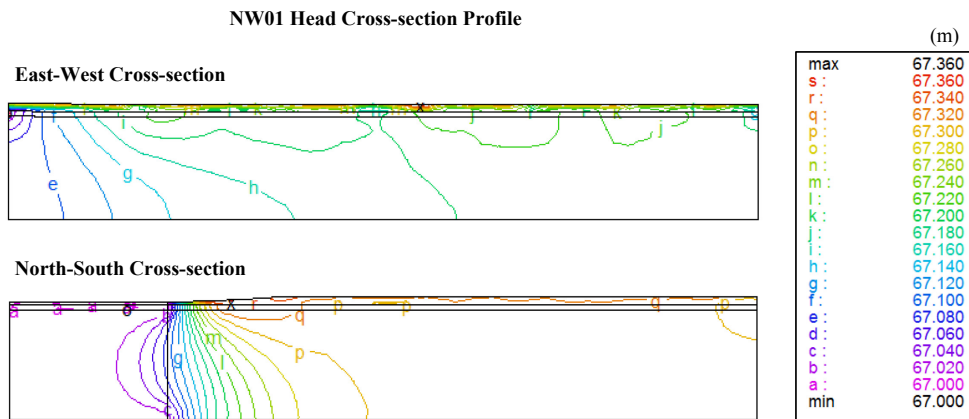


Figure 6-33: End of simulation porewater head profile for model B

Cross-sections of porewater pressure head at tiltmeter depth are plotted with each sensor direction (Figure 6-34 to Figure 6-37). In general, Site TL06 has much smaller height difference in porewater pressure than site NW01, mostly due to the fact that NW01 has a discharge area with constant head. The porewater pressure head at TL06 is higher in regions with lower elevation (i.e. closer groundwater table), with a difference of 0.12m. The porewater pressure head at site NW01 is becoming lower approaching the discharge area. At the open area in top-left part of the model, groundwater is almost constant. A total head difference of 0.9m is observed in this Model.

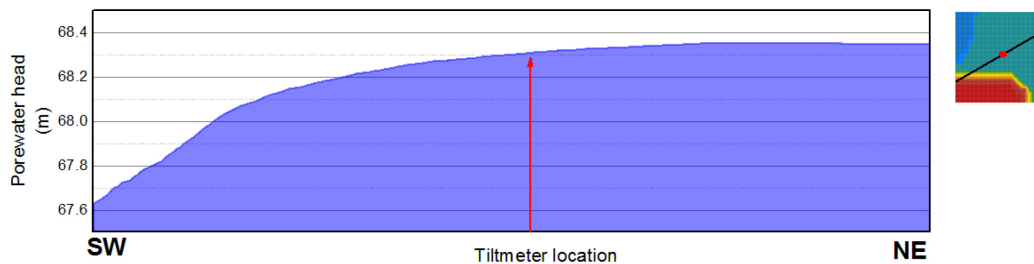


Figure 6-34: Porewater pressure head at SW-NE direction

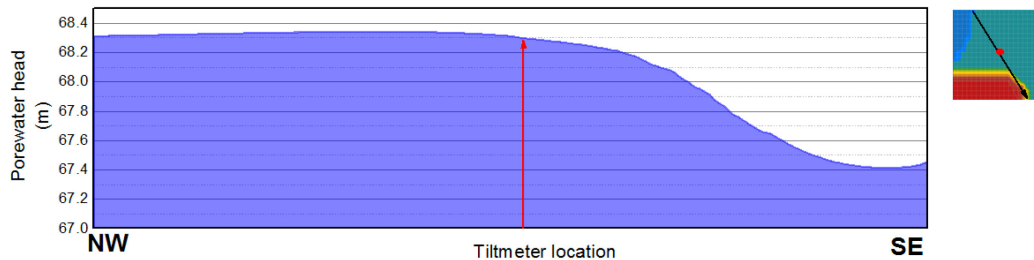


Figure 6-35: Porewater pressure head at NW-SE direction

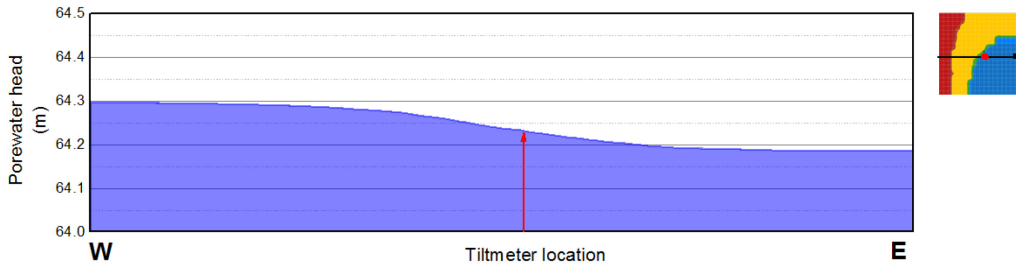


Figure 6-36: Porewater pressure head at W-E direction

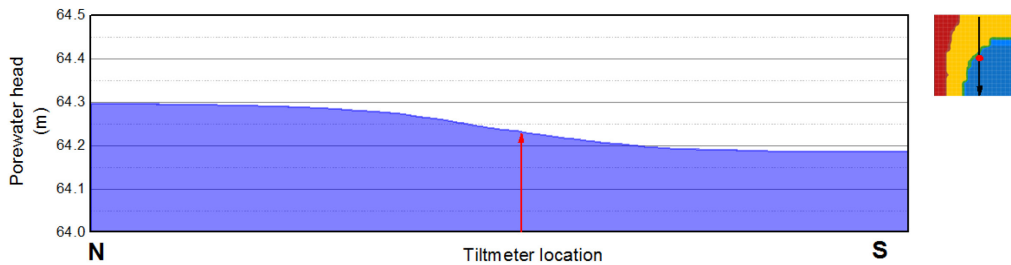


Figure 6-37: Porewater pressure head at N-S direction

Porewater pressure gradient at tiltmeter location for the four sensor directions are plotted with time in Figure 6-38. Despite the large head difference in Site NW01, porewater pressure gradient is in the same range for the two models, because of location of tiltmeter. In TL06, although porewater head is in a flat surface, tiltmeter is located at the steepest spot. Whereas in NW01, tiltmeter is located in the open area and the azimuth of sensor is parallel to the maximum direction of porewater pressure gradient. According to similar gradient, it is expected the two models have similar tilt.

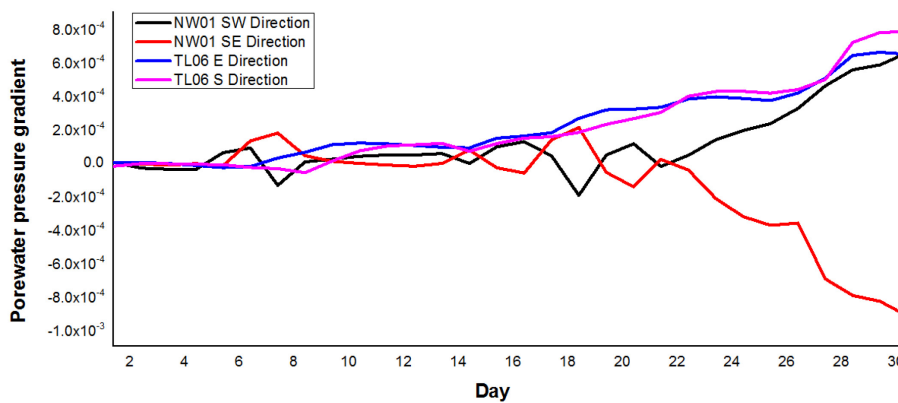


Figure 6-38: Porewater pressure gradient

The daily PWP transfer file from seepage modelling is incorporated in deformation modelling as initial and final conditions and deformation is resolved. Figure 6-39 shows a planar view of displacement at -30m depth. Horizontal displacement is generally centered where elevation changes and becomes small where elevation holds constant. Figure 6-40 shows vertical profiles of

displacement. Similar to 2D simulation, despite the boundary effect, displacement follows a linear decay with depth.

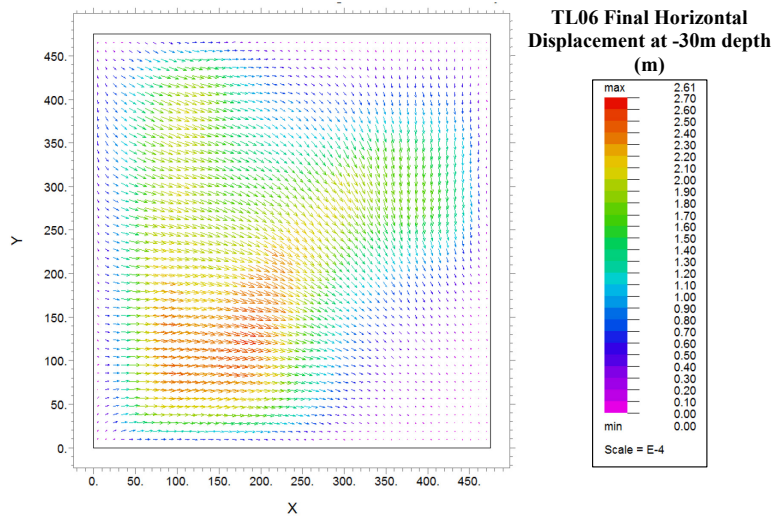


Figure 6-39: End of simulation displacement (-30m) vector map from Model A

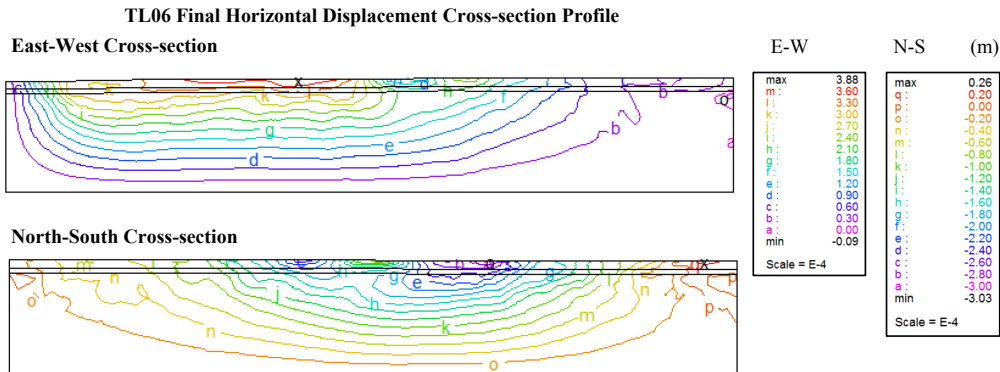


Figure 6-40: End of simulation displacement (-30m) profile from Model A

Figure 6-41 compares simulated and observed tilt patterns obtained between May 18th and June 15th, 2013. The modelling results show generally weak correlations. Higher correlations are only found in certain directions for partial time periods (e.g. N-S direction between June 5th and June

15th).

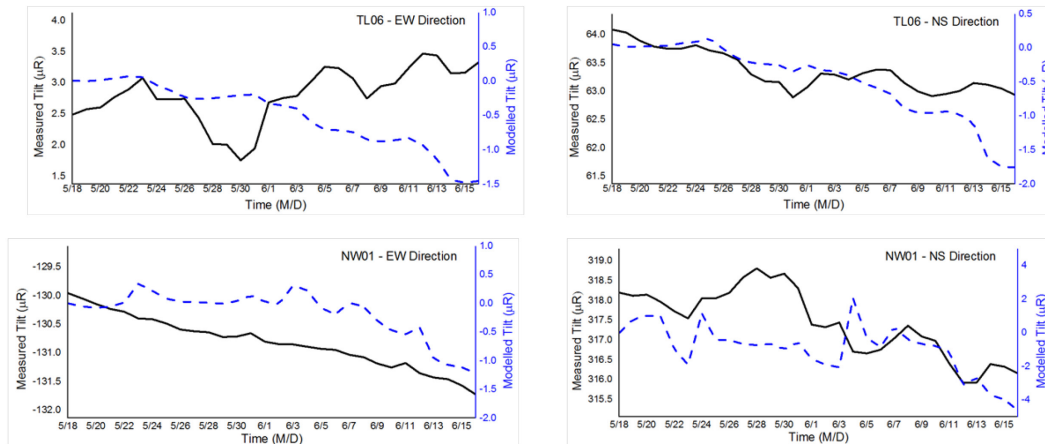


Figure 6-41: Modelled tilt pattern compared with filtered original data

6.3.2.2 Discussion

Tilt patterns for two tiltmeter locations, two orientations are modelled based on 30 days of metrological data. For all the obtained patterns, the occurrence of rainfall is responded with fluctuations in tilt. Similar to the 2D model, infiltration is determined by combining meteorological factors (precipitation, evaporations and runoff). This appearance is consistent with the method of applying a rain function proposed by several authors. While infiltration is the deciding factor in defining the amplitude of this fluctuation, the actual tilt pattern is shaped by boundary condition and topography of the model, as both determine local rainwater distribution. Tilt pattern is also orientation sensitive. Sensors show an overall positive correlation to rainfall and the sensor from NW01 SE direction has a negative correlation. The difference of the correlations is obviously determined by the gradient of pore water pressure in that direction. Tiltmeter sensor in alignment with maximum slope of groundwater is more sensitive to rainfall induced tilt, theoretically a uniform groundwater table, despite the fluctuations created by surface climate, will not produce tilt signals.

Model A (NW01) is creating tilt pattern with large amplitude, especially in the N-S direction. This can be explained as the presence of a surface lake acts as discharge area in the model and drives large porewater pressure gradient in the N-S direction. Tiltmeter sensor in alignment with direction between recharge and discharge areas are more sensitive to rainfall.

Model B (TL06) has shown smaller and consistent amplitude of tilt than that of Model A. As the only factor creating groundwater gradient is surface topography. The generally flat surface at TL06 site has resulted in smooth groundwater table. Local topography has very limited power in creating the gradient in groundwater after rainfalls.

The simulated tilt pattern from 3D models generally follows a weak correlation with observed tilt pattern. The major limitation of this model includes a lack of detailed regional groundwater regime and unaccounted localized rainstorms. The dynamic distribution of porewater pressure is the

superposition of initial groundwater profile plus the distribution of episodic rainwater. As a lack of regional groundwater mapping, the initial groundwater profile is set as a steady state. Any existing flow of groundwater and existing shape of groundwater table will affect the modelling results. Therefore for more accurate modelling of rainfall pattern, a hydrogeological survey is necessary. While the distribution of episodic rainwater is simulated in the 3D model, one aspect of uncertainty is the scale of the rainstorm. The model simulates rainfall in a large scale like a blanket over the area. While actually in the place of southeastern Saskatchewan, localized rainstorms are also common. This is represented as a centralized precipitation area that is moving. This is accounted in the simulation and may bring uncertainty to modelling results. This 3D study is focused on evaluating the impact local topography and the presence of surface water on the two tiltmeter stations. Results from 3D simulation can be used to validate and improve the previous 2D simulation. The characterization of groundwater table shape and raining pattern is not characterized in this study, however in future work this can greatly help increase the accuracy of the model.

6.4 Discussion

Rainfall induced tilt has always been major type of noise in tiltmeter array monitoring. Due to its episodic nature and large amplitude, rainfall induced tilt may obscure or even alter the real signals. Sensitivity of rainfall is quite site-specific. In Aquistore, tiltmeters responds to rainfalls with weak but definite patterns. A statistical analysis shows that tiltmeter shows fluctuating signals during rainfalls the pattern last for days. Tiltmeters in Aquistore are installed in a flat terrain and deep at 30m depth. The effect of direct rain mass loading and the subsequent underground flow is too feeble to explain induced tilt signals. The effect of pore-elastic deformation is therefore modelled and compared with observed tilt pattern.

Tilt pattern captured after rainfalls is created by horizontal deformation, which is caused by differential pore pressure in the horizontal direction. Lateral gradient in pore water pressure is determined by both local and regional factors including topography, hydrogeological conditions, surface runoff conditions, anisotropic homogeneous etc. A 2D model is proposed that assume a varying gradient and calculate the induced tilt. 3D models are used to test the factors influencing the gradient including topography and hydrogeological conditions. The models show that the pattern of tilt is directly determined by rain infiltration determined from climate conditions while the amplitude of tilt is determined by the gradient. Modelled tilt fit observed tilt pattern in sensors of certain azimuth.

According to the model, the sensitivity tiltmeter to rainfall is determined by the installation geometry including depth, surface topography, and nearby recharge and discharge areas. With generally flat site in Aquistore, the weak response of rainfall in tiltmeter is mostly determined by global groundwater regime as well local hydrogeological conditions. With the available climate data, the

episodic appearance of rainfall induced tilt can be determined as well as quantified according the back regression factor determined by modelling. Further modelling can benefit from local groundwater characterization as well as more baseline information from further tiltmeter locations.

CHAPTER 7 Conclusion and Recommendation

Surface tiltmeter array is a part of MMV program in Aquistore project to monitor surface deformation induced by geologic CO₂ storage. Surface deformation will be adequately interpreted by combining 15 tilt vectors covering the estimated CO₂ plume, within a 25 km² area. As tiltmeters are accommodated in 30 m boreholes in Aquistore, the noise effects of thermal and surface conditions on readings have been greatly minimized. The addition of a remote data acquisition system and a weather station enables real-time interpretation of tilt signals related to individual events, including injection and surface atmospheric activities.

Three years of continuous tilt data have been collected in two stations, representing baseline conditions without the influence of CO₂ injection. Baseline reading in Aquistore consists of tilt signals induced by earth tides, atmospheric activities, and seismic events. Table 7-1 summarizes the characterized noise signals from baseline data analysis in Aquistore.

Table 7-1: Characterized noise signals in Aquistore

Type	Pattern	Scale in Aquistore	Periodicity
Earth tide signal	Sinusoidal wave	less than 0.1 μR	Semidiurnal
Barometric pressure	Episodic fluctuations	Up to 1 μR	No
Rainfall signal	Random fluctuations	Up to 0.5 μR	No
Thermal signal	Sinusoidal wave	Negligible	Annual
Seismic signal	Spikes	Up to 3 μR	None

Earth tide signals have the smallest amplitude and a semidiurnal periodicity. Their scale barely changes with depth. The presence of smooth earth tide signals throughout baseline data indicates that the tiltmeter is fully coupled to the ground. Using a simplified earth model, theoretical tidal signals are estimated and compared with observed patterns. Besides a high correlation coefficient, observed amplitudes are about 40% larger. This factor arises because the earth is not purely rigid as the model assumes, but can be applied to future pattern estimates. Earth tide signals can be subtracted from tiltmeter data.

Atmospheric signals are induced by meteorological activities from the surface. The deep burial design in Aquistore has greatly reduced the scale of atmospheric signals. Two significant contributions found in Aquistore are barometric signal and rainfall signal, as both involve a mass redistribution effect. Barometric signals have twice the scale (up to 1 μR) of rainfall signals, and follow air pressure in a linear relationship with a coefficient of 0.5 μR/kPa. After subtracting barometric signals from baseline data, rainfall signals are revealed, with a generally weaker correlation to precipitation. The atmospheric-tilt model is used to estimate tilt patterns from discrete precipitation data. Boundary conditions and topography are the two factors used in defining the direction and amplitude of rainfall signals, as both determine local rainwater distribution. Soil properties, especially permeability and volume change index, affect patterns in the temporal and dimensional scales. This model gives a coarse prediction of tilt pattern due to a lack of full spatial

characterization of the groundwater table or rainfall intensity. Its accuracy is greatly enhanced when this information becomes available.

Tiltmeters can capture seismic signals from both local and distant activities. These signals are identifiable by rapid spikes that can reach 5 μ R. The scale is directly proportional to the energy level, which is determined by the magnitude of the activity and its distance from the tiltmeter. Straightforward subtraction can be used to remove seismic signals, as they only affect baseline data for several hours.

Thermal signals come from thermoelastic deformation of the earth due to surface heat propagation. Assuming a homogeneous space under thermal isotherms with a constant slope, the amplitude of thermal signals is proportional to temperature variation on the slope. The impact of daily temperature fluctuations is only considered at shallow depth (less than 3 m) due to strong attenuation. Seasonal temperature variations can normally reach 20 m under the surface, but factors such as loose surface material and high thermal conductivity of borehole casings can increase this reach. The downhole thermal sensor of tiltmeter recorded a temperature drop of 0.03°C in the initial 6 months and no long-term trend in two-year period. Theoretical thermoelastic tilt created by this temperature pattern will not reflect in tiltmeter reading and therefore thermal signals do not exist in Aquistore tiltmeters with 30 m burial depth. Tiltmeter sensor also exhibits temperature dependent behavior. This effect can be negated by conducting thermal compensation tests on tiltmeter sensors. However the minimal downhole temperature fluctuation observed in Aquistore will not produce signal of this origin either.

Based on this research on tiltmeter array design, deployment and baseline data analysis, the evaluation of tiltmeter performance in Aquistore has provided several recommendations for future projects. The burial depth of 30m in Aquistore has proven to be effective in reducing major noise signals. It is recommended that future tiltmeter array applications for reservoir surveillance adopt a deep design (more than 10 m). This research does not include analysis of noise signals from tectonic movement and cavity effect which may be a dominant source of long-term signal drift. The effect of long-term tectonic movement can be estimated by additional field tests, including rotating tiltmeter periodically to observe the direction of background drift. Borehole cavities effects can be better understood by reinstalling tiltmeter in boreholes to observe the initial tilt response. For the noise signals analyzed in this research, earth tide signal is unavoidable, but it serves as a good indication of installation quality. By analyzing earth tide signals, a preliminary evaluation can be conducted for newly installed tiltmeters. Tiltmeter with poor revelation of tidal signal should be repositioned for better sensitivity. The nature of rainfall signals can be better understood with records of local groundwater dynamics. A continuous water well near the tiltmeter site is recommended to best understand the impact of rainfall and regional groundwater conditions. Tiltmeter will be less sensitive to rainfalls in areas with flat topography. As large porewater gradient centralizes near local recharge and discharge areas, tiltmeter sites should avoid lakes, rivers and

operating water wells. For thermal signals, thermal compensation tests are necessary for tiltmeter exposed to significant temperature fluctuations. The analysis on thermoelastic tilt indicates that a burial depth more than 10 m can reduce thermoelastic signal below the detection limit. By installing a tiltmeter at various depths of a single borehole, local thermal parameters can be obtained which can be used to predict thermoelastic tilt signals.

In cases where noise signals have to be reduced, one of the three general methodologies proposed in this thesis can be applied depending on statistical properties of the signal. Statistical regression method can be used to quantify linearly-provoked tilt signal including earth tide and barometric pressure. For the impact of surface precipitation, the numerical modelling approach is best at estimating the scale of induced tilt signal for tiltmeter installed below groundwater table. As tiltmeter sensor exhibits temperature dependent behavior, thermal compensation test is necessary for tiltmeter experiencing strong temperature fluctuations. Combining signal characteristics with individual reduction method, a systematic approach is advised when processing large quantify of tiltmeter surveillance results (as shown in Table 7-1). With the removal of noise signals from tilt measurement, the tiltmeter array technology is closer towards providing accurate and unbiased surveillance of CO2 injection and storage.

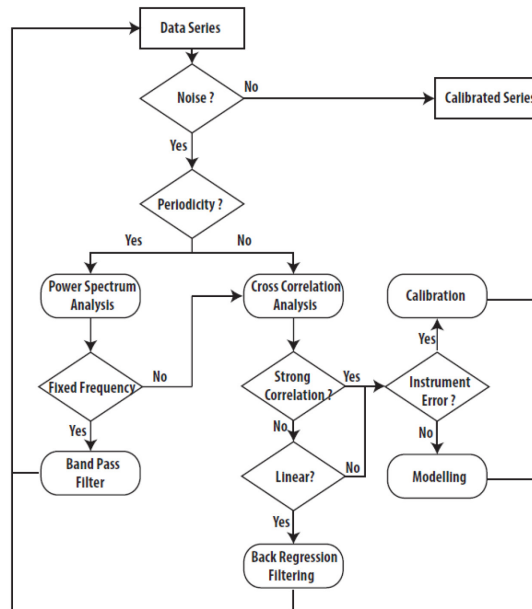


Figure 7-1: Systematic approach in reducing tiltmeter noise signals

References

- [1] J. Gibbins and H. Chalmers, “Carbon capture and storage,” *Energy Policy*, vol. 36, no. 12, pp. 4317–4322, Dec. 2008.
- [2] E. Rubin, L. Meyer, and H. de Coninck, “IPCC Special Report Carbon Dioxide Capture and Storage-Technical Summary,” 2005.
- [3] S. I. Plasynski, J. T. Litynski, H. G. McIlvried, and R. D. Srivastava, “Progress and New Developments in Carbon Capture and Storage,” *CRC. Crit. Rev. Plant Sci.*, vol. 28, no. 3, pp. 123–138, Apr. 2009.
- [4] Global CCS Institute, “Global CCS Institute January 2013 Update,” Ottawa, 2013.
- [5] A. Chadwick, R. Arts, E. Ola, P. Williamson, and G. Williams, “Geophysical monitoring of the CO₂ plume at Sleipner, North Sea,” in *Advances in the geological storage of carbon dioxide*, Springer Netherlands, 2006, pp. 303–314.
- [6] National Round Table on the Environment and the Economy, “Achieving 2050: A Carbon Pricing Policy for Canada,” 2009.
- [7] D. White, “Monitoring CO₂ storage during EOR at the Weyburn-Midale Field,” *The Leading Edge*, vol. 28, p. 838, 2009.
- [8] S. I. Plasynski, J. T. Litynski, H. G. McIlvried, D. M. Vikara, and R. D. Srivastava, “The critical role of monitoring, verification, and accounting for geologic carbon dioxide storage projects,” *Environ. Geosci.*, vol. 18, no. 1, pp. 19–34, Mar. 2011.
- [9] R. Sweatman and G. R. Mccolpin, “Monitoring technology enables long-term CO₂ geosequestration,” *Exploration & Production*, no. November, Houston, Nov-2009.
- [10] B. Voight and R. Hoblitt, “Remarkable cyclic ground deformation monitored in real-time on Montserrat, and its use in eruption forecasting,” *Geophys. ...*, vol. 25, no. 18, pp. 3405–3408, Sep. 1998.
- [11] H. Wang, H. T. Hsu, and Y. Z. Zhu, “Prediction of surface horizontal displacements, and gravity and tilt changes caused by filling the Three Gorges Reservoir,” *J. Geod.*, vol. 76, no. 2, pp. 105–114, Feb. 2002.

- [12] N. R. Goultly and R. Gilman, "Repeated creep events on the San Andreas Fault near Parkfield, California, Recorded by a strainmeter array," *J. Geophys. Res.*, vol. 83, no. B11, p. 5415, 1978.
- [13] C. Wright, E. Davis, and L. Weijers, "Downhole tiltmeter fracture mapping: a new tool for directly measuring hydraulic fracture dimensions," in *SPE annual technical Conference*, 1998.
- [14] Halliburton, "Tilt Fracture Mapping." [Online]. Available: http://www.halliburton.com/public/pe/contents/Data_Sheets/web/H/H08316.pdf.
- [15] M. Wilson and M. Monea, "IEA GHG Weyburn CO2 monitoring & storage project. Summary report 2000-2004," 2004.
- [16] K. Worth, D. White, R. Chalaturnyk, J. Sorensen, C. Hawkes, B. Rostron, J. Johnson, and A. Young, "Aquistore Project Measurement, Monitoring, and Verification: From Concept to CO2 Injection," *Energy Procedia*, vol. 63, pp. 3202–3208, 2014.
- [17] S. Samsonov, D. White, M. Craymer, K. Murnaghan, R. Chalaturnyk, and G. Zambrano-narvaez, "Monitoring Ground Deformation at the Aquistore CO2 Storage Site in SE Saskatchewan , Canada," 2012. [Online]. Available: ftp://geod.nrcan.gc.ca/pub/GSD/craymer/pubs/aquistore_agu2012fall_poster.pdf.
- [18] S. Francisco, M. R. Craymer, J. A. Henton, M. Piraszewski, J. Silliker, J. C. Lavergne, and S. Samsonov, "Preliminary results of continuous GPS monitoring of surface deformation at the Aquistore underground CO2 storage site," 2013. .
- [19] S. Whittaker and K. Worth, "Aquistore: A fully integrated demonstration of the capture, transportation and geologic storage of CO2," *Energy Procedia*, vol. 4, pp. 5607–5614, Jan. 2011.
- [20] S. Marsic, W. Roadarmel, M. Machovoe, and E. Davis, "Improving Reservoir Monitoring in EOR Environments Using Microdeformation-Based Technologies," in *Proceedings of SPE Western Venezuela Section South American Oil and Gas Congress*, 2011.
- [21] A. Aryee, "Evaluation of the Impact of Reclamation Regulations and Guidelines on Ecological Rehabilitation Practices at the Estevan Surface Coal Mines (1996-1999), Saskatchewan," *Environ. J.*, vol. 34, no. 2, pp. 71–85, 2006.
- [22] Pinnacle, "TiltTalk Professional User's Manual." .

- [23] R. Sleeman, H. . Haak, M. . Bos, and J. J. . van Gend, "Tidal tilt observations in the Netherlands using shallow borehole tiltmeters," *Phys. Chem. Earth, Part A Solid Earth Geod.*, vol. 25, no. 4, pp. 415–420, Jan. 2000.
- [24] J. Levine, C. Meertens, and R. Busby, "Tilt observations using borehole tiltmeters: 1. Analysis of tidal and secular tilt," *J. Geophys. ...*, vol. 94, no. 88, pp. 574–586, 1989.
- [25] F. Wyatt, G. Cabaniss, and D. Agnew, "A comparison of tiltmeters at tidal frequencies," *Geophys. Res. ...*, vol. 9, no. 7, pp. 743–746, 1982.
- [26] D. Milbert, "SOLID." 2014.
- [27] L. Petrov and J.-P. Boy, "Study of the atmospheric pressure loading signal in very long baseline interferometry observations," *J. Geophys. Res.*, vol. 109, no. B3, p. B03405, 2004.
- [28] G. Dal Moro and M. Zadro, "Subsurface deformations induced by rainfall and atmospheric pressure: tilt/strain measurements in the NE-Italy seismic area," *Earth Planet. Sci. Lett.*, vol. 164, no. 1–2, pp. 193–203, Dec. 1998.
- [29] R. Edge, T. Baker, and G. Jeffries, "Borehole tilt measurements: aperiodic crustal tilt in an aseismic area," *Tectonophysics*, vol. 71, pp. 97–109, 1981.
- [30] H.-J. Kämpel, J. a. Peters, and D. R. Bower, "Nontidal tilt and water table variations in a seismically active region in Quebec, Canada," *Tectonophysics*, vol. 152, no. 3–4, pp. 253–265, Sep. 1988.
- [31] L. Longuevergne, N. Florsch, F. Boudin, L. Oudin, and C. Camerlynck, "Tilt and strain deformation induced by hydrologically active natural fractures: application to the tiltmeters installed in Sainte-Croix-aux-Mines observatory (France)," *Geophys. J. Int.*, vol. 178, no. 2, pp. 667–677, Aug. 2009.
- [32] C. Ricco, I. Aquino, and C. Del Gaudio, "Ground tilt monitoring at Phlegraean Fields (Italy): a methodological approach," *Ann. Geophys.*, vol. 46, no. December, pp. 1297–1314, 2003.
- [33] J. Berger, "A note on thermoelastic strains and tilts," *J. Geophys. Res.*, vol. 80, no. 2, pp. 274–277, 1975.
- [34] J. Harrison and K. Herbst, "Thermoelastic strains and tilts revisited," *Geophys. Res. Lett.*, vol. 4, no. 11, pp. 535–537, 1977.

- [35] L. Prawirodirdjo, Y. Ben-Zion, and Y. Bock, "Observation and modeling of thermoelastic strain in Southern California Integrated GPS Network daily position time series," *J. Geophys. Res.*, vol. 111, no. B2, p. B02408, 2006.
- [36] Y. Ben-Zion and P. Leary, "Thermoelastic strain in a half-space covered by unconsolidated material," *Bull. Seismol. Soc. Am.*, vol. 76, no. 5, pp. 1447–1460, 1986.
- [37] R. Freeze and J. Cherry, *Groundwater*. New Jersey: Printice-Hall, 1979.
- [38] H. L. Penman, "Natural Evaporation from Open Water, Bare Soil and Grass," *Proc. R. Soc. A Math. Phys. Eng. Sci.*, vol. 193, no. 1032, pp. 120–145, Apr. 1948.
- [39] G. Gitirana, M. Fredlund, and D. Fredlund, "Numerical modelling of Soil-atmosphere interaction for Unsaturated Surfaces," *ASCE*, pp. 658–669, 2006.
- [40] G. W. Wilson, "Soil evaporative fluxes for geotechnical engineering problems," University of Saskatchewan, 1990.
- [41] D. G. Fredlund and H. Rahardjo, "Soil Mechanics for Unsaturated Soils," *Stress Int. J. Biol. Stress*, p. 517, 1993.
- [42] M. D. Fredlund, G. W. Wilson, and D. G. Fredlund, "Use of the grain-size distribution for estimation of the soil-water characteristic curve," *Can. Geotech. J.*, vol. 39, no. 5, pp. 1103–1117, Oct. 2002.
- [43] D. Fredlund and A. Xing, "Equations for the soil-water characteristic curve," *Can. Geotech. J.*, vol. 31, no. 3, pp. 521–532, 1994.
- [44] M. Van Genuchten, "A closed-form equation for predicting the hydraulic conductivity of unsaturated soils," *Soil Sci. Soc. Am.*, vol. 8, pp. 892–898, 1980.
- [45] W. Gardner, "Some steady-state solutions of the unsaturated moisture flow equation with application to evaporation from a water table," *Soil Sci.*, 1958.
- [46] D. Fredlund, A. Xing, and S. Huang, "Predicting the permeability function for unsaturated soils using the soil-water characteristic curve," *Can. Geotech. ...*, 1994.
- [47] E. Leong and H. Rahardjo, "Permeability functions for unsaturated soils," *J. Geotech. ...*,

no. 12, pp. 1118–1126, 1997.

- [48] D. G. Fredlund and N. R. Morgenstern, “Constitutive relations for volume change in unsaturated soils,” *Can. Geotech. J.*, vol. 13, no. 3, pp. 261–276, Aug. 1976.
- [49] H. Vu and D. Fredlund, “The prediction of one-, two-, and three-dimensional heave in expansive soils,” *Can. Geotech. J.*, vol. 737, pp. 713–737, 2004.

Appendix A Standard Working Procedure for Tiltmeter Station Installation

1. General

This SOP details the requirements for Installation a tiltmeter station to measure ground tilt. This method specifies the tools, instrumentation and procedures to lock a tiltmeter downhole and provide communication using radio and satellite network.

2. General Safety Precautions and Corresponding SWP

1.1. There are risks in tiltmeter station installation in the field including tripping hazard, heavy lifting induced body injury.

1.2. This method covers the procedures in tiltmeter station installation.

1.3. The corresponding Safe Work Practices include:

1.3.1. SWP – Tiltmeter Station Installation

2. Summary of Installation Method

2.1. One tiltmeter is deployed downhole connected by cable to surface radio communication box as well as other supporting accessories. After communication between remote computer and downhole tiltmeter is successful, lock tiltmeter with sand and finish ground work.

3. Significance and Use

3.1. Multiple tiltmeters deployed over monitoring area provide a resolution of surface deformation. It is used widely in hydraulic fracturing tests to monitor fracturing performance. It can also be used to various monitoring programs. The quality of installation of each tiltmeter station greatly influences the performance of the whole system.

4. Components of installation

4.1. Downhole instruments

4.1.1. Tiltmeter

4.1.2. Communication cable

4.1.3. Aircraft cable

4.1.4. Silica sand

4.2. Surface instruments

4.2.1. Radio box

4.2.2. Solar panel for radio box

4.2.3. Tiltmeter battery box

4.2.4. Tiltmeter solar panel

4.2.5. Surface installation pipe

5. Pre-Test Installation Checks

5.1. Safety checks and document the site condition.

5.2. Determine direction of North for solar panels orientation using compass.

5.3. Determine the direction of master radio station for radio box orientation (using a map of well sites when necessary). Radio station mast is visible from a large distance due to the lack of surface relief and the height of the mast.

5.4. Check the stability and integrity of the borehole casing and surface installation pole. Make sure surface installation pole has enough strength to hold the radio box and solar panels. Check if the opening of borehole casing is clear and tiltmeter can slide in smoothly.

6. Installation Procedure

6.1. Put tiltmeter downhole

6.1.1. Fully extend the aircraft cable and data cable on the ground. Make the two parallel to each other.

6.1.2. Use plastic ties to attach the two cables every 3 meters.

6.1.3. Connect the data cable to tiltmeter connector and tie the aircraft cable to the loop on top of tiltmeter.

6.1.4. Raise tiltmeter vertically over the casing opening and slowly put down into the inner PVC pipe using aircraft cable until it reaches the bottom.

6.1.5. Lift tiltmeter a little up and down again to make sure it is sitting stable on the borehole bottom.

6.1.6. Extend extra cables straight on the ground.

6.2. Surface installation

6.2.1. Mount the radio box in upright position on the surface pole using U-bolts.

6.2.2. Mount two solar panels using U-bolts on the surface pole and face north direction. The mounting on the surface pole is shown in Figure A-1 below:



Figure A-1: Solar panel and radio box setup on steel pole

6.2.3. Put tiltmeter battery inside the radio box.

6.2.4. Attach the data cable from downhole tiltmeter to battery box and the cable from battery box to radio box connector. Figure A-2 below shows setup with the radio box:



Figure A-2: setup inside radio box

6.2.5. Fix the aircraft cable to the surface pole, adjust its looseness and make sure there is no tension

6.2.6. Attach power cords from solar panels to its connector on radio box and tiltmeter battery box. Cable wiring and connection is shown in Figure A-3:



Figure A-3: Cable wiring and connection

6.2.7. Use the power switch inside radio box to power the system.

6.3. Communication test

6.3.1. Communication test between downhole tiltmeter and remote computer including tiltmeter detection, changing settings and data downloading.

6.3.2. On computer end, use TiltTalk software to search for tiltmeter after field instruments is powered. If field instruments are wired correct, connection can be established in a few minutes. Detect new tools in the setup tab and choose refresh all in expand view. Newly installed tiltmeter should show up and be connected. After connection is on, try to change settings in the control tab. After tiltmeter takes some readings, try to download data. If all the above procedures are successful, communication test is completed. Figure A-4, Figure A-5 and Figure A-6 below show screen shots of the above procedures.

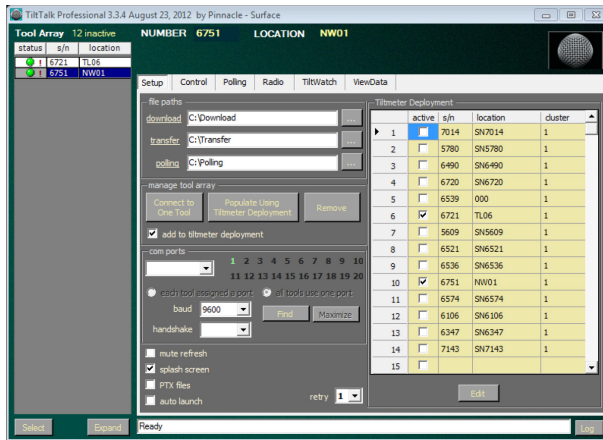


Figure A-4: Setup tab of TiltTalk shows all tiltmeters information

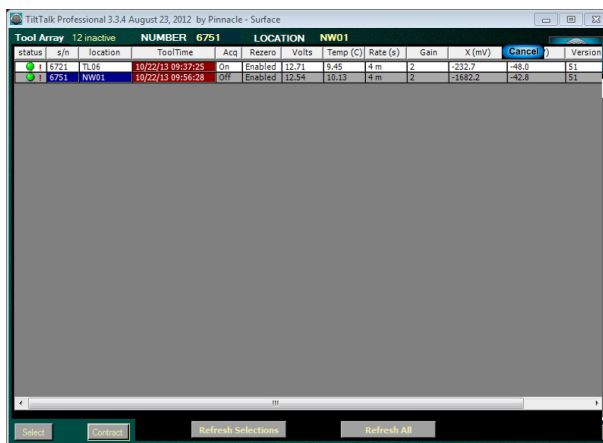


Figure A-5: “Expand” tool array table shows all active tiltmeter information, “Refresh All” to detect new tiltmeters

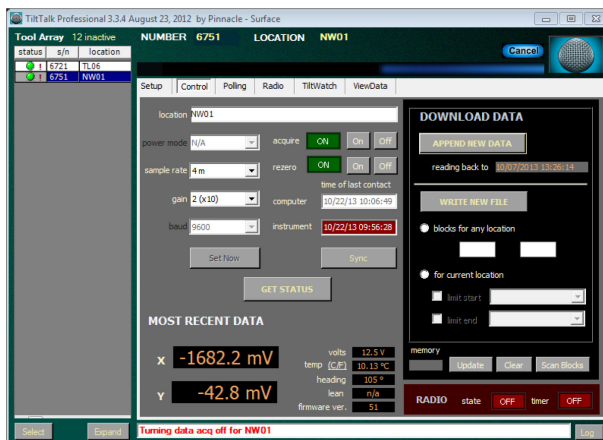


Figure A-6: Control tab of TiltTalk shows command window for each tiltmeter, including acquire status, changing settings and download data

6.3.3. If connection cannot be established, try to diagnose the problem by checking signal lights of each component and the connection between different units.

6.3.4. Tiltmeter communication can also be tested while tiltmeter is still in the surface. Additional test should still be performed after tiltmeter is put downhole to check if the communication is functioning well.

6.4. Finishing the installation

6.4.1. After communication is successful, close and lock the radio box.

6.4.2. Put ~1 L of sand downhole using a measuring cup. This volume is determined by using PVC pipe of the same inner diameter and tiltmeter in laboratory and it should cover half of tiltmeter height. This volume can be adjusted in field if there is some loss of sand (in between the two casings) during operation.

6.4.3. Put extra-length cable inside the borehole casing and lock the opening of surface borehole casing with cap. A finished tiltmeter station is shown in the Figure A-7 below.



Figure A-7: Finished tiltmeter station

6.4.4. Clean the site.

Appendix B Field Installation Logs

The following section provides a summarized account of events prior and during the deployment and completion of tiltmeter sites to provide the reader with a sense of the activities that are undertaken when designing and installing a surface tiltmeter array monitoring system.

November 2012 field trip

November 2012 field trip focused on the initial deployment of two tiltmeter sites and the communication system. Two tiltmeter sites were deployed at site TL06 and NW01. Master Radio station was installed near site TL06.

November 1st - Load vehicles at University of Alberta. Instruments are loaded on a pickup and a cube van and secured to the deck.

November 2nd - Leave Edmonton for site at noon.

November 3rd - Arrive at Estevan. Report to field administration and take field safety training.

November 6th – Install tiltmeter station at site NW01. Steel cabinet and solar panels are installed on the surface pipe first. Then put down tiltmeter using aircraft cable. 0.5 L more sand is used to lock tiltmeters as there is some loss in the casing. Finish all connections at surface. Signals indicate all parts working.

November 7th – Install tiltmeter station at site TL06 using the same procedures as in NW01. Install master radio station near site TL06. Make a steel frame structure using steel bars. Install the master radio cabinet and solar panels on the structure. Due to strong wind, the installation of mast is postponed.

November 8th – Install mast for master radio station. Assemble all parts to the mast before lifting it up. After the mast is erected, communication test is performed. Connects to both tiltmeter sites are successful from Edmonton. Finish site TL06.

November 9th –After successfully collected one day's data, left Estevan for Edmonton in the afternoon.

November 10th – Arrive at Edmonton

February 2013 field trip

February 2013 field trip focused on the installation of weather station and tests on tiltmeter following the initial data analysis.

February 17th – Pick up vehicle and load equipment at University. Leave for Estevan at noon.

February 18th – Arrive at Estevan. After a primary scan of the site, choose a flat ground 2m north of master radio station as the location of weather station.

February 19th – Install Weather station according to the manual. Connect weather station cabinet with modem from master radio station using internet cable. Communication test failed after the communication.

February 20th – After reconnect all cables, communication test becomes successfully. Validation of collected data with government meteorological data shows good agreement.

February 21st – Check existing tiltmeter sites. Loose supporting aircraft cable to relief tension. Some basic noise tests are conducted. No significant data deviation is detected from collected data. Leave for Edmonton in the afternoon.

February 22nd – Arrive at Edmonton.

September 2013 field trip

September 2013 field trip focused on the inspection of tiltmeter site after one year's operation and preparation of upcoming tiltmeter borehole drilling. This trip also took place with Aquistore Fluid Recovery System (FRS) test.

September 16th - Pick up vehicle and load equipment at university.

September 17th – Leave Edmonton for Estevan.

September 18th – Arrive at Estevan in the afternoon. Finish FRS test. Locate tiltmeter borehole materials (steel and PVC pipes are found at well site while couplers are missing). Confirm tiltmeter borehole drilling materials and schedule.

September 19th –Check tiltmeter sites. Leave tiltmeter equipment at SaskaPower warehouse. Drilling should start today but due to wet weather machinery cannot access site. Leave for Edmonton in the afternoon.

September 20th – Arrive at Edmonton.

Appendix C Tiltmeter Temperature Compensation Test

Testing equipment

The purpose of the calibration test is to find the actual tiltmeter reading under different temperatures and compare it with the real tilt. To measure the real tilt, LVDT and high accuracy gauges are used. A stable testing frame is built to house the tiltmeter with controllable temperature and mount LVDT and gauges to take measurement. The testing frame consists of three systems, the temperature chamber system that controls the testing temperature, measuring system that takes tilt reading, and testing structure that is used to fix the above instruments and the tiltmeter.

Testing Structure is shown in the Figure C-1 below. Tiltmeter is fixed in a steel pipe with sand. The height of the sand in the pipe is about the height of the tiltmeter. The communication cable of the tiltmeter connects the tiltmeter with the battery box outside. The steel pipe is fixed on the rotation wheel using two ring clamps. Once the steel pipe is put on, two o-rings are placed inside the clamps and the clamps are tightened using screws. There is a dial on the rotation wheel that can loose or tighten the wheel. A steel arm is fixed horizontally on the wheel that is used to measure vertical displacement on the other end. All the above instruments sit on a steel structure that is stably sitting on the ground.

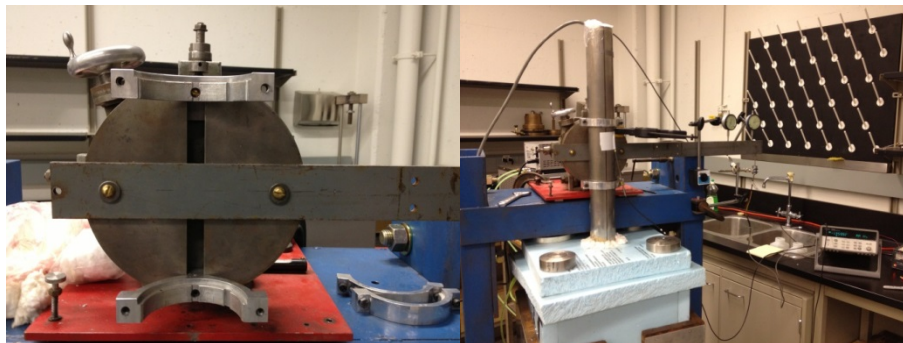


Figure C-1: Rotation arm and testing frame

Temperature Chamber is a system that is used to maintain the tiltmeter in a certain constant temperature. A programmable temperature controller is used to circulate liquid with pre-set temperature to a spiral coil that is stationed inside a big box made of heat insulation foam board. The extra space in the box is filled with heat insulation popcorn. Any opening in this system is clogged with thermal cotton. Temperature control device and environmental chamber is shown in Figure C-2.



Figure C-2: Temperature control device and environmental chamber

Measuring System consists of two reading gauge and a LVDT. These gauges are measuring the vertical displacement of a rotating arm. The tiltmeter is fixed by the rotation arm so that the vertical displacement of the rotation arm can be converted to tilt when the rotation is minimal. The two reading gauge can take a minimum reading of 0.001mm, while LVDT is connected to a data logger that can display the displacement of a minimum 0.001mm. The length of the arm is measured so that tilt can be computed out by divide the vertical displacement by the length of the arm. By having three tilt any error in one can be figured out easily and the average good readings is more accurate. Also taken by the data logger are two temperature probes that are fixed on top and bottom of the steel pipe that contains the tiltmeter. While the upper probe can represent the room temperature, the bottom probe is sitting inside the chamber that can give the actual temperature of the tiltmeter. The data logger is taken readings every 5 seconds. Two gauges and LVDT is shown in Figure C-3.

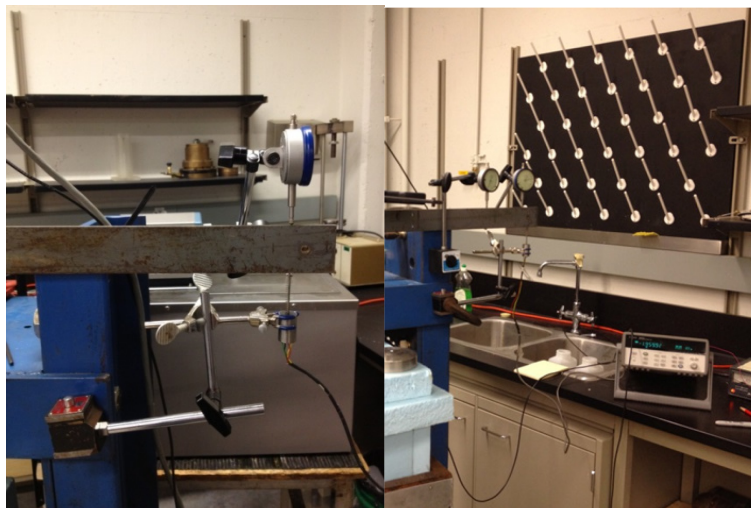


Figure C-3: Measuring gauges and LVDT

Testing procedures

1. Prepare the tiltmeter. The steel pipe comes with two pieces. Put the tiltmeter into the lower piece. Attach the tiltmeter cable to the port and stick the temperature probe to about 30cm above the bottom of the tiltmeter. Align the mark on the tiltmeter with the mark on the steel

pipe so that X direction is unknown during the test. Put sand into the pipe to about the height of the tiltmeter. Put the upper piece of the pipe and align the marks. Use Steel O-ring to connect the two pieces. Put heat insulation cotton to the opening of the pipe.

2. Assemble the pipe. Put the steel pipe into the chamber and face the mark to the left hand side. Lift the pipe about 10cm above the bottom of the chamber and tighten it on the wheel using the O-shaped clamps and O-rings. Seal the opening on top of the chamber using cotton. Put the pipe as vertical as possible. Attach the second temperature probe on the exposed pipe. Tighten the wheel using the dial and use the clamp to further tighten it.
3. Test the tiltmeter reading by loosening the clamp first, and then tilt the tiltmeter by spinning the dial of the wheel at a small pace. Watch the LVDT for the degree of the tilt. For most cases a delta reading of 0.2mm is adequate for one turn, which in tiltmeter is about 2000mV or 500uR in tilt. After tilting, tighten the wheel again and take the reading of two gauges and LVDT, Tilt showed in the Tilttalk software.
4. For one temperature, the tilt readings of the tiltmeter should be within $\pm 300\text{uR}$ (1500mV) and it's best to have discrete values. In total 10 different values should be taken before and testing axis be rotated. Then take another 10 readings for the other axis.
5. For each tiltmeter, 4 different temperatures are tested, usually -1, 4, 9 and 14 degree Celsius, which is the estimated range of temperatures to be encountered in the field.
6. After each test, data is retrieved from data logger and Tilttalk for process in the next stage.

Data processing and results

The data obtained from each calibration is listed in Table C-1:

Table C-1: Data obtained from temperature compensation test

Tiltmeter Information	Serial Number, Default calibration factor
Temperature Data	Two temperature probe data, Tiltmeter temperature record
Gauge Reading	Two reading gauge, LVDT
Tiltmeter Reading	X tilt, Y tilt

The gauge reading is converted to tilt by dividing the length of each arm. Then the tilt reading is converted to a series of shattered points through dividing the delta tilt with corresponding delta X or Y tilt, so that for each X or Y reading, there is a corresponding tilt. In this way the actual calibration factor is determined. An example is given below in Table C-2.

Table C-2: A sample calculation for temperature dependency coefficient

Tilt #	Dial#1 (mm)		Dial#2 (mm)		LVDT (mm)		Y-Axis (mV)	
	Before	After	Before	After	Before	After	Before	After
1	1.557(A)	1.295(B)	1.643	1.432	-2.042	-2.310	1280(D)	1754(E)
2	1.295	1.564	1.432	1.649	-2.31	-2.034	-1754	1378
Tilt #	Before	After	Before	After	Before	After	$C = \frac{A-B}{L} / (D-E) * D$	
1	189.3(C)	-259.4	186.0	-254.9	187.3	-256.7		
2	-258.0	202.7	-254.0	199.5	-256.1	201.2		

After the corresponding tilt is computed from the table above, the shattered plot of X or Y reading and corresponding tilt can be plotted. A trend line can be generated. Usually the dispersion ratio of the trend line should be above 0.99 or a double check should be done to ensure no error occurred while processing the data. There will be three trend lines corresponding the three gauge reading. The average gradient of the trend line is the actual calibration factor for the tiltmeter at the tested temperature. Figure C-4 below is an example of a shattered plot for a tiltmeter at -1 degree Celsius bath temperature.

For each temperature, a calibration factor can be estimated. Then the relationship between temperature and calibration factor can be plotted and its trend line reveals the behavior of tiltmeter with temperature (Figure C-5). This trend can be used to calibrate the tiltmeter when temperature changes in the field.

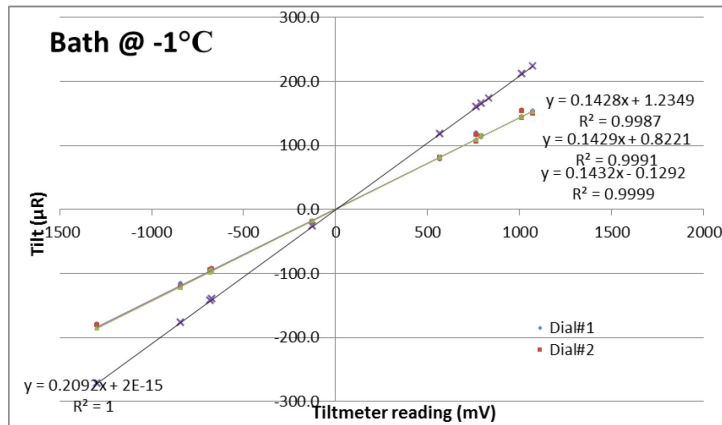


Figure C-4: Temperature dependency coefficient at -1°C

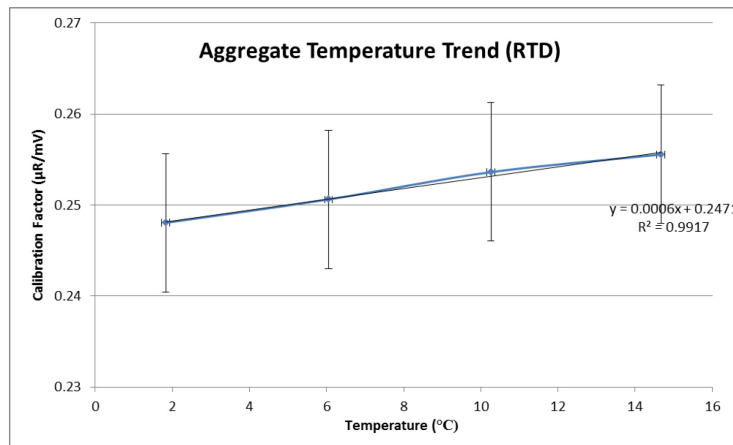


Figure C-5: Calibration factor with temperature